

# **Synthesis and Characterisation of Indole-based Materials for Organic Electronic Applications**

**Robert Andrew Valentine**



**Thesis submitted for the degree of PhD**

**The University of Edinburgh**

**September 2009**

## **Declaration**

I hereby declare that this thesis has been entirely composed by myself and that the work described herein is my own except where clearly stated either in acknowledgement, reference or text. It has not been submitted either in whole or in part for any other degree, diploma or other qualification.

Robert A. Valentine

September 2009

*For Nicola,*

*without whom I wouldn't have started and certainly wouldn't have finished*

## Acknowledgements

This thesis would not have been possible without the help of an awful lot of people and they deserve all the praise in the world.

Firstly, my supervisor Neil Robertson for his continuing support and guidance, as well as for taking a chance and giving me this opportunity to champion the cause of indole chemistry.

For their help with NMR, Mass Spectrometry and CHN analysis thanks must go to John Miller, Alan Taylor and Sylvia Williamson respectively. Special mention needs to Patricia Richardson that I understand any computational chemistry is almost entirely due to her continued efforts. For teaching me more in a week than anyone has a right to learn thanks must go to Maxim Shkunov and David Sparrowe of Merck Chemicals Ltd for their help with film and semiconductor characterisation. Acknowledgement must also be made of the Cheung group at the Scottish Microelectronics Centre, for both their time and advice in regard to FET measurements. Thanks need to go Andrew Mount and John Henry for their help with the Electrochemistry of 2,3-diindoles and the Yellowlees group for their help with both electrochemistry in general and spectroelectrochemistry.

Then there is the Robertson group and the various people who have passed through it over my time in Edinburgh. Thank you all for the advice, chats and distractions but most importantly the tea.

Linda and Allan who for reasons I have yet to fathom agreed to let me take advantage of their hospitality. I promise you will have your to yourself soon.

To my parents who continued to put up with my student status without complaint as well as their support both emotional and occasionally financial.

Finally Nicola, for your understanding, support and occasional kicks in the right direction, I don't know how you have put up with me but I can't thank you enough for it.

## Abstract

This thesis presents the synthesis and characterisation of conjugated indoles with a view to assessing their potential for electronic applications. Four different families of indole-based species have been investigated, 2,3-diindoles, indolo[3,2-a]carbazoles, indolo[3,2-a, 3',2'-c]carbazoles and indolo[2,3-a]carbazoles. Characterisation was carried out through a combination of electrochemistry, absorption spectroscopy, emission spectroscopy and hybrid-DFT calculations. Additional characterisation using field-effect transistor measurements and spectroelectrochemistry was undertaken where required.

Three of the families investigated 2,3-diindoles, indolo[3,2-a]carbazoles and indolo[3,2-a, 3',2'-c]carbazoles, are the results of new, high-yield synthetic routes. This includes the first reported use of microwave synthesis in the production of an indolocarbazole species. The electronic properties of each of these systems and the indolo[2,3-a]carbazoles are reported. Adaptation of the electronic properties of each of these systems was observed through the investigation of the effects of substituents at different positions around the conjugated core of the molecule.

This work also reports the first coordination compound formed with an indolocarbazole ligand. The ruthenium[bipyridine]<sub>2</sub>benzo[c]indolo[2,3-a]carbazole display a number of interesting properties caused by the significant HOMO character on the

benzo[c]indolo[2,3-a]carbazole ligand. This was observed through both computational and spectroelectrochemical methods.

# Contents

|                  |     |
|------------------|-----|
| Declaration      | i   |
| Dedication       | ii  |
| Acknowledgements | iii |
| Abstract         | iv  |
| Contents         | vi  |
| Abbreviations    | ix  |
| Structures       | x   |

|                                 |          |
|---------------------------------|----------|
| <b>Chapter 1 - Introduction</b> | <b>1</b> |
| 1.1 – Transistors               | 2        |
| 1.2 – Semiconducting Materials  | 3        |
| 1.3 – Plastic Electronics       | 7        |
| Organic Semiconductors          | 8        |
| 1.4 – Device Engineering        | 19       |
| Solution Processing             | 20       |
| 1.5 – Conclusions and Aims      | 21       |
| 1.6 – References                | 22       |

|  |           |
|--|-----------|
| <b>Chapter 2 – Experimental Techniques</b> | <b>27</b> |
| 2.1 – Photochemistry                       | 28        |
| 2.2 – Computational Methods                | 29        |
| Geometry Optimisation Calculations         | 29        |
| Time-Dependant DFT                         | 30        |
| 2.3 – FET Measurements                     | 30        |
| 2.4 – Spectroelectrochemistry              | 32        |
| 2.5 – References                           | 33        |

|  |           |
|--|-----------|
| <b>Chapter 3 – 2,3-Diindoles and Indolo[3,2-a]carbazoles</b> | <b>35</b> |
| 3.1 – Introduction   | 35        |
| 3.2 – Synthesis  | 40        |
| 2,3-Diindoles  | 41        |
| Indolo[3,2-a]carbazoles                                      | 42        |

|   |    |
|---|----|
| 3.3 – Electrochemistry  | 43 |
| 2,3-Diindoles   | 43 |
| Indolo[3,2-a]carbazoles                                       | 46 |
| 3.4 – UV/Vis Spectroscopy                                     | 50 |
| 2,3-Diindoles   | 50 |
| Indolo[3,2-a]carbazoles                                       | 51 |
| Indole monomers vs. 2,3-Diindoles vs. Indolo[3,2-a]carbazoles | 53 |
| 3.5 – Emission Spectroscopy                                   | 55 |
| 2,3-Diindoles   | 55 |
| Indolo[3,2-a]carbazoles                                       | 58 |
| 2,3-Diindoles vs. Indolo[3,2-a]carbazoles                     | 60 |
| 3.6 – DFT Calculations  | 61 |
| 2,3-Diindoles   | 61 |
| Indolo[3,2-a]carbazoles                                       | 65 |
| 3.7 – TD-DFT  | 68 |
| 3.8 – FET Measurements  | 71 |
| 2,3-Diindoles   | 71 |
| Indolo[3,2-a]carbazoles                                       | 72 |
| 3.9 – Conclusions   | 74 |
| 3.10 – Experimental   | 76 |
| 3.11 – References   | 80 |

|   |           |
|---|-----------|
| <b>Chapter 4 – C3-Symmetric Triindoles</b>          | <b>84</b> |
| 4.1 – Introduction                                  | 84        |
| C3-Symmetric Triindoles                             | 88        |
| 4.2 – Synthesis                                     | 90        |
| 4.3 – Electrochemistry                              | 94        |
| C3-Symmetric Triindoles                             | 94        |
| Indolo[3,2-a]carbazoles vs. C3-Symmetric Triindoles | 98        |
| 4.4 – UV/Vis Spectroscopy                           | 99        |
| C3-Symmetric Triindoles                             | 99        |
| Indolo[3,2-a]carbazoles vs. C3-Symmetric Triindoles | 101       |
| 4.5 – Emission Spectroscopy                         | 103       |
| C3-Symmetric Triindoles                             | 103       |
| Indolo[3,2-a]carbazoles vs. C3-Symmetric Triindoles | 106       |
| 4.6 – DFT Calculations                              | 107       |
| C3-Symmetric Triindoles                             | 107       |
| Indolo[3,2-a]carbazoles vs. C3-Symmetric Triindoles | 110       |



|   |            |
|---|------------|
| 4.7 – FET Measurements                                      | 112        |
| 4.8 – Conclusions   | 112        |
| 4.9 – Experimental  | 114        |
| 4.10 – References   | 116        |
| <b>Chapter 5 – Indolo[2,3-a]carbazoles</b>                  | <b>118</b> |
| 5.1 – Introduction  | 118        |
| 5.2 – Indolo[2,3-a]carbazoles                               | 123        |
| 5.2.1 – Synthesis   | 123        |
| 5.2.2 – Electrochemistry                                    | 123        |
| 5.2.3 – UV/Vis Spectroscopy                                 | 128        |
| 5.2.4 – Emission Studies                                    | 131        |
| 5.2.5 – DFT Calculations                                    | 133        |
| 5.2.6 – TD-DFT  | 134        |
| 5.3 – Ruthenium Bisbipyridyl Benzo[c]indolo[2,3-a]carbazole | 137        |
| 5.3.1 – Synthesis   | 137        |
| 5.3.2 – Electrochemistry                                    | 138        |
| 5.3.3 – UV/Vis Spectroscopy                                 | 141        |
| 5.3.4 – Emission Studies                                    | 143        |
| 5.3.5 – Spectroelectrochemistry                             | 143        |
| 5.3.6 – DFT Calculations                                    | 145        |
| 5.4 – Conclusion  | 148        |
| 5.5 – Experimental  | 150        |
| 5.6 – References  | 151        |
| <b>Chapter 6 – Future Work</b>                              | <b>154</b> |

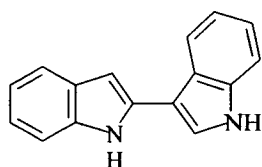
## **Abbreviations**

|      |                                    |
|------|------------------------------------|
| DCM  | Dichloromethane                    |
| DFT  | Density Functional Theory          |
| DMF  | Dimethyl Formamide                 |
| DMSO | Dimethyl Sulfoxide                 |
| DSSC | Dye Sensitized Solar Cell          |
| FET  | Field Effect Transistor            |
| HOMO | Highest Occupied Molecular Orbital |
| LCD  | Liquid Crystal Display             |
| LUMO | Lowest Occupied Molecular Orbital  |
| RFID | Radio Frequency Identification     |
| TFT  | Thin Film Transistor               |

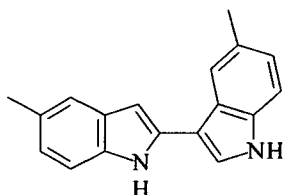
# Structures

## Synthesised Compounds

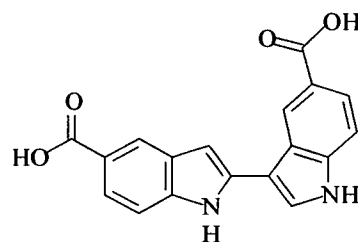
### 2,3'-Diindoles



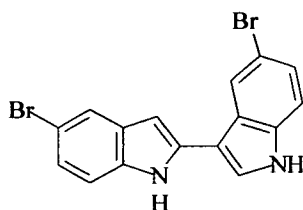
1a – 2,3'-diindole



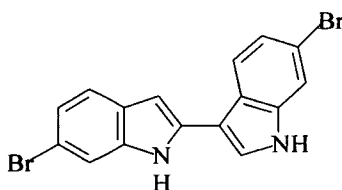
1b – 5,5'-dimethyl-2,3'-diindole



1c – 2,3'-diindole-5,5'-dicarboxylic acid

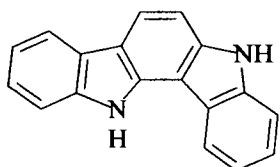


1d – 5,5'-dibromo-2,3'-diindole

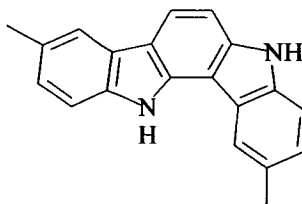


1e – 6,6'-dibromo-2,3'-diindole

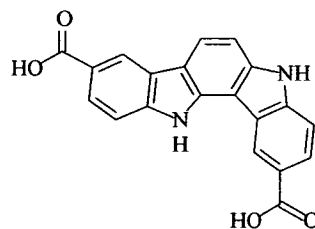
### Indolo[3,2-a]carbazoles



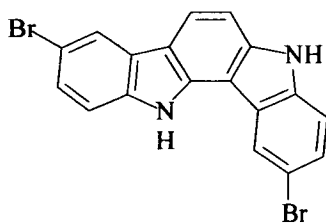
1a – Indolo[3,2-a]carbazole



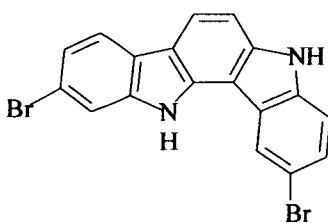
2b – 2,9-dimethylindolo[3,2-a]carbazole



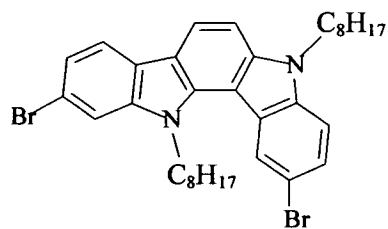
2c – indolo[3,2-a]carbazole-2,9-dicarboxylic acid



2d – 2,9-dibromoindolo[3,2-a]carbazole

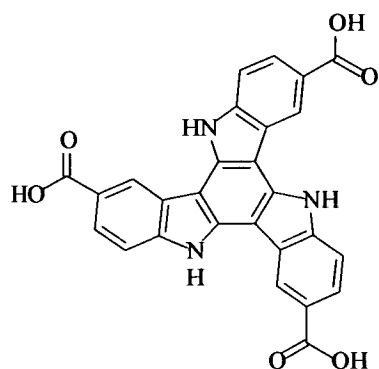


2e – 3,10-dibromoindolo[3,2-a]carbazole

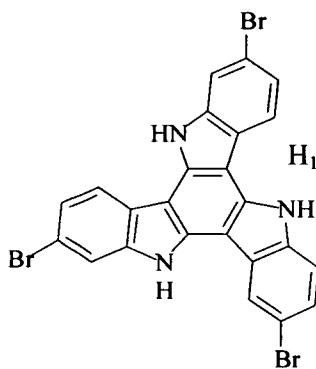


3 – 5,12-dioctyl-3,10-dibromoindolo[3,2-a]carbazole

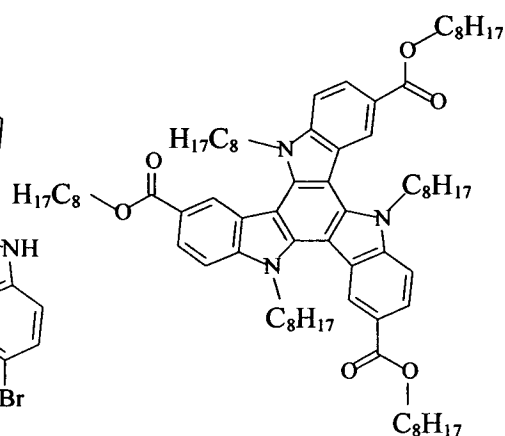
### C3-Symmetric Indole Trimers



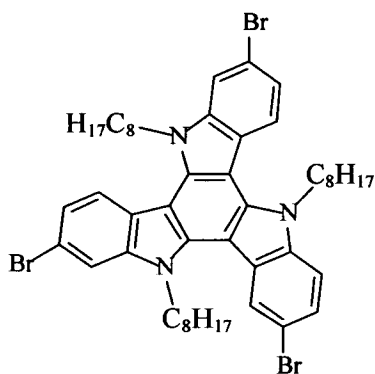
**4a** – indolo[3,2-a;3'2'-c]carbazole-2,7,12-tricarboxylic acid



**4b** – 3,8,13-tribromoindolo[3,2-a;3'2'-c]carbazole

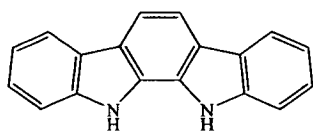


**5a** – 5,10,15-trioctyl indolo[3,2-a;3'2'-c]carbazole-2,7,12-trioctylester

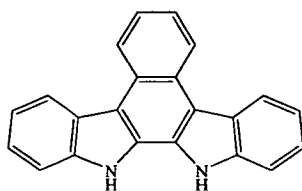


**5b** – 5,10,15-trioctyl-3,8,13-tribromoindolo[3,2-a;3'2'-c]carbazole

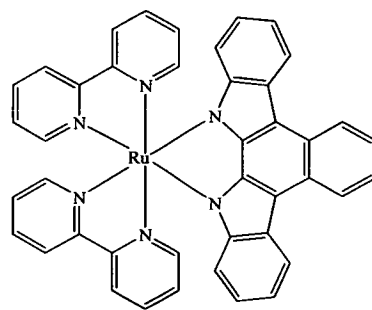
### Indolo[2,3-a]carbazoles



**a** – indolo[2,3-a]carbazole



**6b** – benzo[c]indolo[2,3-a]



**7** – Ru(bipy)<sub>2</sub>,**6b**

## **Chapter 1**

# **Introduction to Organic Semiconducting Materials**

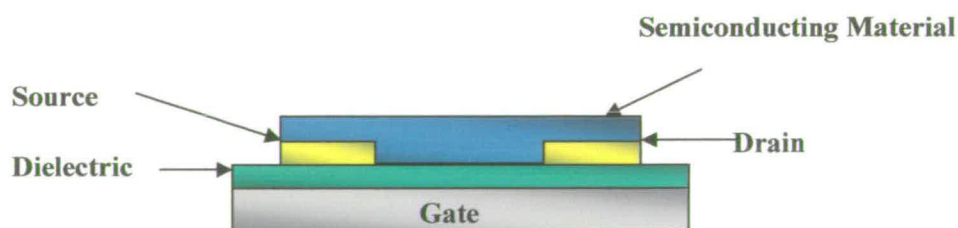
The history of the human race may be categorised by great technological innovation, from the Stone Age, Iron Age and Bronze Age, to the industrial revolution. It is in the nature of the human species to strive for an improved life through the creation of new tools and work practices. A number of factors including the exponential increase in population and mass education initiatives have given rise to a rate of industrial creativity of unprecedented levels. The sheer quantity of new and innovative advancements make it difficult to put a label on the current era of human history, however the consensus appears to be divided between the electronics age and the plastic age.

The field of electronics has grown with the ability to finely control the flow of electricity allowing the development of increasingly sophisticated devices. At a basic level this control comes from a number of switches which direct the flow of electricity. On a

macroscopic scale such as powering a light bulb the flow can be physically controlled by an operator through the use of a single switch. The increasingly intricate devices necessary for modern living require a vast array of switches in order to function and fully process information, hence a form of microscopic switch is required in order to control complex devices. This switch takes the form of a transistor. Through the application of an external stimulus, a transistor can be made to either allow the flow of electric current or prevent it. A series of transistors, which may be in any combination of ‘on’ or ‘off’ positions, allow a myriad of options and thus the fine control required to run electronic devices.

## 1.1 - Transistors

Invented in 1947 by Brittain, Bardeen and Shockley, a transistor is largely based around the intrinsic properties of semiconducting materials. A typical three-electrode field effect transistor is shown in Fig. 1.1



*Figure 1.1 – A typical bottom-gate field-effect transistor*

The source and drain electrodes are connected to the circuit. Under normal conditions the semiconducting material acts as an insulator and no current can flow between the two electrodes. However, if a charge is placed on the gate electrode an opposing charge is formed in the semiconductor. The presence of this charge between the source and drain electrodes allows current to flow between the two, completing the circuit. The continuing improvement in transistor technology is the fundamental reason behind the proliferation of electronic devices available. Engineering advances have significantly reduced transistor size greatly increasing the potential number of transistors within a processor resulting in a vast improvement in computing power. Chemical advances have also played a significant role in the improvements in transistor technology through improving the capabilities of the semiconducting materials involved.

## **1.2 - Semiconducting Materials**

The first evidence of semiconducting materials became apparent in 1833 when Michael Faraday discovered that the conductivity of silver sulphide increased upon heating.<sup>1</sup> The most effective semiconducting materials have since been found to be some group IV elements including silicon and germanium or compounds based on group III and group V elements such as gallium arsenide and indium nitride.

Semiconducting materials can be explained through band theory as illustrated in Fig. 1.2. The presence of a large number of atoms results in the splitting of energy levels into an increasingly large number of molecular orbitals. As the number of atoms increases, the difference between energy levels decreases until the point where the energy levels amalgamate to become bands, specifically a conduction band and a valence band. In a semiconducting material the energy difference between the empty conduction and filled valence bands is small enough that external stimuli can cause the valence band to become partially filled, this then gives rise to charge carriers.

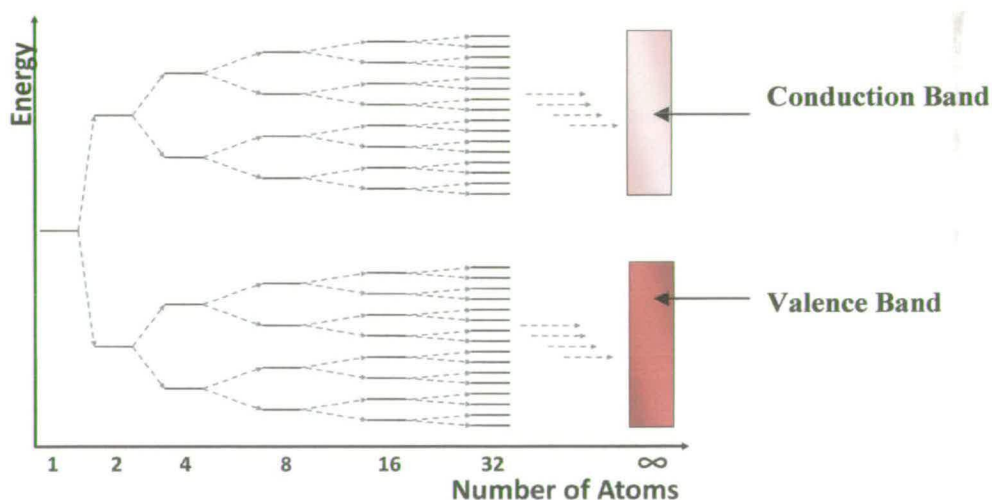


Figure 1.2 – Illustration of the band theory explanation for semiconducting materials

The single most important intrinsic property of a semiconductor is the charge mobility. Charge mobility is the rate at which an induced charge can move through a material and some typical values for these properties are illustrated in Table 1.1.

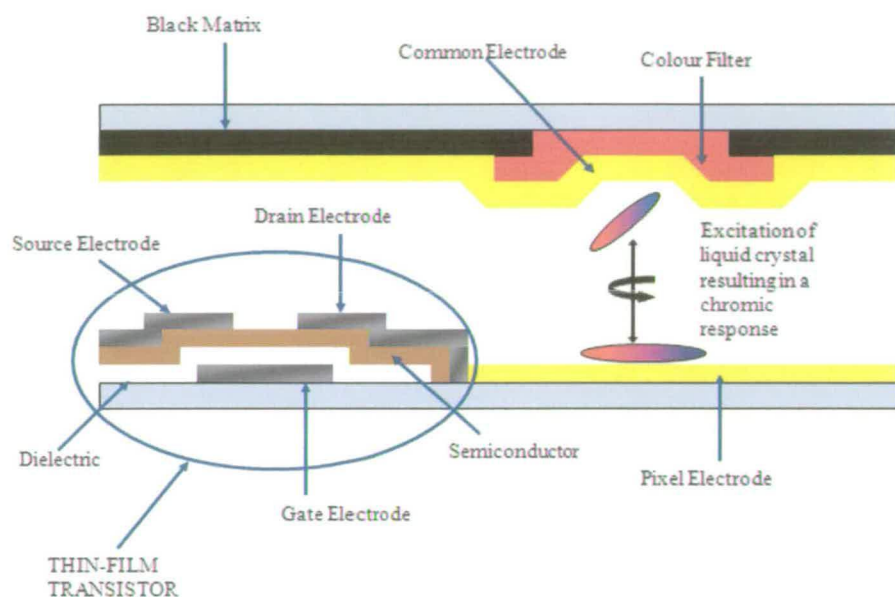


|                  | Mobility $\text{cm}^2/\text{Vs}$ |
|------------------|----------------------------------|
| Silicon          | 1400                             |
| Gallium Arsenide | 9000                             |
| Indium Nitride   | 2000                             |

*Table 1.1 – Typical values for charge mobility of a number of inorganic semiconductor*

The charge mobility values seen for these materials are the result of a number of processes. In the case of silicon these processes include the purification of the starting material until it is 99.999999% followed by subsequent doping with a small amount of group III or group V material. This provides a very small excess of charge carrying species and reduces the band gap of the silicon to the point where mobilities of the order of  $1400 \text{ cm}^2/\text{Vs}$  are possible.

This improved charge mobility through purification comes at significant cost. For computational applications this cost can be offset by the consumers' willingness to pay for the final product. In applications such as liquid crystalline displays, Fig. 1.3, arrays of thin-film transistors are used within each pixel to stimulate liquid crystalline materials



*Figure 1.3 – Diagrammatic representation of a pixel within an LCD display*

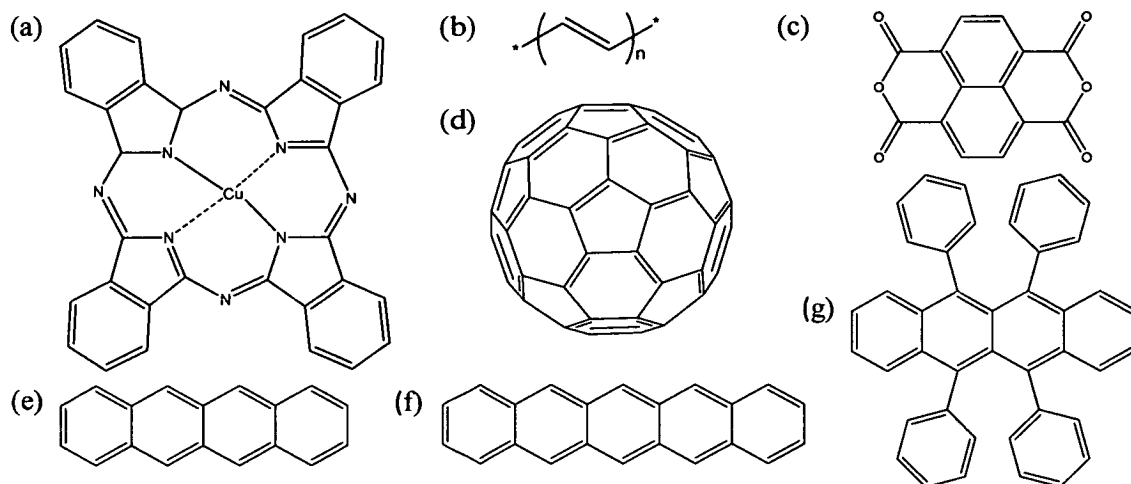
resulting in a chromic response. Given the number of transistors involved in such a large area application, the costs of using ultra-high purity materials become prohibitive. Instead these and other large-area applications such as photovoltaics or low-cost applications such as RFID (Radio-Frequency Identification) tags, often take advantage of  $\alpha$ -Si (amorphous silicon). This is a less pure form of silicon but as a result of this impurity, the quality of the films of material produced is reproducible, with a charge mobility of  $\approx 1 \text{ cm}^2/\text{Vs}$ . Despite the lowered costs of purification steps, the same expensive manufacturing costs are incurred when producing  $\alpha$ -Si based transistors as when forming those based on ultra-pure silicon. This has led to the search for

alternative semiconducting materials which offer either an improved performance at a similar manufacturing cost or a similar performance at reduced cost.

### **1.3 - Plastic Electronics**

Plastic is the generic term used to describe a multitude of synthetic organic solids. Synthetic plastics have been known since 1855<sup>3</sup> and a wide range of extremely useful commercially produced plastics have been observed including, Bakelite, polystyrene and PVC. The vast majority of these ‘plastic’ materials are polymeric and the potential commercial application of such materials has led to significant levels of research funding being awarded to the new field of polymer science.

The study of organic-inorganic hybrid materials led to the discovery of organic based semiconductors such as copper phthalocyanine, Fig 1.4a<sup>4</sup> and highly conductive materials such as perylene-iodine complexes.<sup>5</sup> However, when, in 1977, it was discovered that doped polyacetylene, Fig. 1.4b, was also highly conductive,<sup>6</sup> the new field of plastic electronics was born.<sup>7</sup>



**Figure 1.4.** – Examples of Organic Semiconductors. a) Copper Pthalocyanine, b) Polyacetylene c) naphthalene tetracarboxylic dianhydride, d)  $C_{60}$ , e) tetracene, f) pentacene, g) rubrene

Plastic electronics is a term used to describe electronic systems made up primarily of organic materials. While most known organic materials are insulators many others have recently been discovered which act as conductors,<sup>8,9</sup> and even others which act as low temperature superconductors,<sup>10,11</sup> however the most significant advancement in organic electronics has been in the field of organic semiconducting materials.

### **Organic semiconductors**

From Huckel Theory it is understood that conjugated organic materials also have filled or empty bands formed from molecular orbitals. This equates to the band theory

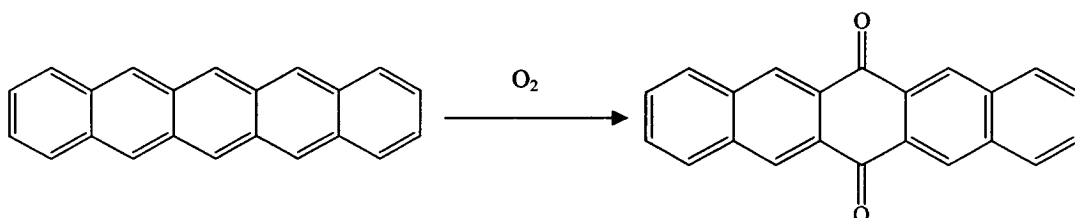
diagram, Fig 1.2. With an increased number of conjugated bonds the energy gap between the highest occupied molecular orbital (HOMO) and lowest unoccupied molecular orbital (LUMO) decreases.

A wide range of conjugated organic materials have been discovered with a suitable HOMO- LUMO band gap, Fig 1.4, <sup>12-16</sup> however, it was in 1997 with the discovery of hole mobility in pentacene, Fig 1.4f, that research into small molecule organic-based electronic materials began in earnest. The discovery by Jackson et al of hole mobility of  $0.6\text{cm}^2/\text{Vs}$  <sup>17</sup> put mobility values of organic semiconductors within an order of magnitude of  $\alpha$ -Si and for the first time organic semiconductors became a viable alternative for large area applications. Optimisation of pentacene based transistors through improvements in processing and transistor technology have led to the current highs for hole mobility of  $3\text{cm}^2/\text{Vs}$  for a thin-film pentacene-based transistor <sup>18</sup> and  $35\text{cm}^2/\text{Vs}$  for a single crystal pentacene-based transistor. <sup>19</sup>

Both thin-film and single crystal-based transistors have a number of potential applications, however for device purposes thin-film transistors are more commonly used. <sup>20</sup> The primary reason for this is the reproducibility of results for thin-films due to the uniformity of the systems in conjunction with the ease of large-scale processibility in comparison to single crystal-based transistors.

While pentacene and the related acene family such as tetracene, Fig. 1.4e, and rubrene, Fig1.4g, are widely recognised as the most effective organic semiconductors, the larger acenes demonstrate a number of properties which prevent the more widespread use of such materials.

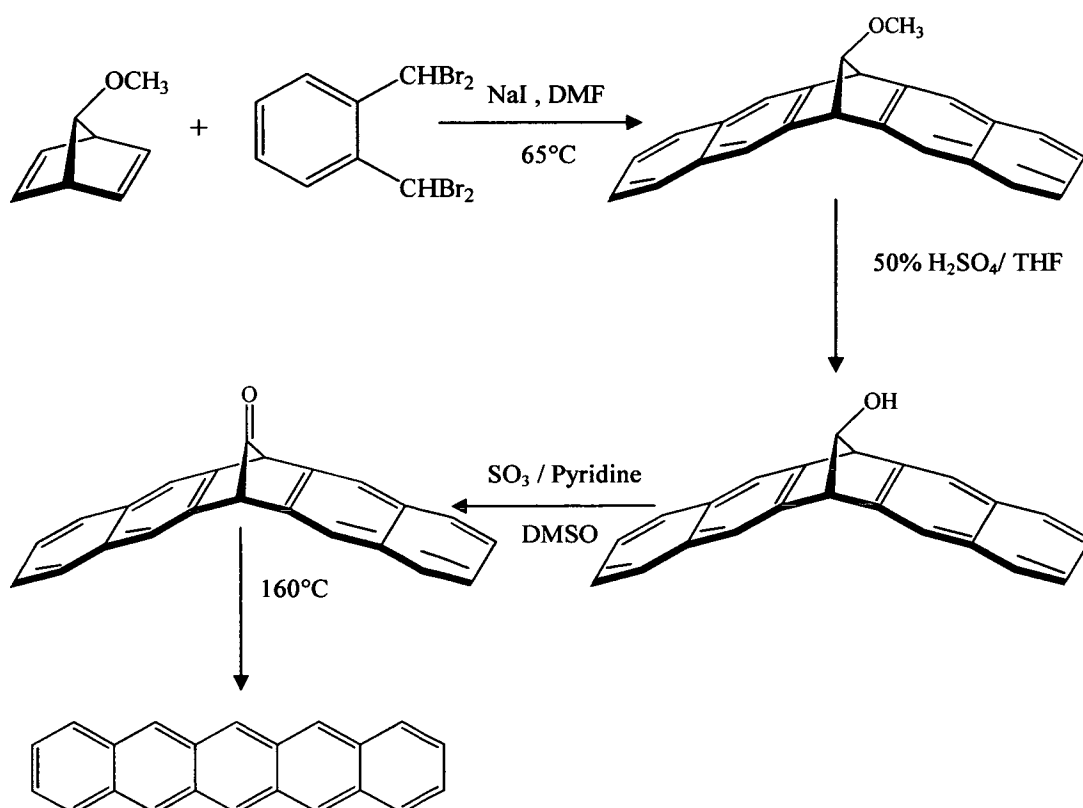
- Many systems, including pentacene, are unstable in air, Scheme 1.1. This causes problems in terms of material synthesis, device formation and device stability, all of which increase cost.



*Scheme 1.1 – Reaction of pentacene with air*

- The nature of the highly conjugated organic molecules means that the bulk materials are very stable and due to the strength of the interactions between  $\pi$ -systems, are often insoluble. This means that in a number of cases, rather than forming transistors from relatively inexpensive solvent-based processing techniques the same expensive processing techniques required for inorganic based transistors must be employed for organic devices.
- Synthesis of large conjugated systems may also be problematic due to the complexity of systems involved. This may be observed through the laboratory synthesis of pentacene Scheme 1.2.<sup>20</sup> The complexity of the synthesis as well as

the difficulties in reproducing such a synthesis on an industrial scale mean that pentacene is primarily obtained as a minor by-product of the oil industry. As such pentacene currently retails at £218.69 / gram for 99.9% pure and £453/g for 99.995% pure (prices from Sigma-Aldrich and correct as of September 2009).



*Scheme 1.2 – Laboratory synthesis of pentacenes*

While demonstrating the effectiveness of organic semiconductors as potential replacements for  $\alpha\text{-Si}$  the failures of the acene family indicate the need for the discovery of new materials with potentially interesting electronic properties to more effectively fulfil the criteria for low-cost or large area applications.

It is clear from Figure 1.4 that organic semiconductors share a number of important characteristics.

- All are highly conjugated with a large number of  $\pi$ -electrons. The presence of these electrons and the corresponding orbitals make possible the transfer of charge which results in semiconducting properties.
- With the exception of  $C_{60}$ , Fig. 1.4d, all are made up of large planar units. This allows for more effective overlap of orbitals ultimately leading to greater charge transfer potential.

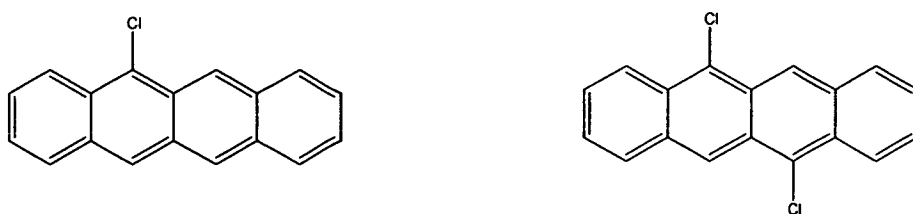
For large area and low cost applications the primary focus for new materials is a similar or improved performance to  $\alpha$ -Si at a much reduced cost. Based on the demonstrated failures of pentacene three further idealised characteristics for new organic semiconductors present themselves.

- The systems should be cheap and relatively simple to synthesise from readily available starting materials. This will allow for simple bulk synthesis on a scale suitable for industry.
- Systems should ideally be air stable.
- Systems should be soluble in a solvent suitable for solution processing as costs incurred are greatly reduced in comparison to standard vacuum deposition procedures.



While the first of these criteria is largely dependent on the nature of the core conjugated system, thus making control difficult, the second and third criteria can largely be controlled by application of synthetic organic chemistry to the periphery of the conjugated system. Most of this chemistry is done at the periphery of the core unit, however, adaptation of the periphery of conjugated system can still have a significant effect on the electronic properties of the system core. This has been effectively demonstrated by Moon et al<sup>22</sup> and their investigation into substituted tetracene.

Tetracene, is the four ring analogue to pentacene, though more air stable than pentacene, tetracene reacts with oxygen over time causing a significant reduction in device performance. In comparison 5-chlorotetracene, Fig 1.5a, is both air-stable and solution processible, however hole mobility dropped from  $1.3 \text{ cm}^2/\text{Vs}$  for tetracene,<sup>23</sup> to  $1.4 \times 10^{-4} \text{ cm}^2/\text{Vs}$  for 5-chlorotetracene, Table 1.2, purely due to the electron withdrawing effect of the chloro group on the conjugated core.



**Figure 1.5.** – (a) 5-chlorotetracene and (b) 5, 11-dichlorotetracene

|                         | Structure   | Mobility $\text{cm}^2/\text{Vs}$ |
|-------------------------|-------------|----------------------------------|
| tetracene               | herringbone | 1.3                              |
| 5-chlorotetracene       | herringbone | $1.4 \times 10^{-4}$             |
| 5, 11-dichlorotetracene | $\pi$ stack | 1.6                              |

**Table 1.2.** – Crystal packing structure and Charge mobility of tetracene derivatives

Further adaptation of the tetracene core with the addition of a further chloro group at the 11 position, Fig 1.5b, results in a dramatic increase in the hole mobility to  $1.6\text{cm}^2/\text{Vs}$ . This may largely be attributed to the presence of the extra chloro group causing a change to the packing structure of the solid material from a herringbone to slipped  $\pi$ -stack. This gives a much greater orbital overlap for the HOMO and LUMO levels between molecules, which in turn allows increased charge-transfer. While neatly illustrating the potential for modification of the periphery to increase air stability and allow solution processing, this example also demonstrates two other important aspects of the search for new organic semiconductors.

- The potential for outlying groups to improve the intrinsic properties of the core system, in this case through packing effects.
- The potential for introducing heteratoms into a conjugated system to improve functionality.

Both of these factors play an important role in the quest for new organic materials. The introduction of heteroatoms in particular plays a vital role due to both the effect of the

heteroatoms themselves and the subsequent chemistry, which may be used to further improve material properties. As may be noted from Fig 1.4, the majority of known organic electronic materials are based around a highly conjugated carbon core. Due to the difficulties inherent in carbon-carbon bond formation expansion of this highly conjugated core through carbon-carbon bonding can be a difficult process. The introduction of heteroatoms may allow expansion of the conjugated core through readily available carbon-heteroatom bond formation.

Functionalisation of known organic semiconductors has been used extensively as a route to new functional electronic properties. The acene family in particular has been subject to numerous attempts to functionalise the periphery of the core unit. These adaptations have attempted to improve or maintain the existing properties of the acene system, while removing some of their inherent disadvantages.

The range of modifications made to the periphery of a conjugated system may affect the intrinsic properties through a number of means. In the case of 5,11-dichlorotetracene, the edge-to-face interactions within the herringbone packing structure are disrupted by the presence of the halo-groups. This results in a change to face-to-face transitions interactions and increased  $\pi$ -overlap. The intrinsic electronic properties of tetracene and anthracene may also be enhanced through the addition of phenyl groups to form rubrene, Fig 1.6a and 9,10-diphenylanthracene, Fig 1.6c, respectively. This results in a charge

mobility of  $15 \text{ cm}^2/\text{Vs}$  for rubrene<sup>24</sup> and  $13 \text{ cm}^2/\text{Vs}$  for 9,10-diphenylanthracene<sup>25</sup> single-crystal based semiconductors. The steric interactions between the substituent groups and the acene ring system force the pendant phenyl rings to align perpendicular to the core. This causes an increase in the  $\pi$ -overlap due to the interactions between the peripheral phenyl groups and neighbouring molecules within the herringbone packing structure.

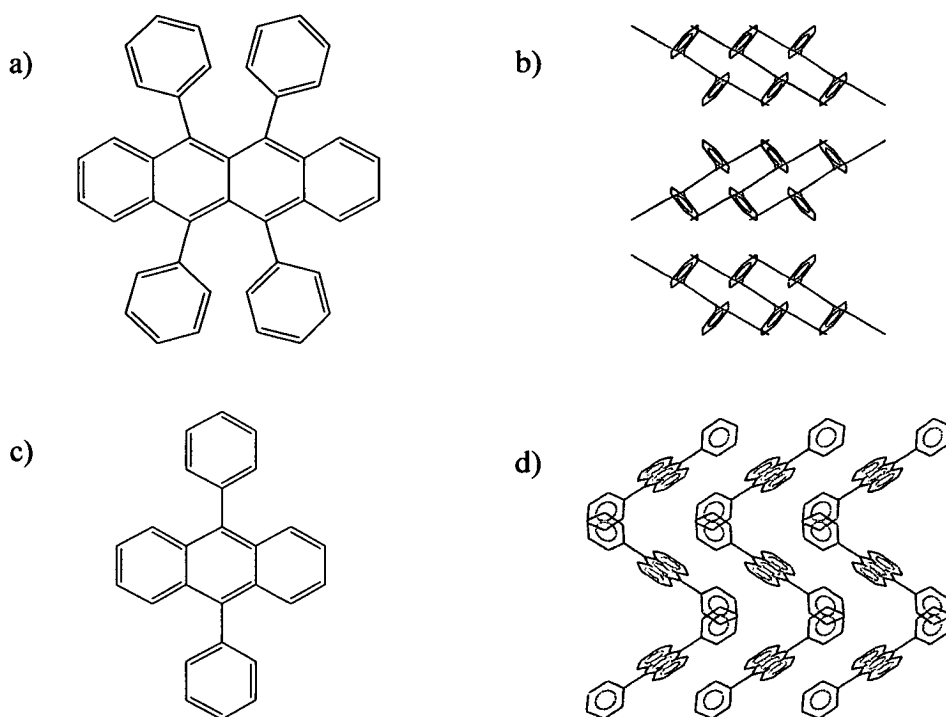
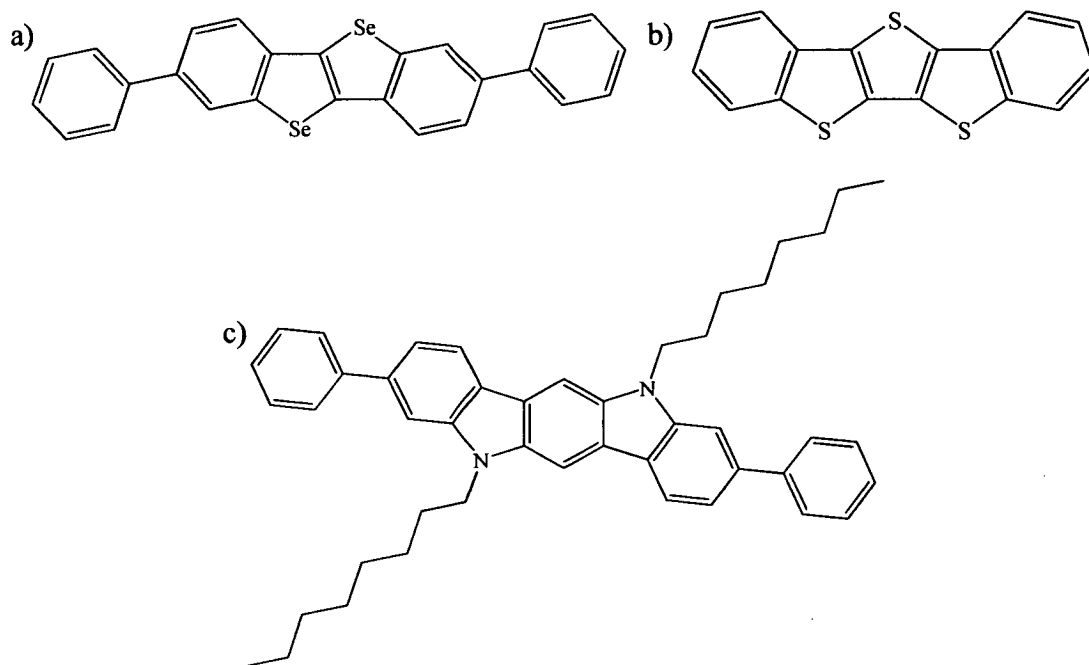


Figure 1.6 – a) Rubrene, b) Rubrene crystal structure<sup>26</sup> c) 9,10-diphenylanthracene and d) 9,10-diphenylanthracene crystal structure<sup>27</sup>

The introduction of heteroatoms or functional groups to the periphery of the conjugated core may cause significant changes to the material properties. However changes to the

material properties can also be made through the introduction of heteroatoms to the core itself. Due to the extensive research into the acene family much investigation of heteroacenes has also been undertaken.<sup>28-30</sup> The various heteroatoms introduced to the system result in numerous acene analogues, often without disadvantages of the acenes themselves. Systems such as the tetracene analogue 2,7-diphenylbenzo[d]benzoselenopheno[3,2-b]selenophene, Fig 1.7a,<sup>31</sup> and the pentacene analogues

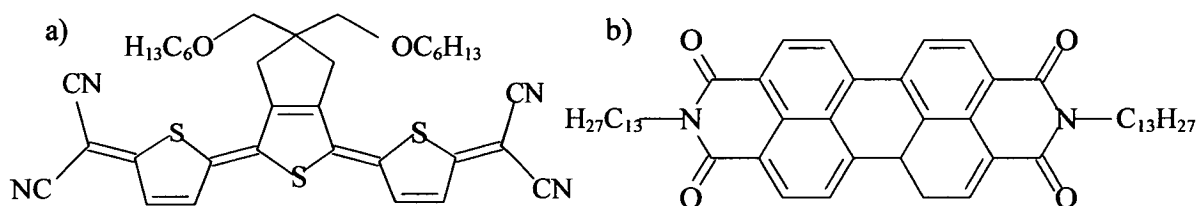


**Figure 1.7** - 2,7-diphenyl-benzo[d]benzoselenopheno[3,2-b]selenophene, b) dibenzo[d,d']thieno[3,2-b;4,5-b']dithiophene, c) 5,11-dioctyl-3,9-diphenylindolo[3,2-b]carbazole

dibenzo[d,d']thieno[3,2-b;4,5-b']dithiophene, Fig 1.7b,<sup>32</sup> and 5,11-dioctyl-3,9-diphenylindolo[3,2-b]carbazole, Fig 1.7c,<sup>33</sup> exhibit charge mobilities of  $0.31\text{cm}^2/\text{vs}$ ,

0.51 cm<sup>2</sup>/Vs and 0.40 cm<sup>2</sup>/Vs respectively but are all air stable and are soluble in a variety of solvent systems.

Another of the factors preventing more widespread commercial use of organic semiconductors is the disparity between materials with a high hole mobility and those with a high electron mobility. Devices such as diodes require a p-n junction such that both an electron-transport material and a hole-transport material are required to make the diode function. The most effective organic semiconductors, including the acenes and hexabenzocoronene are all p-type semiconductors with mobility values  $\leq 1\text{cm}^2/\text{Vs}$ .<sup>18,21,34-36</sup> Though recent efforts have discovered high electron mobility in C<sub>60</sub>,<sup>37</sup> a more commonly used method is the use of electronegative heteroatoms within the core. This is observed in recent work by a number of groups on systems as disparate as the thiophene derivatives, Fig 1.8a, with an electron mobility of 0.16 cm<sup>2</sup>/Vs<sup>38</sup> and 2,9-ditridecylanthra[2,1,9-def;6,5,10-d'e'f']diisoquinoline-1,3,8,10-tetrone, Fig 1.8b, with an electron mobility of 2.1 cm<sup>2</sup>/Vs<sup>39</sup>



**Figure 1.8** – a) 2,2'-[[5,5-bis[(hexyloxy)methyl]-5,6-dihydro-1H-cyclopenta[c]thiophene-1,3-diyliidene]di-5,2-thiophenediyliidene]bispropanedinitrile, b) 2,9-ditridecylanthra[2,1,9-def;6,5,10-d'e'f']diisoquinoline-1,3,8,10-tetrone, Fig1.8b

## **1.4 – Device Engineering**

It has previously been noted that devices based on traditional inorganic semiconductors involve expensive manufacturing costs. These costs arise not only from the expenses involved in the purification of the semiconducting material, but from the cost of depositing the material onto a transistor substrate

For inorganic systems, this deposition is primarily through vapour or vacuum deposition techniques at high temperatures, typically above 400°C. Deposition of organic materials may also take place through vapour or vacuum deposition techniques, though not necessarily at such high temperatures. As a result, different substrates may be used, including other plastics. The ability to deposit materials onto plastic substrates allows the production of new products, specific to organic electronic material based devices, such as the Plastic Logic eReader™, a thin, lightweight device to replace books and other paper-based products.

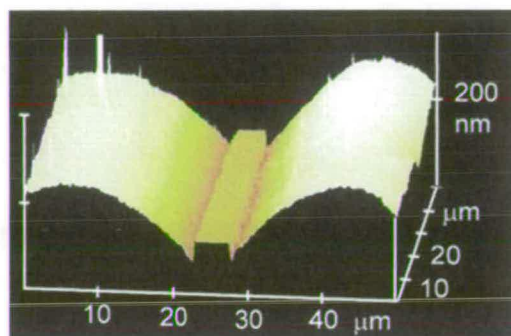
Vapour deposition of a material allows for the controlled growth of molecular thin-films and gives films with a high degree of molecular order ideal for devices where higher mobilities are required. However, use of soluble organic materials as a basis for electronic devices allows the use of solution processing techniques for device manufacture.

## ***Solution Processing***

Solution processing is a much more cost-effective method of thin-film production, though the films formed may have charge mobilities up to an order of magnitude lower than those formed by other techniques. A range of solution processing techniques are available, including spin and drop coating,<sup>40</sup> Langmuir-Blodgett film formation<sup>41</sup> and inkjet printing.<sup>42,43</sup> While at present the molecular order of films deposited via solution is often lower than those deposited by vapour, a number of different methods, including the application of a magnetic field to the film during manufacture,<sup>44,45</sup> are being developed to improve the long-range order of such films.

The low costs incurred in the solution processing already make devices formed via solvent based deposition ideal for low-cost applications such as RFID tags. The use of printing technology for electronic applications is another step towards the mass production of low-cost electronic devices. Advances in both the organic materials used and inkjet printing technology mean that it is now possible to print transistors onto a substrate forming entirely organic devices. These printed devices have improved with printing technology to the point where device size, nominally the distance between source and drain electrodes has shrunk from between 5 and 50 $\mu\text{m}$ <sup>46</sup> to 250 and 300nm at the time of writing, Fig 1.9.<sup>47</sup>

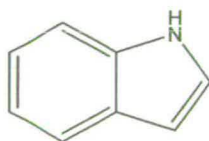




*Figure 1.9 – AFM demonstrating the channel width of devices formed through inkjet printing*

## 1.5 - Conclusion and Project Aims

This project is focused on the synthesis and characterisation of a series of heteroatomic aromatic systems based on the indole moiety, Fig 1.10, and investigating the electronic properties of such systems. Of the four different series of systems under investigation, three are closely related to the well known indolo[3, 2-b] carbazole series of organic semiconductors,<sup>48-50</sup> while the other provides information regarding the mechanism of formation for one series of compounds and a vital step in the synthesis of another.



*Figure 1.10 – Indole*

While this project is primarily aimed at the discovery and characterisation of new systems for organic electronic applications, it may also be noted that the one family of indole based materials under investigation display the potential to act as ligand to a wide range of metal centres. As such preliminary research into the properties of this family of compounds as ligands has begun, the ultimate aim of which is to combine two areas of research for the Robertson group at the University of Edinburgh, organic materials and metal-based dyes for use in dye sensitised solar cells and other photovoltaic applications.

Each chapter of this thesis will begin with a discussion of the background literature related to each field of study. A more detailed summary of the aims of each individual investigation is also provided at the beginning of each chapter.

## 1.6 – References

1. Faraday, M (1833). *Experimental Researches in Electricity, Volume 1*. London: Green Lion Press; (November 1, 2000).
2. Edward Chauncey Worden. Nitrocellulose industry. New York, Van Nostrand, 1911, p. 568. (Parkes, English patent #2359 in 1855)
3. D. D. Eley, *Nature*, 1948, **162**, 819
4. H. Akamatu, H Inokuchi, Y Matsunaga, *Nature*, 1954, **173**, 168.
5. H. Shirakawa, E.J. Louis, A.G. MacDiarmid, C.K. Chiang, A.J. Heeger, *J. Chem. Soc. Chem. Commun.*, 1977, **16**, 578.

6. Y. Yang, F. Wudl, *Adv. Mater.*, 2009, **21**, 1401
7. T. Imakubo, N. Tajima, M. Tamura, R. Kato, Y. Nishio, K. Kajita, *Synth. Met.*, 2003, **133-134**, 181
8. N. Tajima, A. Tajima, M. Tamura, Y. Nishio, K. Kajita, *Synth. Met.*, 2003, **133-134**, 147
9. A. G. Lebed, P. Bak, *Phys. Rev. Lett.*, 1989, **63**, 1315
10. S. Kimura, T. Maejima, H. Suzuki, R. Chiba, H. Mori, T. Kawamoto, T. Mori, H. Moriyama, Y. Nishio, K. Kajita, *Chem. Commun.*, 2004, 2454
11. H. Usta, A. Facchetti, T. J. Marks, *J. Am. Chem. Soc.*, 2008, **130**, 8580.
12. Y. Song, C. Di, X. Yang, S. Li, W. Xu, Y. Liu, L. Yang, Z. Shuai, D. Zhang, D. Zhu, *J. Am. Chem. Soc.*, 2006, **128**, 15140
13. Y. Sun, K. Xiao, Y. Liu, J. Wang, J. Pei, G. Yu, D. Zhu, *Adv. Func. Mat.*, 2005, **15**, 818
14. M. Mas-Torrent, M. Durkut, P. Hadley, X. Ribas, C. Rovira, *J. Am. Chem. Soc.*, 2004, **126**, 984
15. G. Gahungu, J. Zhang, T. Barancira, *J. Phys. Chem. A*, 2009, **113**, 255
16. D.J. Gundlach, Y.Y. Lin, T.N. Jackson, S.F. Nelson and D.G. Schlom. *IEEE Elec. Dev. Lett.*, 1997, **18**, 87.
17. H. Klauk, M. Halik, U. Zschieschang, G. Schmid, W. Radlik, W. Weber. *J. App. Phys.*, 2002, **92**, 5259.
18. O. D. Jurchescu, J. Baas, T. T. M. Palstra, *App. Phys. Lett.*, 2004, **84**, 3061
19. D. Braga, G. Horowitz, *Adv. Mat.*, 2009, **21**, 1473

20. K. Y. Chen, H. H. Hsieh, C. C. Wu, J. J. Hwang, T. J. Chow, *Chem. Commun.*, 2007, **10**, 1065.
21. H. Moon, R. Zeis, E-J. Borkent, C. Besnard, A.J. Lovinger, T. Siegrist, C. Kloc, Z. Bao., *J. Am. Chem. Soc.*, 2004, **126**, 15322.
22. C. Goldmann, S. Haas, C. Krellner, K. P. Pernitsch, D. J. Gundlach, B. Batlogg, *J. App. Phys.*, 2004, **96**, 2080
23. V. Podzorov, S.E. Sysoev, E. Loginova, V.M. Pudalov, M.E. Gersehenson. *Appl. Phys. Lett.* 2003, **83**, 3504.
24. A. K. Tripathi, M. Heinrich, T. Siegrist, J. Pflaum, *Adv. Mat.*, 2007, **19**, 2097
25. B.D. Chapman, A. Checco, R. Pindak, T. Siegrist, C. Kloc, *J. Cryst. Growth*, 2006, **290**, 479
26. J. M. Adams, S. Ramdas, *Acta Cryst. B*, 1879, **35**, 679
27. Q. Miao, M. Lefenfield, T.-Q. Nguyen, T. Siegrist, C. Kloc, C. Nuckolls, *Adv. Mat.*, 2005, **17**, 407
28. J. A. Merlo, C. R. Newman, C. P. Gerlach, T. W. Kelley, D. V. Muyres, S. E. Fritz, M. F. Toney, C. D. Frisbie, *J. Am. Chem. Soc.*, 2005, **127**, 3997
29. S. A. Odom, S. R. Parkin, J. E. Anthony, *Org. Lett.*, 2003, **5**, 4245
30. M. M. Payne, S. A. Odom, S. R. Parkin, J. E. Anthony, *Org. Lett.*, 2004, **6**, 3325
31. K. Takimiya, Y. Kunugi, Y. Konda, H. Ebata, Y. Toyoshima, T. Otsubo, *J. Am. Chem. Soc.*, 2006, **128**, 3044
32. J. Gao, R. Li, L. Li, Q. Meng, H. Jiang, H. Li, W. Hu, *Adv. Mater.*, 2007, **19**, 3008.

33. P. T. Boudreault, S. Wakim, N. Blouin, M. Simard, C. Tessier, Y. Tao, M. Leclerc, *J. Am. Chem. Soc.*, 2007, **129**, 9125
34. M. L. Tang, A. D. Reichardt, N. Miyaki, R. M. Stoltenberg, Z. Bao, *J. Am. Chem. Soc.*, 2008, **130**, 6064
35. A. M. Van de Craats, J. M. Warman, A. Fechtenkotter, J. D. Brand, M. A. Harbison, K. Mullen, *Adv. Mater.*, 1999, **11**, 1469
36. X. Gao, Y. Wang, X. Yang, Y. Liu, W. Qiu, W. Wu, H. Zhang, T. Qi, Y. Liu, K. Lu, C. Du, Z. Shuai, G. Yu, D. Zhu, *Adv. Mater.*, 2007, **19**, 3037
37. K. Itaka, M. Yamashiro, J. Yamaguchi, M. Haemori, S. Yaginuma, Y. Matsumoto, M. Kondo, H. Koinuma, *Adv. Mater.* 2006, **18**, 1713
38. S. Handa, Eigo Miyazaki, Kazuo Takimiya, and Yoshihito Kunug, *J. Am. Chem. Soc.*, 2007, **129**, 11684
39. S. Tatemichi, M. Ichikawa, T. Koyama, Y. Taniguchi, *App. Phys. Lett.*, 2006, **89**, 112108
40. M. M. Payne, S. R. Parkin, J. E. Anthony, C.-C. Kuo, T. N. Jackson, *J. Am. Chem. Soc.*, 2005, **127**, 4986
41. D. Natali, M. Sampietro, L. Franco, A. Bolognesi, C. Botta, *Thin Solid Films*, 2005, **472**, 238
42. C. Reese, Z. Bao, *J. Mater. Chem.*, **16**, 329-333, (2006)
43. J.-U. Park, M. Hardy, S. J. Kang, K. Barton, K. Adair, D. K. Mukhopadhyay, C. Y. Lee, M. S. Strano, A.G. Alleyne, J. G. Georgiadis, P. M. Ferraira, J. A. Rogers, *Nat. Mater.*, 2007, **6**, 782

44. I. O. Shklyarevskiy, P. Jonkheijm, N. Stutzmann, D. Wasserberg, H. J. Wondergem, P. C. M. Christianen, A. P. H. J. Schenning, D. M. de Leeuw, Z. Tomovic, J. Wu, K. Müllen, J. C. Maan, *J. Am. Chem. Soc.*, 2005, **127**, 16233
45. B. Hu, L. Yan, M. Shao, *Adv. Mater.*, 2009, **21**, 1500
46. Y. Yang, S.C. Chang, J. Bharathan, J. Liu, *J. Mater. Sci.: Mater. Electron.*, 2000, **11**, 89
47. H. Sirringhaus, T Kawase, R.H. Friend, T. Shimoda, M. Inbasekaran, W. Wu, E.P. Woo, *Science*, 2000, **290**, 2123
48. M. Belletete, N. Blouin, P. T. Boudreault, M. Leclerc, G. Durocher, *J. Phys. Chem. A*, 2006, **110**, 13696
49. H. Zhao, X. Tao, F. Wang, Y. Ren, X. Sun, J. Yang, Y. Yan, D. Zou, X. Zhao, M. Jiang, *Chem. Phys. Lett.*, 2007, **439**, 132
50. Y. Wu, Y. Li, S. Gardner, B. S. Ong, *J. Am. Chem. Soc.*, 2005, **127**, 614

## Chapter 2

# Experimental Techniques

Throughout the course of this investigation, a number of analytical techniques have been used to characterise the synthesised materials. Such techniques include Cyclic Voltammetry, UV/VIS Absorption Spectroscopy, Emission Studies, Computational Chemistry, Field-Effect Transistor measurements and for one species Spectroelectrochemistry. This chapter describes the equipment involved in the analyses throughout this study.

All electrochemical studies were carried out using a DELLGX110PC with General Purpose Electrochemical System (GPES), version 4.8 software, connected to an Autolab system containing a PGSTAT20 potentiostat. A three electrode configuration was used with a 0.5 mm Pt diameter working disc electrode, a Pt rod counter electrode and an Ag/AgCl (saturated KCl) reference electrode which was further referenced against ferrocenium/ferrocene which was measured at 0.55 V. Experiments were carried out in 0.1 M tetrabutyl ammonium tetrafluoroborate (TBABF<sub>4</sub>) in dry, degassed DMF as the electrolyte solution. Alternatively a 0.3 M

TBABF<sub>4</sub> electrolyte solution in dry, degassed DCM was used. In each case approximately 1 mmol of compound was used.

## 2.1 - Photochemistry

Photochemistry has long been used as a technique to investigate the electronic properties of molecular species. This study used both Absorption and Emission Spectroscopy techniques to investigate the energy levels of both the ground and excited electronic states.

UV/Vis Absorption Spectroscopy has been used to discover the energy between the S<sub>0</sub> ground state and the S<sub>1</sub> excited state of the newly synthesised systems, Fig. 2.1.

Emission studies investigated the various processes through which the absorbed photochemical energy is lost for each system, i.e. a comparison of the rate between fluorescence and the longer-lived phosphorescence.

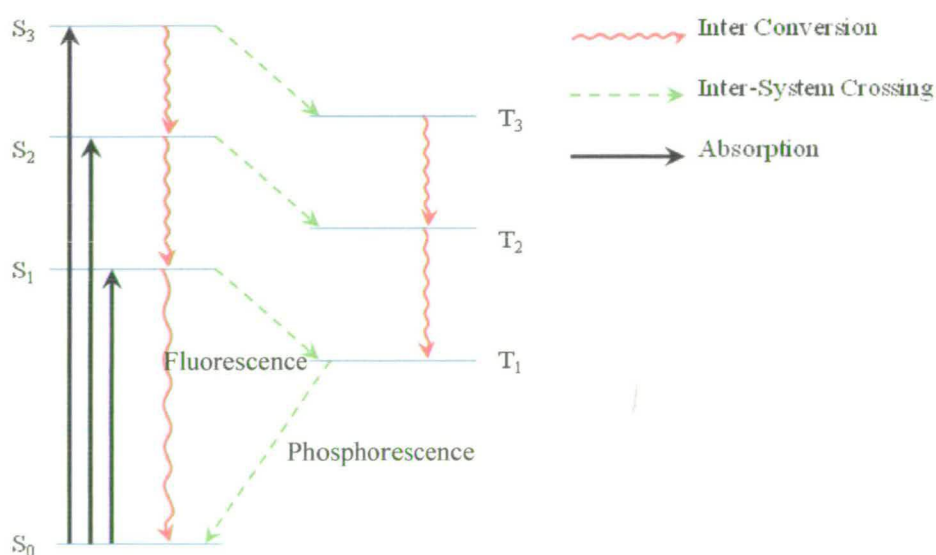


Figure 2.1 – Jablonski Diagram illustrating the various photochemical processes



---

All UV/VIS absorption spectra were recorded using a Perkin-Elmer Lambda 9 spectrophotometer connected to a PC using UV Winlab software. Emission studies were undertaken using a PC connected to a Horiba-Jobin-Yvon Fluoromax-P Spectrometer and measured using ISASCAN software. All samples were measured in a 1 cm<sup>3</sup> cell with ethanol as the solvent. Species studied at 77K were investigated through the formation of a frozen glass of the solution used for the 293K measurement

## 2.2 - Computational Methods

The increased availability of necessary software in combination with enhanced computing power has made theoretical calculations an increasingly relevant analytical tool in regard to chemical research. While computational calculations designed to accurately assess the charge mobility are still in the embryonic stages of development,<sup>1</sup> use of calculations to investigate the properties of frontier orbitals including orbital energies and orientation are increasingly accurate. Here Density Functional Theory (DFT) has been used to study the energy and geometry of frontier molecular orbitals, while time dependent DFT (TD-DFT) has been used to investigate the nature of the electronic transitions between frontier orbitals.

### *Geometry Optimisation Calculations*

Unless otherwise stated the geometry of each system was calculated with DMSO included in the system via a polarisable continuum model.<sup>2</sup> This was done after

previous optimisation of a gas phase system to more accurately reflect the observed data from solution-based experiments.

All calculations were carried out using the Gaussian 03 program<sup>3</sup> with the Becke three parameter hybrid exchange, Lee Yang-Parr correlation functional (B3LYP) level of theory.<sup>4</sup> All atoms were described by the 6-31G\* basis set<sup>5</sup> with the exception of the Ruthenium atom of compound 7 which was described via a Hay-Wadt VDZ (n + 1) ECP basis set.<sup>6</sup> All structures were input through Arguslab.<sup>7</sup> Molecular orbitals were generated with the cubegen function from Gaussian 03.

### ***Time Dependant DFT (TD-DFT)***

TD-DFT calculations have been carried out using a DMSO polarisable continuum model. In each case the number of singlet transitions calculated varied in order to provide a simulation as close as possible to the observed transitions. The simulated spectra were generated using the Gabedit 2.1.8 freeware program, using a full-width half-maximum value of 3300cm<sup>-1</sup>.<sup>8</sup>

## **2.3 - FET Measurements**

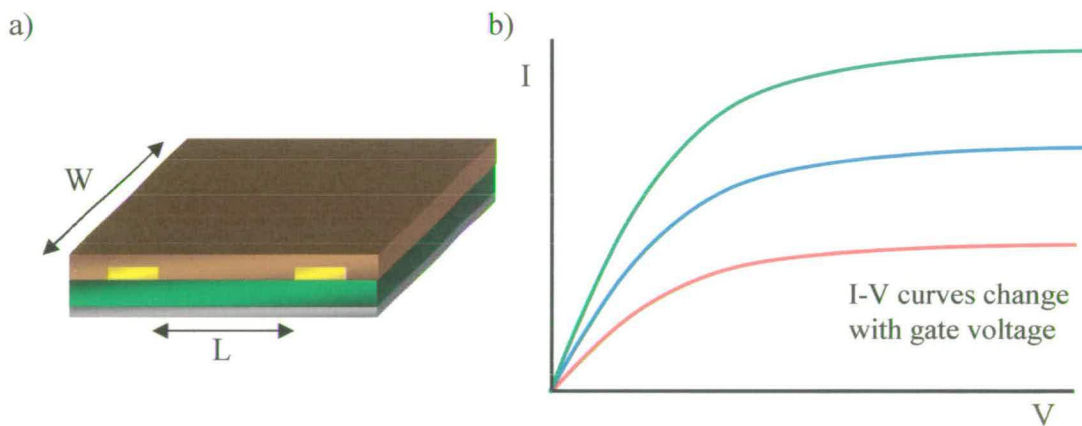
While numerous techniques exist to measure the intrinsic charge mobility of a species,<sup>9-17</sup> the most relevant is the use of field effect transistors. As the most common use of a semiconducting material is in a transistor, using a transistor to measure charge mobility, provides a measure of not just the charge mobility of a species but also the charge mobility of a species in a device-type environment.

---

Mobility is measured through calculation of the second differential of the I-V curve between the source and drain electrodes relative to the charge placed on the gate electrode. Equation 2.1 and Fig. 2.2.

$$\mu = \frac{\partial^2 I_{sd}}{\partial V_{sd} \partial V_g} \frac{L}{CW}$$

**Equation 2.1** – Measure of mobility in thin-film FET where  $L$  = path length,  $W$  = width and  $C$  = capacitance per unit area of the dielectrode material.



**Figure 2.2** – a) FET device as used in the measurement of charge mobility  
b) Typical series of I-V curves based on an organic semiconductor.

Devices were fabricated on pre-patterned substrate with a  $10\mu\text{m}$  channel between gold source and drain electrodes with a  $300\mu\text{m}$   $\text{SiO}_2$  dielectric.

Before deposition of the organic semiconductor substrates were washed with ethanol, deionised water, acetone and isopropyl alcohol then dried under nitrogen. The low

melting point of the species under investigation meant that they were melt coated on to the substrates at 110°C and left for 12 hours before being allowed to cool.

The I-V curves were measured using a Micromanipulator four-probe station connected to a Hewlett-Packard 4156B semiconductor parameter analyser.

## **2.4 - Spectroelectrochemistry**

Spectroelectrochemistry is a technique that allows analysis of electrogenerated species through a combination of cyclic voltammetry and spectroscopy. In this study 7 has been investigated using the Optically Transparent Thin Layer Electrode (OTTLE) technique, which combines electrochemistry with UV/VIS/n-IR spectroscopy. By observing the UV/VIS/n-IR spectrum over the course of a reversible, bulk coulombetry experiment, changes such as absorption band position and intensity may be used to characterize the generated species and hence information can be gained in regard to the frontier molecular orbitals.

The study was carried out in a 0.5 mm thick quartz cell using a 0.1 M TBABF<sub>4</sub>/DMF electrolyte solution. A three electrode system was established with a Pt/Rh gauze working electrode, a Pt wire counter electrode and a Ag/AgCl reference electrode. A Perkin-Elmer Lamda 9 spectrophotometer, connected to a PC with UV Winlab software was used to record the data. The measurement was done at 253 K.

---

## 2.5 – References

1. A Troisi, *Adv. Mater.*, 2007, **19**, 2000
2. B. Menucci, J. Tomasi, *J. Phys. Chem. A*, 2002, **106**, 6102
3. Gaussian 03, Revision C.02, M. J. Frisch, G. W. Trucks, H. B. Schlegel, G. E. B3LYP Scuseria, M. A. Robb, J. R. Cheeseman, J. A. Montgomery, Jr., T. Vreven, K. N. Kudin, J. C. Burant, J. M. Millam, S. S. Iyengar, J. Tomasi, V. Barone, B. Mennucci, M. Cossi, G. Scalmani, N. Rega, G. A. Petersson, H. Nakatsuji, M. Hada, M. Ehara, K. Toyota, R. Fukuda, J. Hasegawa, M. Ishida, T. Nakajima, Y. Honda, O. Kitao, H. Nakai, M. Klene, X. Li, J. E. Knox, H. P. Hratchian, J. B. Cross, V. Bakken, C. Adamo, J. Jaramillo, R. Gomperts, R. E. Stratmann, O. Yazyev, A. J. Austin, R. Cammi, C. Pomelli, J. W. Ochterski, P. Y. Ayala, K. Morokuma, G. A. Voth, P. Salvador, J. J. Dannenberg, V. G. Zakrzewski, S. Dapprich, A. D. Daniels, M. C. Strain, O. Farkas, D. K. Malick, A. D. Rabuck, K. Raghavachari, J. B. Foresman, J. V. Ortiz, Q. Cui, A. G. Baboul, S. Clifford, J. Cioslowski, B. B. Stefanov, G. Liu, A. Liashenko, P. Piskorz, I. Komaromi, R. L. Martin, D. J. Fox, T. Keith, M. A. Al-Laham, C. Y. Peng, A. Nanayakkara, M. Challacombe, P. M. W. Gill, B. Johnson, W. Chen, M. W. Wong, C. Gonzalez, J. A. Pople, Gaussian, Inc. Wallingford CT, 2004.
4. A.D. Becke, *J.Chem.Phys.*, 1993, **98**, 5648
5. C. Lee, W. Yang, R.G. Parr, *Phys. Rev. B*, 1988, **37**, 785
6. P.J. Hay, W.R. Wadt, *J. Chem. Phys.*, 1985, **82**, 299-310.
7. Arguslab 4.0, M.A. Thompson, Planaria Software LLC, Seattle,  
<http://www.arguslab.com>.

8. Gabedit 2.1.8, A. R. Allouche, <http://gabedit.sourceforge.net>
9. R.G. Kepler, *Phys. Rev.*, 1960, **119**, 1226.
10. J. Mort, G. Pfister (Eds.), *Electronic Properties of Polymers*, Wiley, New York, 1982, pp. 215–265.
11. J.B. Arthur, W. Bardsley, M.A.C.S. Brown, A.F. Gibson, *Proc. Phys. Soc.*, 1955, **68B**, 43.
12. G.H. Gelnick, J.M. Warman, *J. Phys. Chem.*, 1996, **100**, 20035.
13. M. Pope, C.E. Swenberg, *Electronic Processes in Organic Crystals and Polymers*, Oxford University Press, New York, 1999.
14. W. Brutting, P.H. Nguyen, W. Riess, G. Paasch, *Phys. Rev.*, 1995, **B51**, 9533.
15. G. Horowitz, R. Hajlaoui, H. Bouchriha, R. Bourguiga, M. Hajlaoui, *Adv. Mater.*, 1998, **10**, 923.
16. G. Horowitz, R. Hajlaoui, D. Fichou, A. El Kassmi, *J. Appl. Phys.*, 1999, **85**, 3202.
17. N. Karl, K.-H. Kraft, J. Marktanner, *Synth. Met.*, 2000, **109**, 181.

## **Chapter 3**

# **2,3-Diindoles and Indolo[3,2-a] carbazoles**

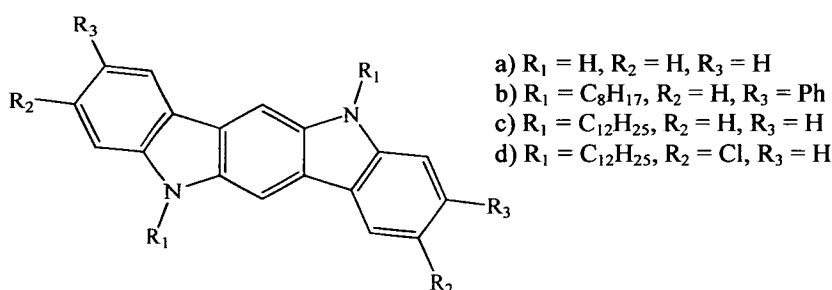
### **3.1 – Introduction**

As noted in Chapter 1, in order for devices based on organic semiconductors to be effective, the organic electronic materials involved must have a high charge mobility.

While a number of systems fulfil this basic criterion, the most successful materials remain the acene series of systems, most notably pentacene <sup>1</sup> and rubrene <sup>2</sup> with single crystal charge mobility values up to 35 cm<sup>2</sup>/Vs and 43 cm<sup>2</sup>/Vs respectively. However, there are a number of problems preventing the widespread use of acenes for semiconductor applications; expense, stability and processibility.

In order to counter these problems two differing techniques are being investigated, the first involves the adaptation of acene-based materials to improve stability and processibility.<sup>3</sup> The second, broader field involves the investigation of alternative materials with similar electronic characteristics but with improved stability and processibility, and ideally, lower cost.<sup>4,5</sup>

The drive for alternative organic semiconductors has recently led to the study of indole-based materials.<sup>6,7,8</sup> Of these indole systems, the most widely studied are the indolo[3,2-b]-carbazoles, Fig. 3.1a. First synthesised in 1963<sup>9</sup> indolo[3,2-b]carbazoles have been seen widely in nature,<sup>10,11</sup> and both the material properties and reactions have been investigated.<sup>12</sup>



**Figure 3.1** – Indolo[3,2-b]carbazole unit

The material properties of the carbazole unit, including both electronic properties and stability, make the indolo[3,2-b]carbazoles an ideal target for organic semiconductor research. This research has taken the form of both small molecule,<sup>13</sup> and polymer

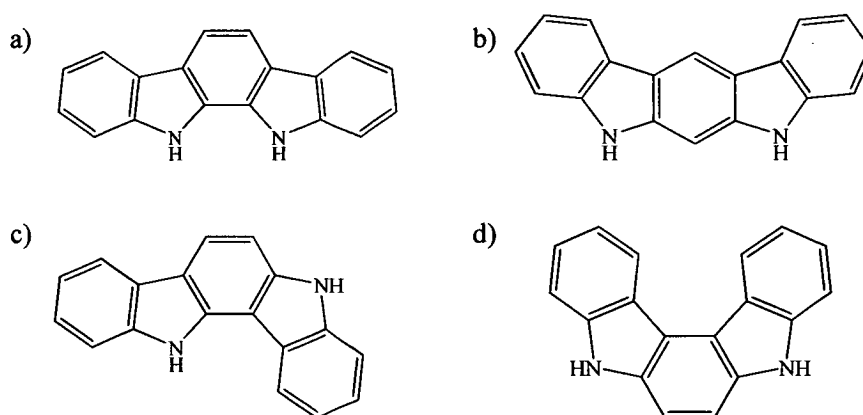


systems<sup>14,15</sup> with a maximum charge mobility of 0.2 cm<sup>2</sup>/Vs found for 3,9-diphenyl-5,11dioctylindolo[3,2-b]carbazole, Fig 3.1b.

The indolo[3,2-b]carbazoles have a number of advantages over the acenes, the most important being processibility. Due to the stability of the materials in air, processing becomes much more cost-effective. The potential to replace the N-H groups with alkyl chains increases the solubility of the systems giving the possibility of solution processing.<sup>16</sup>

The ease with which N-H groups may be changed to N-alkyl groups can also be seen with the addition of other functional groups at other positions within the systems.<sup>17</sup> The potential for functional group switching offers the possibility of tailoring the properties of a material to the requirements of individual applications. The effect of functionalisation can be seen through the removal of the phenyl groups from 3,9-diphenyl-5,11dioctylindolo[3,2-b]carbazole. Assessment of the electronic properties of 5,11-didodecylindolo[3,2-b]carbazole, Fig. 3.1c, has found an electron mobility of 1.2x10<sup>-4</sup> cm<sup>2</sup>/Vs.<sup>18</sup> The same group also reports some unusual electronic properties for indolo[3,2-b]carbazoles. In Chapter 1.3 it was noted that addition of a halo-group to tetracene resulted in a 10000-fold reduction in mobility.<sup>19</sup> This is attributed to the electron-withdrawing effects of the chloro-group, hindering transfer of holes between molecules. The addition of chloro-groups to the 2 and 8 positions to form 2,8-dichloro-

5,11-didodecylindolo[3,2-*b*]carbazole, Fig 3.1d, leads to a mobility of  $0.14 \text{ cm}^2/\text{Vs}$ . Though the possibility of a packing structure change exists in this case, which may also play a considerable role in the mobility improvement, this is not the case in the analogous 3,9-dichloro-5,11-didodecylindolo[3,2-*b*]carbazole. Here an improvement to  $0.01 \text{ cm}^2/\text{Vs}$  is observed, while not of the same order, this is still a remarkable and possibly unexpected improvement. The unusual electronic properties of the indolo[3,2-*b*]carbazoles suggest that further study of indole-based systems may prove fruitful. In particular it is surprising that no previous studies have been carried out on the related indolocarbazole species. Fig 3.2.



**Figure 3.2** – a) Indolo[2,3-*a*]carbazole, b) indolo[2,3-*b*]carbazole, c) indolo[2,3-*c*]carbazole, d) indolo[3,2-*a*]carbazole

Until recently, most research into indole-based materials had been undertaken in the context of the biological systems in which indole-based materials have been found to play a role.<sup>20,21</sup> As a result much of the indole chemistry known is grounded primarily in biological applications.<sup>22,23</sup> Consequently a number of indole systems remain largely

unexplored in a materials chemistry context; this includes a number of highly conjugated indole-based systems, including alternative indolocarbazole systems. This chapter focuses on two systems, Fig 3.3, the 2,3-diindoles and indolo[3,2-a]carbazoles.

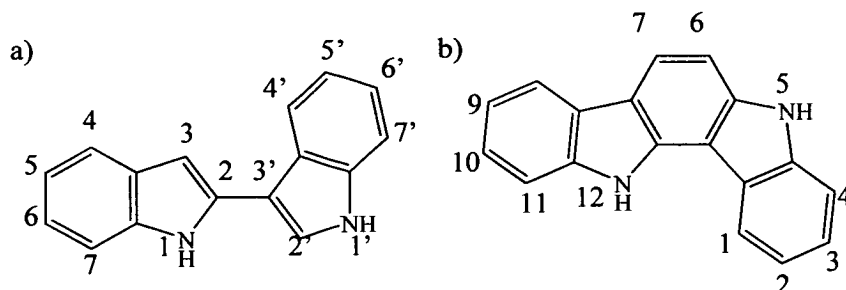
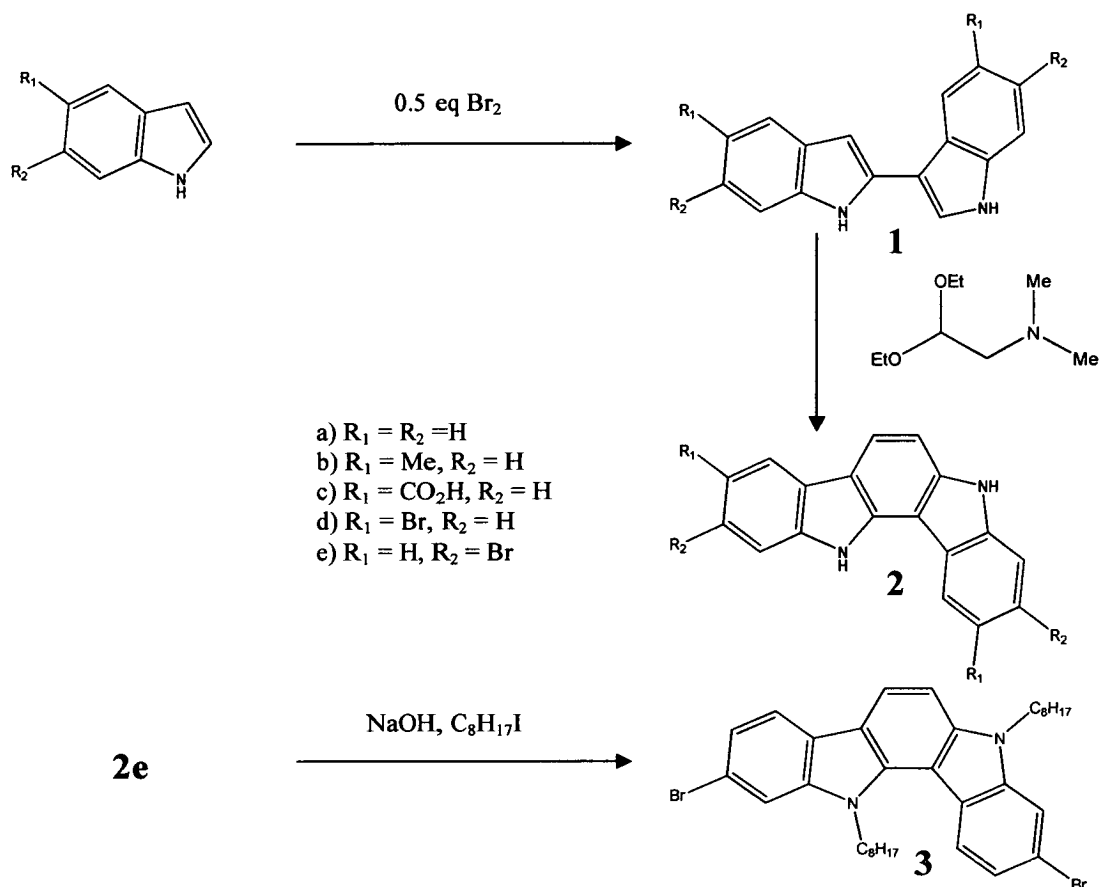


Figure 3.3 – a) 2,3-Diindole and b) Indolo[3,2-a]carbazole

While both of these systems have been synthesised previously, the electronic properties of the systems have not been thoroughly studied. The area of substituted 2,3-diindoles and indolo[3,2-a]carbazoles has also remained largely unexplored.<sup>24</sup> This chapter reports the adaptation and improvement of known syntheses to produce a wide range of conjugated indole-based systems. Cyclic voltammetry, absorption and emission spectroscopy, DFT calculations and FET measurements have been utilised in the characterisation of the material properties of these systems in order to assess the potential of these systems for organic electronic applications.

## 3.2 – Synthesis

Species **1a-e**, **2a-e** and **3** were prepared by the synthetic route summarized in scheme 3.1. The route has been adapted from known syntheses of compounds **1a**, <sup>7</sup> **2a**, <sup>25</sup> and a known route to alkylated indole species. <sup>26</sup> The synthesis has led to two novel families of compounds, the 2,3-diindoles, **1a-e**, and indolo[3,2-a]carbazoles, **2a-e**, and **3**.



Scheme 3.1 - Synthetic route to 2,3-diindoles, **1a-e**, and indolo[3,2-a]carbazoles **2a-e** and **3**.

## 2,3-Diindoles

Synthesis of **1a** has been achieved via a number of synthetic routes,<sup>27,28,29</sup> however none of the syntheses have resulted in pure **1a** and been only one-step. Robertson et al have successfully synthesised 2,3-diindole through the addition of 0.5 equivalents of Br<sub>2</sub> in acetonitrile solution, though this results in a precipitate of **1a**.4/3HBr.<sup>7</sup> In this work the reaction of Br<sub>2</sub> with an acetonitrile solution of 5-methylindole and indole-5-carboxylic acid gives **1b**.4/3HBr and **1c**.4/3HBr respectively.

Attempts to extend this reaction to cyano-, nitro-, amino- and carboxaldehyde 5-substituted indoles gave crude mixtures containing no 2,3-diindole product. In the cases of the cyano and carboxaldehyde systems this is due to competing reactions of Br<sub>2</sub> with the substituent. The nitro and amino cases are discussed further in Section 3.2.

When acetic acid was used as an alternative solvent the reaction gave a yield comparable to that of the acetonitrile reaction. The use of acetic acid allowed the synthesis of **1d** and **1e**, previously prevented for reasons of solubility. Both systems precipitated with 4/3HBr, however sonication in H<sub>2</sub>O removed HBr from the material in each case, turning it from yellow, as with **1a-c**, to off-white. The attempt to remove HBr by the same route was unsuccessful for other 2,3 diindoles.

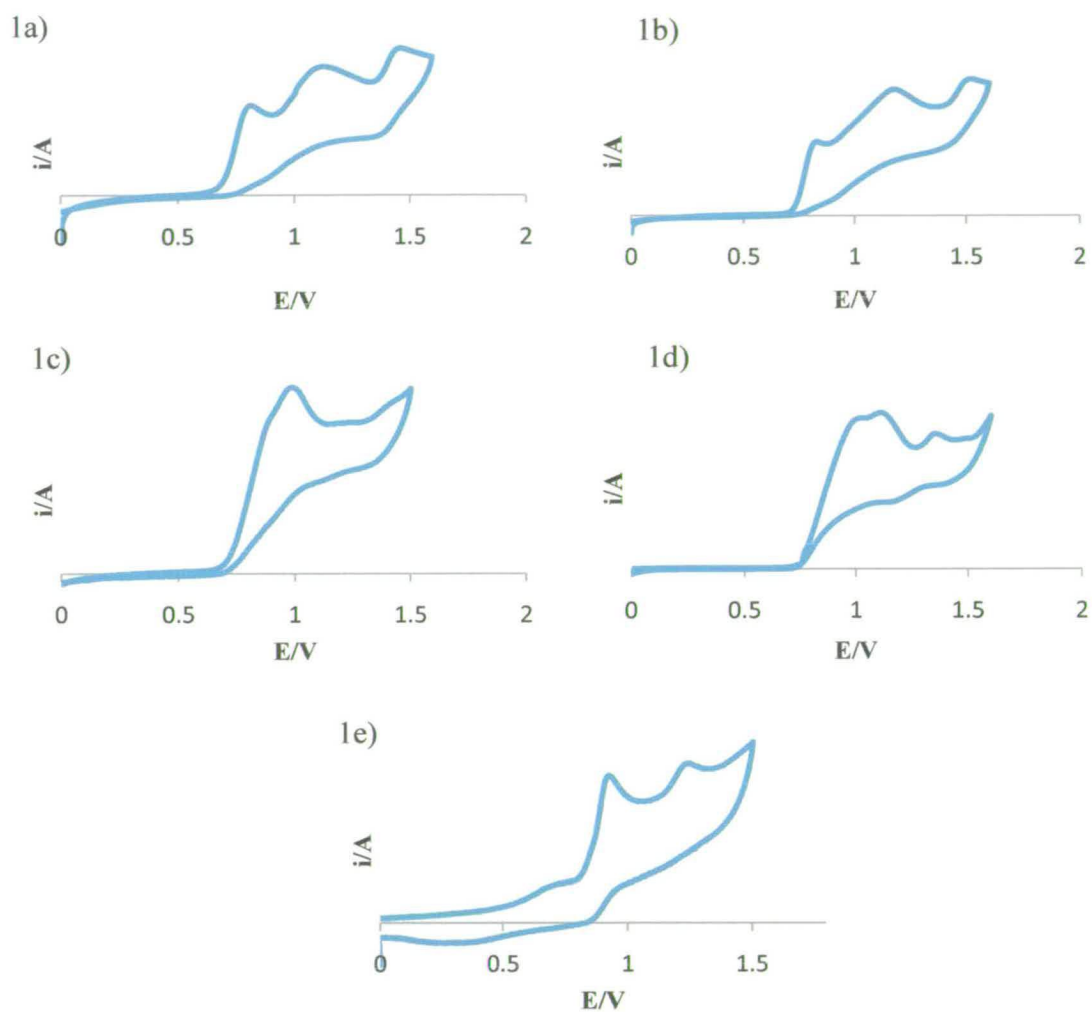
### ***Indolo[3,2-a]carbazoles***

(Dimethylamino)acetaldehyde diethyl acetal has been used in a number of syntheses to form indolocarbazoles, most notably indolo[2,3-a]carbazoles<sup>30,31,32</sup> however, Bergman et al have also reported its use in the synthesis of 5,12-dihydroindolo[3,2-c]carbazole **2a**.<sup>33</sup> These syntheses involve the slow addition of (dimethylamino)acetaldehyde diethyl acetal to a solution of the indole dimer in acetic acid followed by heating at reflux for between 2 and 24 hours depending on the indole species. A 91% yield has been reported for this reaction however, when this reaction was attempted using **1a** formed via the Robertson synthesis this yield dropped to 15% pure product. After the attempted synthesis and purification it was noticeable that much of the removed material was dark green. A dark green colour has been previously noted for a number of partially oxidized indolocarbazole species.<sup>34</sup> While the purified solid **2a** remained stable in air, this was not the case in solution. To reduce the amount of time in solution the reaction was carried out in a microwave reactor. Due to the nature of the microwave heating, solvents can be heated much more effectively and super-heated beyond the normal boiling point. This has been found to drastically increase the rate of reaction and in many cases the reaction efficiency. When the microwave synthesis of **2a** was attempted, the yield of pure product increased to 48%. The microwave reactor was subsequently used in the successful synthesis of indolo[3,2-a]carbazole species **2b-2e**, however **2b** was found to be unstable in air and readily oxidised, all other syntheses progressed as expected. The synthesis of **3** was carried out from **2e** through known synthetic methodology.<sup>29</sup>

## 3.3 – Electrochemistry

### *2,3-Diindoles*

The electrochemical oxidation of indole species **1a-e** gives the series of oxidation potentials seen in Fig. 3.4 and Table 3.1. Systems **1a**, **1b** and **1d**, clearly display three oxidation peaks, each irreversible, the position of the first ranging from 0.80 V for **1b** to 1.01 V for **1d**. Each of these peaks is caused by a single electron process, for **1a** and **1b** each process results in the same change in current, while in the case of **1d** the first oxidation peak appears as a shoulder to the second at 1.10V. This leads to a combined peak height which is approximately twice the size of the third peak at 1.32V. Close inspection of **1c** suggests that this merging of first and second oxidation peaks has been completed resulting in a single peak equivalent to a two electron process. That this is a two electron process may be judged from the height of the third oxidation peak beginning to appear at 1.4V, the maximum of which is unfortunately masked by the onset of solvent oxidation.



**Figure 3.4** – Cyclic Voltammograms of the oxidation of species **1a-e** against Ag/AgCl reference in 0.1MTBAPF<sub>4</sub>/DMF

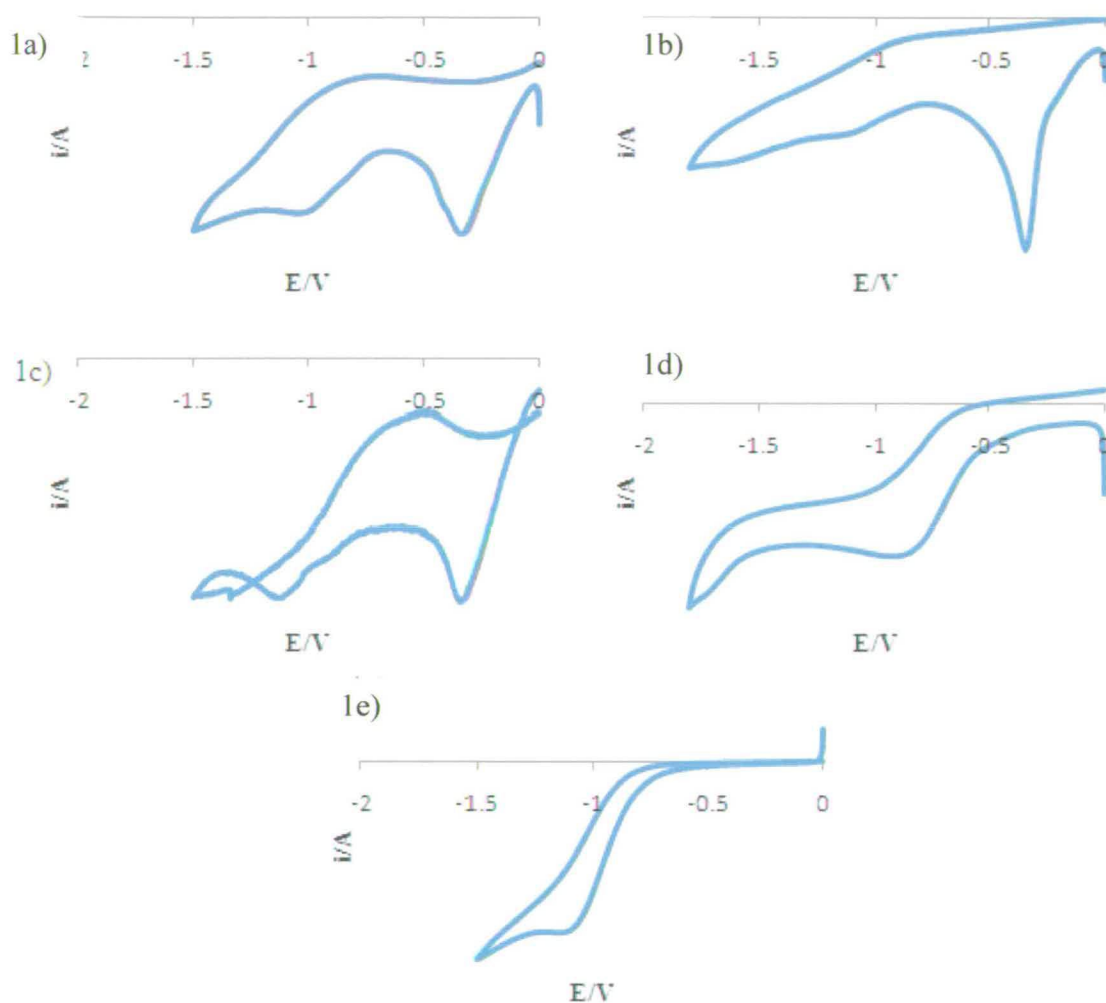
|           | Oxidation |      |      | Reduction |       |
|-----------|-----------|------|------|-----------|-------|
|           | E/V       | E/V  | E/V  | E/V       | E/V   |
| <b>1a</b> | 0.83      | 1.17 | 1.50 | -0.33     | -1.04 |
| <b>1b</b> | 0.80      | 1.08 | 1.43 | -0.32     | -1.01 |
| <b>1c</b> | 0.99      |      |      | -0.31     | -1.12 |
| <b>1d</b> | 1.01      | 1.10 | 1.32 |           | -0.96 |
| <b>1e</b> | 0.92      | 1.23 |      |           | -1.07 |

**Table 3.1** – Redox Potentials of species **1a-e** against Ag/AgCl reference



Investigations undertaken by John Henry of the University of Edinburgh into this series of 5-substituted indole 2,3 dimers led to the conclusion that the electrochemical oxidation profiles seen here are the result of the formation of indole tetramers.<sup>35</sup> This is similar to the electrochemical oxidation of indole monomers, which as stated previously results in the formation of cyclic, asymmetric indole trimers.<sup>36,37</sup>

Species **1a-c** each have a reduction peak between -0.3V and -0.4V, fig 3.5, table 3.1. This is due to the reduction of H<sup>+</sup> from the HBr also present from the product and gradually disappears over the course of electrochemical investigation. This is confirmed by its non-appearance in **1d** and **1e** where the HBr was successfully removed prior to analysis. The reduction peak at around -1V appears for all 2,3-diindole systems suggesting that it is entirely diindole based rather than due to any substituent.



**Figure 3.5** – Cyclic Voltammograms of the reduction of species 1a-e against Ag/AgCl reference in 0.1MTBABF<sub>4</sub>/DMF

### *Indolo[3,2-a]carbazoles*

Oxidation of each of the indolo[3,2-a]carbazole species, Fig 3.6, Table 3.2, results in a single oxidation peak, which for the 2,9-disubstituted species appears between 0.98 V and 1.27 V in the order **2b** < **2a** < **2d** < **2c**.

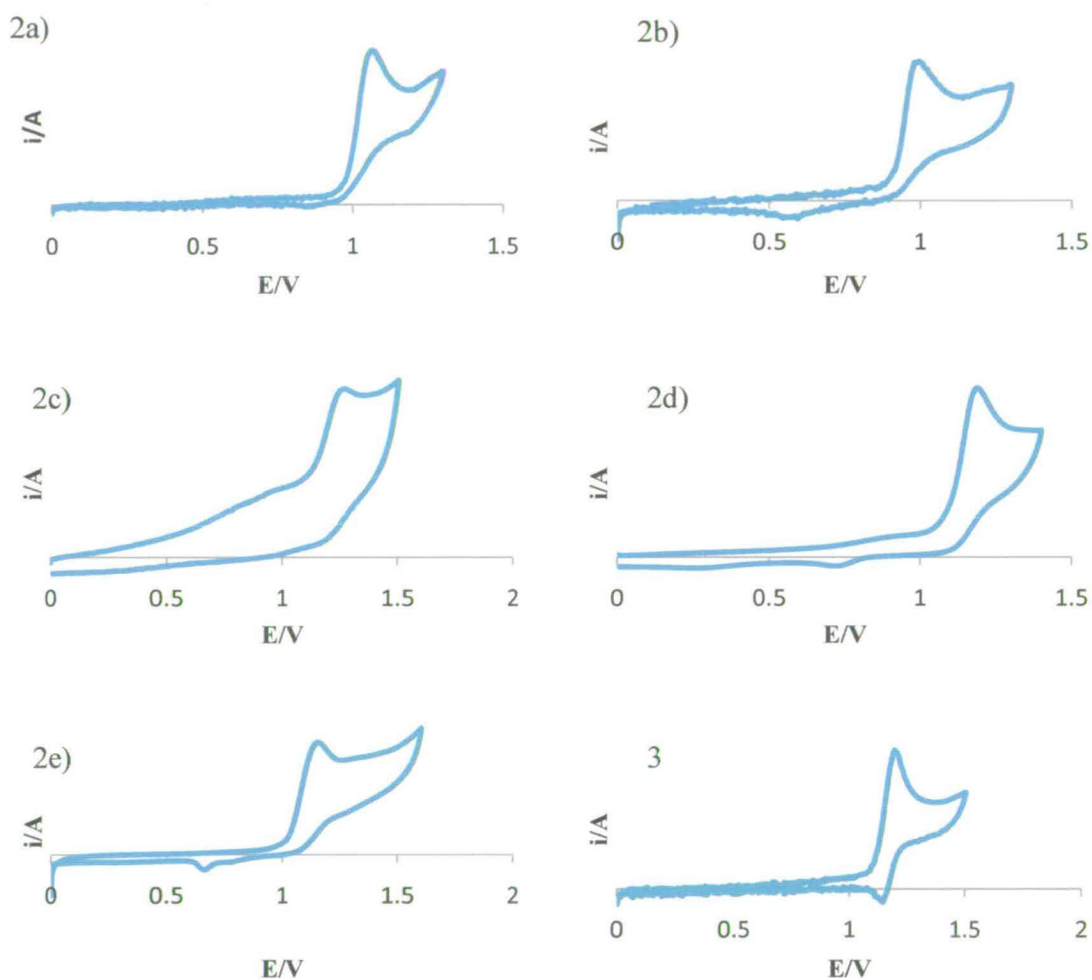
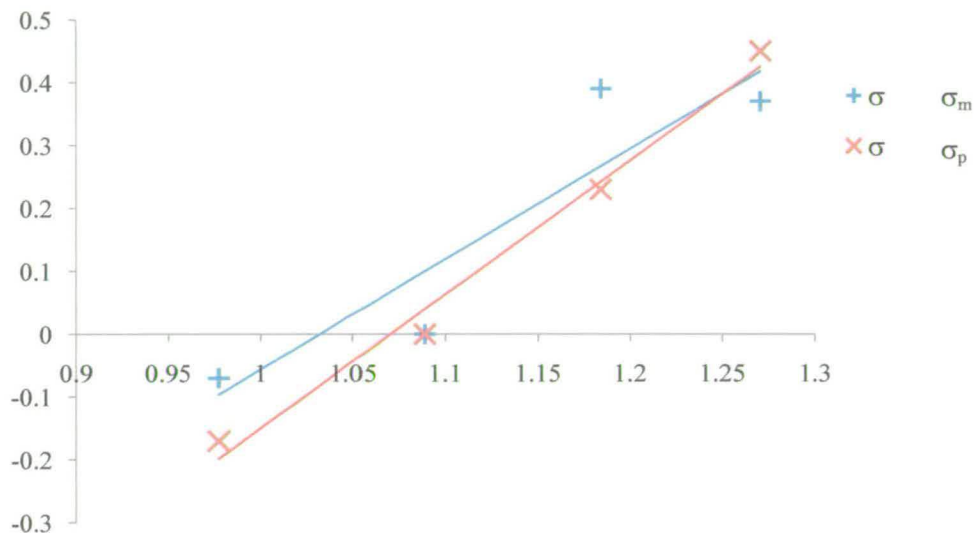


Figure 3.6 – Cyclic Voltammograms of the oxidation of species 2a-e and 3 against Ag/AgCl reference in 0.1MTBABF<sub>4</sub>/DMF

|    | Oxidation | Reduction |
|----|-----------|-----------|
| 2a | 1.09      | -         |
| 2b | 0.98      | -         |
| 2c | 1.27      | -1.02     |
| 2d | 1.18      | -1.01     |
| 2e | 1.18      | -0.87     |
| 3  | 1.17      | -0.87     |

Table 3.2 – Redox Potentials of species 2a-e and 3 against Ag/AgCl reference

When analysed in regard to the meta and para Hammett parameters,  $\sigma_m$  and  $\sigma_p$  respectively, Fig 3.7, it is clear that the oxidations most clearly follow  $\sigma_p$ .

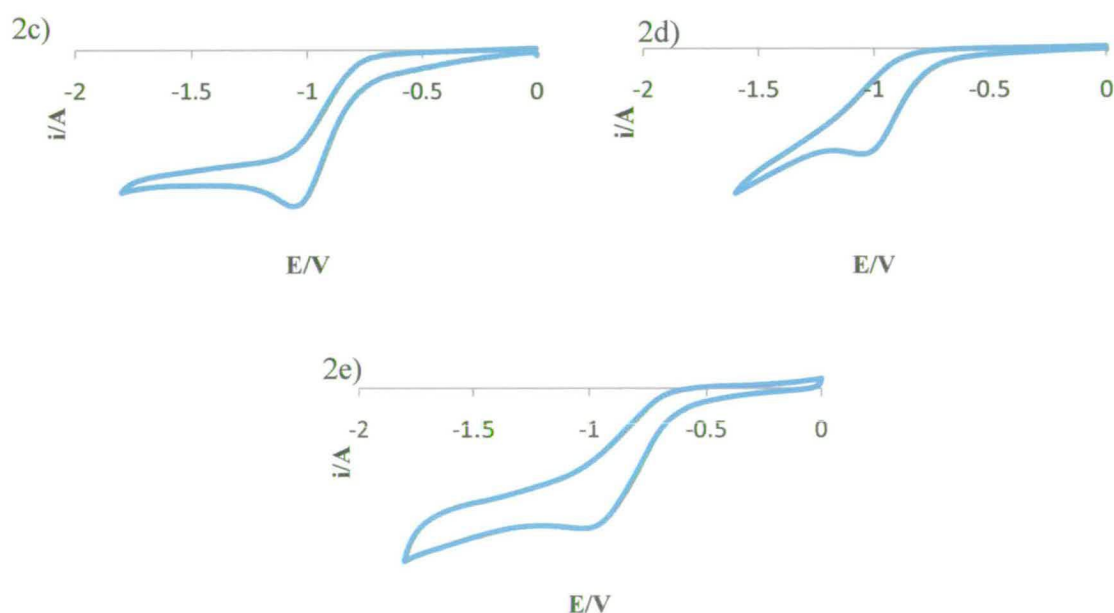


**Figure 3.7** – Plot of Oxidation potential vs. Hammett Parameters  $\sigma_m$  and  $\sigma_p$  for 2a-d

The Hammett parameter relates to the equilibrium constant for reactions involving substituted benzoic acids. In systems such as indole, where the positions both meta and para to the substituent are bonded to another group it provides an effective assessment of which group is responsible for the electronic character of the system. The graph seen in fig 3.7 makes it clear that the N-H group of the indoles is the dominant sub-unit of this species. This is discussed further in Section 3.6.

Another point of note is that for compounds **2a-e**, the first oxidation is irreversible, while for **3** it becomes quasi-reversible. This is in agreement with the work by Ambrose et al,<sup>38</sup> who found that carbazole based materials display irreversible oxidations due to N-N cation coupling in the oxidized species. In the case of **3**, with the indole N blocked through alkylation, N-N interaction becomes much more difficult, hence the oxidation becomes more reversible.

In contrast to the dimer species, only three of the indolo[3,2-a]carbazoles undergo a reduction, **2c**, **2d** and **2e**. Fig 3.8 and table 3.2. This strongly suggests that any observed reduction is substituent based.



**Figure 3.8** – Cyclic Voltammograms of the reduction of species **2c-e** against Ag/AgCl reference in 0.1M TBABF<sub>4</sub>/DMF

### 3.4 – UV/Vis Spectroscopy

#### Indole 2,3 dimers

The UV/Vis spectroscopy for compounds **1a-e**, fig 3.9 and table 3.3, suggests that with the exception of **1c**, each system displays one very broad absorption peak. The nature of the absorbance for species **1c** is explained in Section 3.6. For the rest of the 5-substituted 2,3-diindoles, **1a**, **1b** and **1d**, the energy of the absorption maximum decreases in the order **1a** > **1b** > **1d**. This is due to the extension of the  $\pi$ -system across additional substituents.

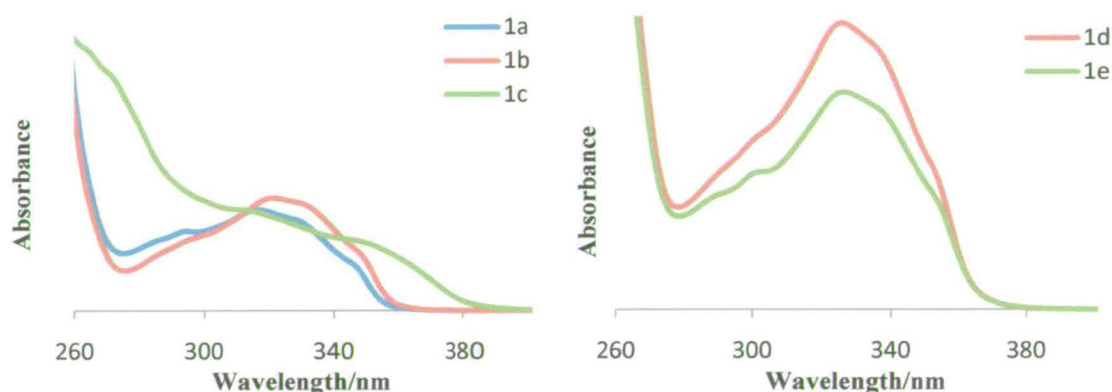


Figure 3.9 – Absorption Spectra for species **1a-e** in DMF

|           | Peak (nm) $\epsilon$ ( $M^{-1}cm^{-1}$ ) |       |
|-----------|--|-------|
| <b>1a</b> | 317                                      | 14700 |
| <b>1b</b> | 321                                      | 18500 |
| <b>1c</b> | 311                                      | 11900 |
| <b>1d</b> | 326                                      | 23700 |
| <b>1e</b> | 326                                      | 29700 |

Table 3.3 – Absorption Peaks and extinction coefficients for species **1a-e** in DMF

**Indolo[3,2-*a*]carbazoles**

The absorption spectra for **2a-e** and **3**, fig 3.10, table 3.4, suggest a much more complicated spectrum than for the equivalent 2,3-diindole species, **1a-e**. Though there is an overlap of peaks in some cases, the pattern of absorptions indicates that the carbazole species have 6 significant transitions around 270nm, 290-300nm, 315nm, 330nm, 345nm and 365nm. Comparison of the 5-substituted indolo[3,2-*a*]carbazoles **2a-2d** for the peaks at 290nm, 345nm and 365nm i.e. the cases in which peaks are clearly visible for all species, shows that the absorbances decrease in energy in the order, **2a** > **2c** > **2b** > **2d**. It is clear from the relationship between the observed spectra that the presence of substituent groups has little effect on the nature of the transition. This implies that the HOMO levels from which the transitions occur vary very little between indolo[3,2-*a*]carbazoles, suggesting the indolocarbazole framework plays the most significant role in the frontier molecular orbitals, which themselves might be expected to have very little substituent-based character. This is discussed further in Section 3.6.

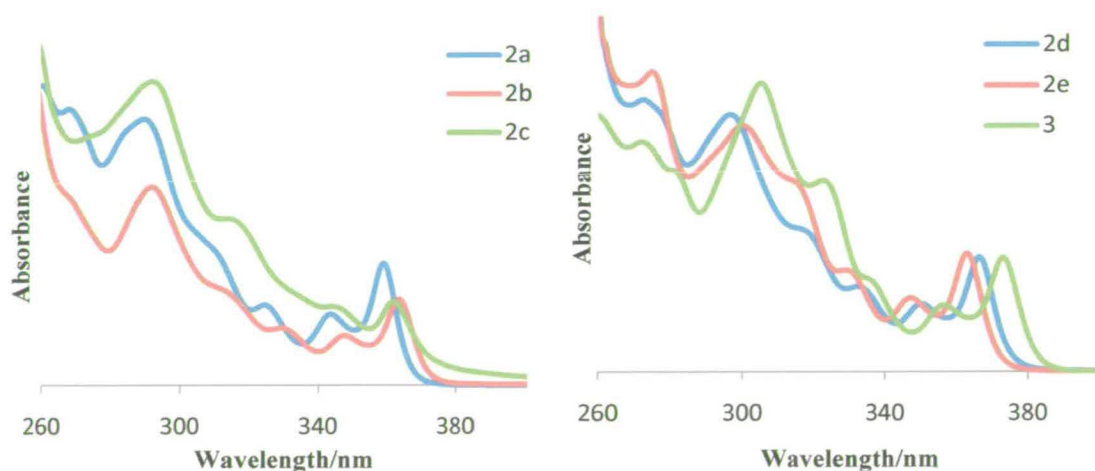


Figure 3.10 – Absorption Spectra for species **2a-e** and **3** in DCM

|           | Peak/nm ( $\epsilon/ M^{-1}cm^{-1} \times 10^3$ ) |            |            |            |            |            |
|-----------|---|------------|------------|------------|------------|------------|
| <b>2a</b> | 268 (55.8)  | 289 (61.6) |            | 324 (18.5) | 344 (16.6) | 359 (33.2) |
| <b>2b</b> |   | 293 (28.2) |            | 329 (9.3)  | 348 (8.2)  | 364 (14.3) |
| <b>2c</b> |   | 292 (45.1) | 314 (23.3) |            | 346 (11.0) | 362 (11.6) |
| <b>2d</b> | 272 (47.7)  | 297 (45.2) | 316 (25.2) | 332 (15.0) | 350 (11.9) | 366 (20.1) |
| <b>2e</b> | 275 (45.3)  | 300 (45.2) | 313 (35.5) | 329 (18.6) | 347 (13.4) | 363 (21.7) |
| <b>3</b>  | 272 (46.6)  | 305 (57.3) | 323 (37.3) | 334 (17.4) | 356 (13.0) | 373 (21.5) |

**Table 3.4** – Absorption Peaks and extinction coefficients for species **2a-e** and **3** in DCM

Investigations between the bromo-based indolo[3,2-a]carbazoles **2d**, **2e** and **3** provide a number of intriguing results. The energy of the transitions for **2d** and **2e** varies in regard to the order. The transitions around 275nm and 300nm are lower energy for **2e**, while those at 315nm, 325nm, 345nm and 365nm are lower energy for **2d**. This implies that significant proportions of the frontier molecular orbitals reside on either the 2 and 9 or the 3 and 10 positions so the substituents play an indirect role in the nature of the transitions. The precise origins of the transitions will be discussed more thoroughly in Sections 3.6 and 3.7.

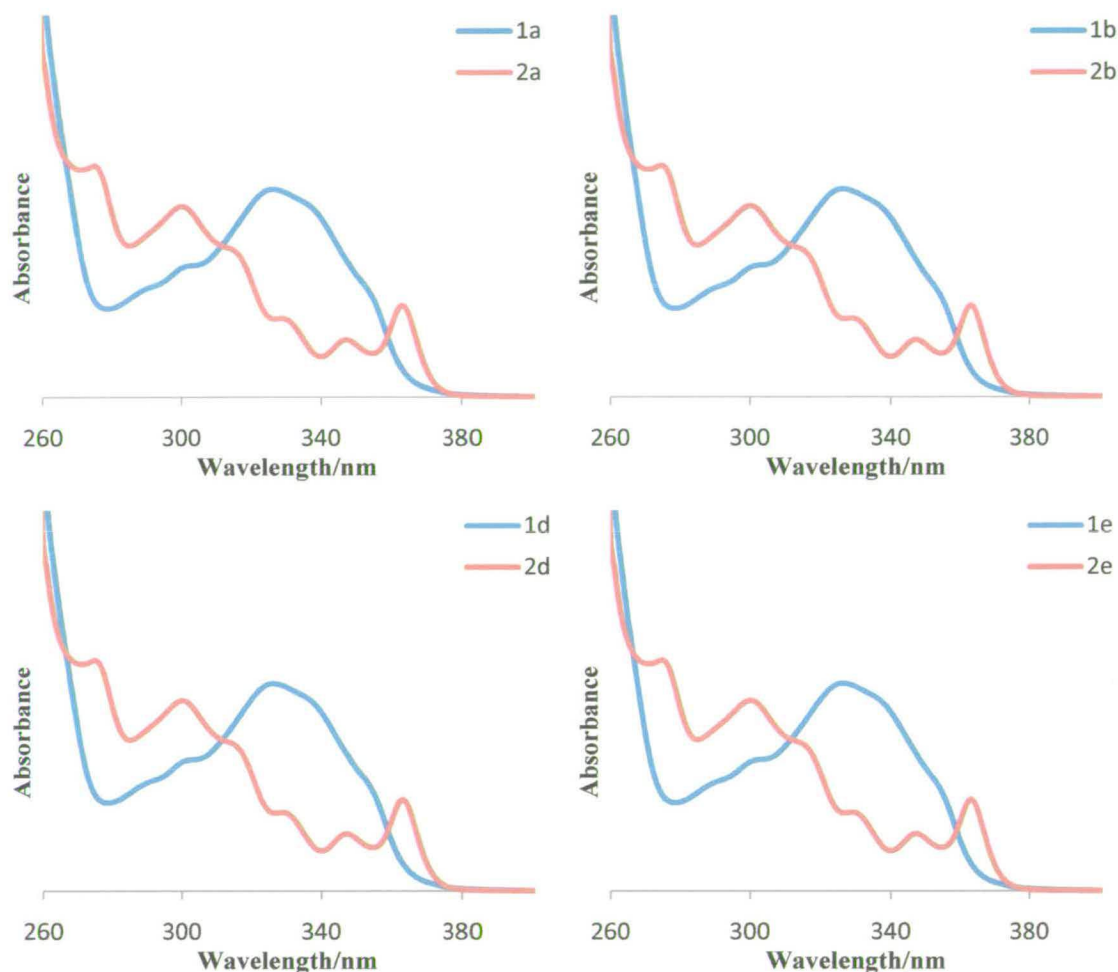
As suggested in regard to 2, 3-diindoles, minor differences in the peak positions are due to minor differences in the level of conjugation caused by various substituents of the indole-based  $\pi$ -system. This has been confirmed through studying the differences in the spectra of **2e** and its alkylated equivalent **3**. The decrease in the energy of absorptions



for **3**, by as much as  $740\text{ cm}^{-1}$  in the case of the lowest energy transition, is due to the inductive effect of the alkyl chains interacting with the  $\pi$ -system.

### ***Indole Monomers vs. 2,3-Diindoles vs. Indolo[3,2-a]carbazoles***

The lowest energy absorption for indole occurs at 285nm.<sup>39</sup> For the 2,3 diindoles investigated in this thesis the lowest energy transition appears between 311nm and 326nm. This decrease in energy comes from the spreading of the  $\pi$ -system across two indole units. As the lowest energy transition decreases significantly it would be expected that the central 2, 3 bond would display a significant proportion of double bond-type character. However, if this bond were significantly conjugated it might be expected that the lowest energy transitions would be much closer to those of the indolo[3,2-a]carbazoles. It is apparent from comparisons of the spectra of the diindole and carbazole species, Fig 3.11, that while the maxima of the 2,3 diindole transitions are much higher energy than the first absorption of the equivalent indolo[3,2-a]carbazoles, the energy range absorbed is similar. It appears that the breadth of the absorption is the result of a number of individual transitions which together form one very broad absorption band.



**Figure 3.11** – Comparisons of the Absorption Spectra for species 2,3-diindole and indolo[3,2-*c*]carbazole species (intensity not shown to scale)

That such a broad transitions are observed for the 2,3-diindole systems is a result of the flexibility of the 2,3-diindole despite some double bond character of the 2,3-bond. The apparent lack of rigidity in the structure means that excitation may occur from a range of rotational conformers, resulting in the broadening of each transition peak as the transition energy will vary for each conformer. The addition of the extra  $C_2H_2$  unit in

each of the indolo[3,2-a]carbazoles prevents this rotation, resulting in the numerous, narrow bands visible in the equivalent spectra.

## 3.5 – Emission Spectroscopy

### *2,3-Diindoles*

Excitation at 320 nm of **1a-e** in EtOH gives rise to emission at room temperature. While excitation of **1d** and **1e** causes only weak emission at 293K, at 77K both **1d** and **1e** are found to be highly emissive, Fig 3.12 and table 3.5. As may be expected the emission spectra of **1a** and **1b** resemble the mirror image of the corresponding excitation spectra, characteristic of fluorescence from the first excited state  $S_1$ .

Alternatively, the emission spectrum of **1c** is significantly different from the corresponding excitation spectrum with the appearance of a very broad second peak implying emission from an alternative excited state. Due to the nature of **1c**, in particular the large Stokes shift, emission appears to occur from a lower energy singlet excited

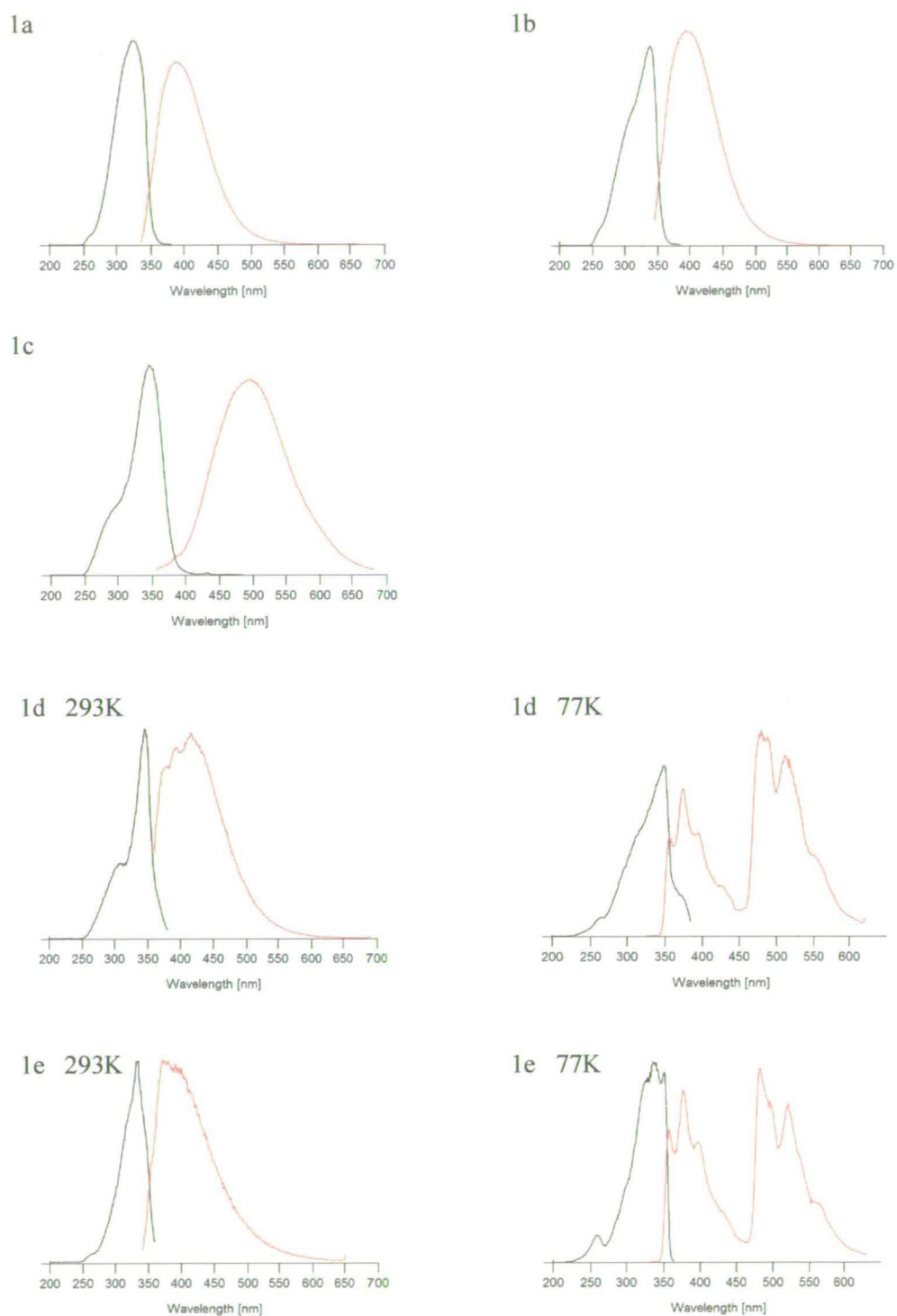


Figure 3.12 – Excitation and Emission spectra for 1a-e at room temperature and 1d and 1e at 77K.

|    | Emission Max |  |
|----|--------------|--|
|    | 293K         | 77K                                    |
| 1a | 390          | -                                      |
| 1b | 397          | -                                      |
| 1c | 496          | -                                      |
| 1d | 375          | 355, 373, 396, 428, 479, 488, 511, 550 |
| 1e | 371          | 357, 376, 397, 430, 482, 493, 520, 560 |

Table 3.5 – Emission Peaks for 1a-e

state compared with the excitation. If this is the case it may be due to poor overlap between the HOMO and the alternative emitting state preventing effective absorption to this level or a significant structural change caused by the presence of the acid groups. This is discussed more thoroughly in Section 3.6.

The presence of bromine in systems **1d** and **1e** allows inter-system crossing to the triplet,  $T_1\pi\pi^*$  state. The  $T_1$  excited state is long-lived as relaxation from this level back to the  $S_0$  ground-state is forbidden, at 293K. This long-lived excited state may be quenched through collisions within the solution with other excited molecules or by trapped  $O_2$ . Upon freezing the solution to 77K, such random collisions are prevented, as such both fluorescence and phosphorescence are observed.

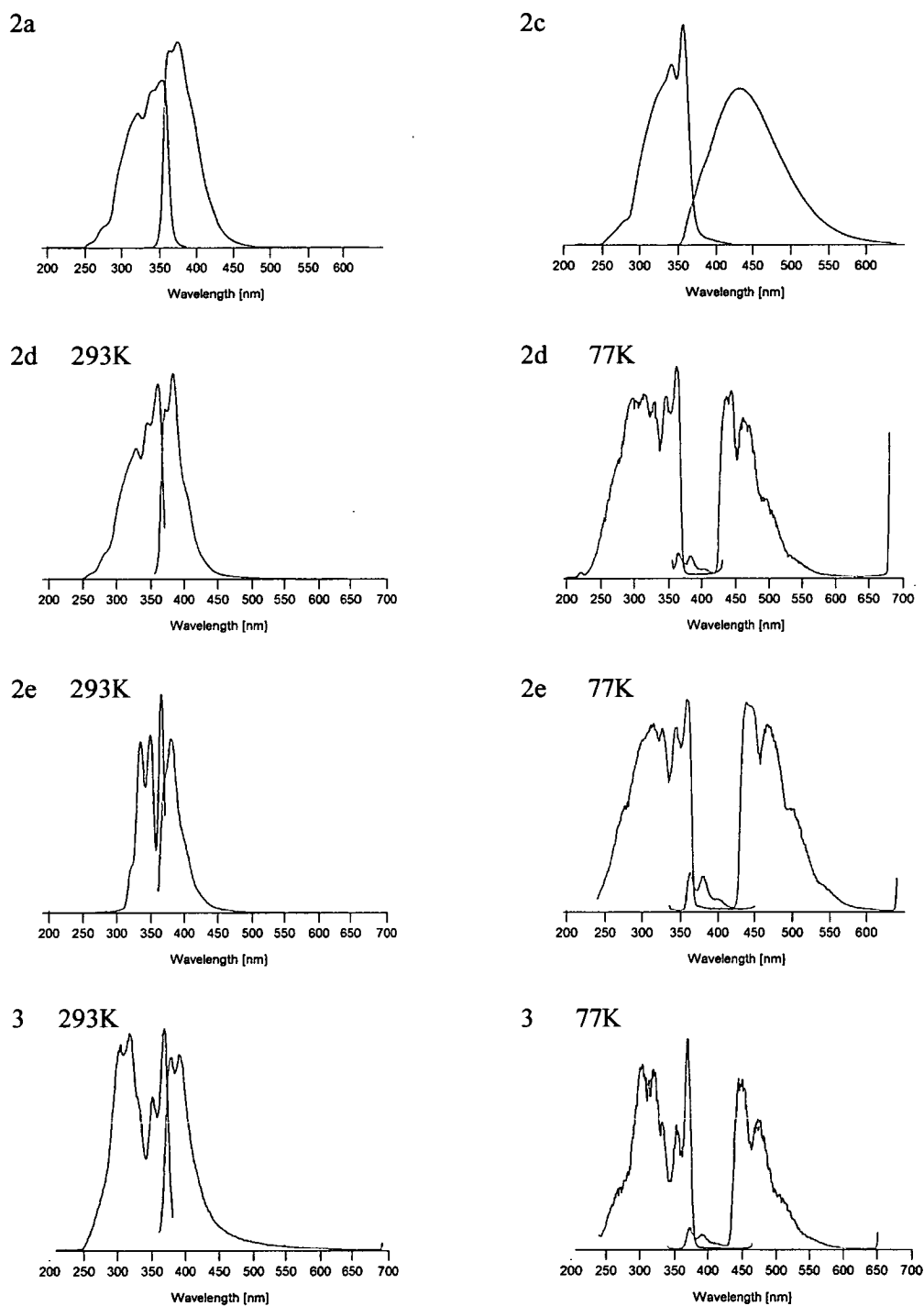
### ***Indolo[3,2-a]Carbazoles***

Compounds **2a**, **2c**, **2d**, **2e** and **3** are all emissive at 293K, while **2d**, **2e** and **3** show additional emissive transitions at 77K, Fig 3.13 and table 3.6. As with **1a**, **2a** closely resembles the mirror image of the excitation spectrum indicative of fluorescence from  $S_1$  to  $S_0$ . The emission from **2b** was not measured due to the impurity of the sample from the lack of stability in air.

The emission spectrum of **2c** is much broader than that of **2a** and as with **1c** varies significantly from the expected spectrum. As with **1c**, possible explanations are discussed more thoroughly in Section 3.6

Unlike **1d** and **1e**, **2d** and **2e** emit at 293K to give clearly resolved spectra. For **2d** this spectrum is very close to that seen for **2a**. This implies that the emission from **2d** comes from excited states with limited bromine character.

Analysis of the 77K data for **2d** and **2e** shows the same emission peaks as 293K but with a significant number of additional peaks, many of much greater size. The absorption area of the spectra for both systems is much changed from that at 293K. While there are no changes to the low energy absorptions many more excitation peaks appear at higher energy as a result of phosphorescence from the  $T_1$  state.



**Figure 3.13** – Excitation and Emission spectra for **2a,2c,2d,2e** and **3** at room temperature and **2d ,2e** and **3** at 77K.

|    | 293K              | 77K                          |
|----|-------------------|------------------------------|
|    | Emission Max (nm) | Emission Max (nm)            |
| 2a | 363, 374          | -                            |
| 2c | 430               | -                            |
| 2d | 368,381           | 365, 383, 402, 440, 461, 486 |
| 2e | 379               | 364, 380, 404, 437, 467, 501 |
| 3  | 376,392           | 372, 390, 405, 446, 572, 500 |

Table 3.6 – Emission Peaks for 2a, 2c, 2d, 2e and 3

### 2,3-Diindoles vs. Indolo[3,2-a]carbazoles

Comparison of the brominated 2,3-diindoles and indolo[3,2-a]carbazoles indicates a much higher ratio of phosphorescence to fluorescence for **2d** and **2e** than for **1d** and **1e**. Given that the same number of bromine atoms are involved this suggests that the carbazole framework plays an important role in promoting inter-system crossing to the  $T_1$  level from the  $S_1$  excited state. The extended  $\pi$ -structure of the indolo[3,2-a]carbazoles, in comparison to the 2,3-diindoles, allows the two bromine atoms to have a greater influence over the system leading to increased bromine character in the excited state.

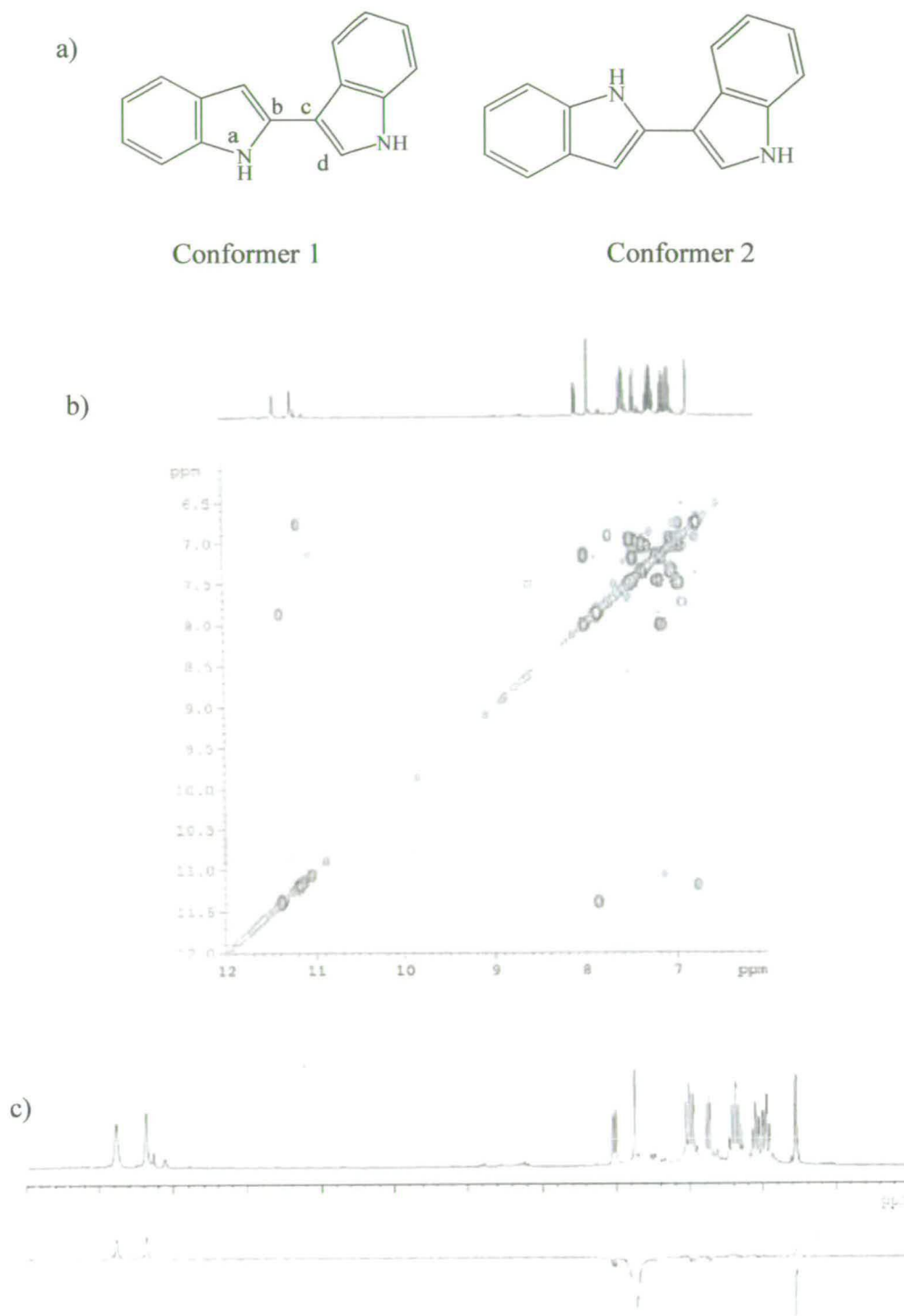


## 3.6 – DFT Calculations

### *2,3-Diindoles*

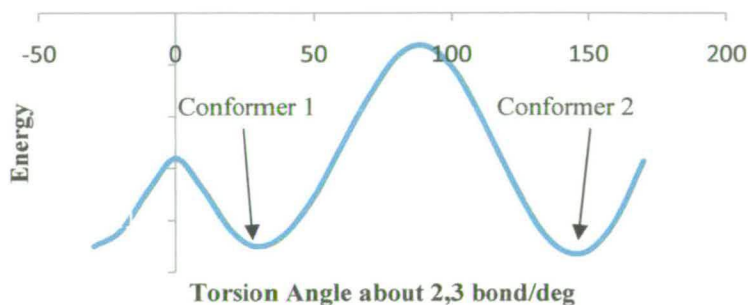
The absorption spectroscopy results from Section 3.4 indicate that while the central 2,3 bond displays significant double bond character, rotation about the 2,3 bond of the diindole species is still possible. This implies that a number of conformations of the species may be observed. Previous computational studies of **1a**, carried out using a B3LYP functional and 6-31G\* basis-set, by Dr Patricia Richardson of the University of Edinburgh,<sup>40</sup> suggest that there are two possible ground-state conformations of this diindole species, Fig 3.15. These conformers are separated by 0.623KJ mol<sup>-1</sup>, with conformer 2 being slightly lower energy. However, 2D-NMR studies carried out by David Reed also of the University of Edinburgh, indicate that only conformer 1 is observed in solution, Fig 3.15.

These studies were repeated for species **1e** using a B3LYP functional and 6-31G\* basis-set giving the ground state energy profile seen in fig. 3.16 In this case conformer 2 was still lower in energy though only by 0.263KJmol<sup>-1</sup> while comparison of <sup>1</sup>H-NMR of **1e** to that of **1a** confirms that conformer 1 is the only configuration present in solution. In order to obtain a more accurate view of the system the torsion angle study was repeated, factoring in the solvation of **1e** by DMSO, the solvent used for the NMR studies, Fig

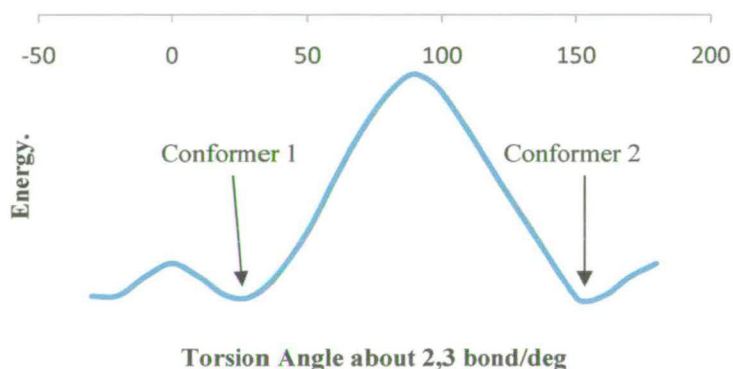


**Figure 3.15** – a) The two possible ground-state configurations of **1a**, b) COSY Spectra of species **1a**, c) NOESY spectra of species **1a**

3.15. In this case it appears that conformer 2 is still the more favourable conformation though now by only  $0.032 \text{ KJmol}^{-1}$ .



*Figure 3.16* –Plot of the ground state energy against the torsional angle about the 2,3 bond for *1e*, labelled a, b, c, d in Fig 3.15

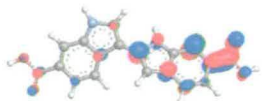
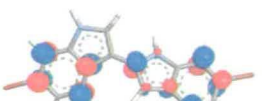
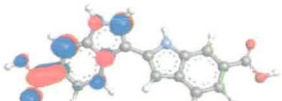
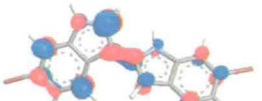
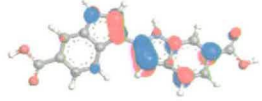
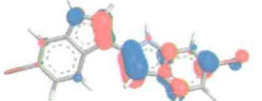
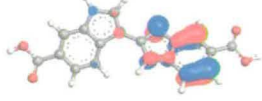
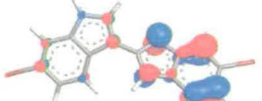
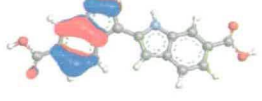



*Figure 3.15* – Plot of the ground state energy against the torsional angle about the 2,3 bond for *1e* in DMSO

Since neither conformer is significantly more energetically favourable, two possible explanations for the exclusive presence of conformer 1 in solution present themselves. The mechanism of the reaction is such that the conformer 1 is the exclusive product and the energy barrier against  $180^\circ$  rotation is too high, or that in the polar solvents used for

<sup>1</sup>H-NMR there is some stabilisation from the interaction between DMSO molecules and the indole nitrogen atoms for conformer 1 but not for conformer 2.

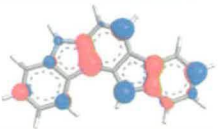
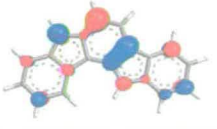
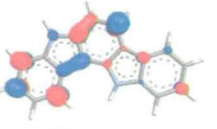
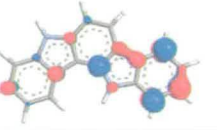
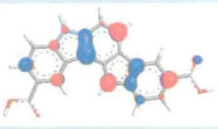
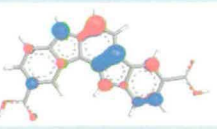

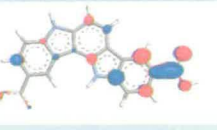

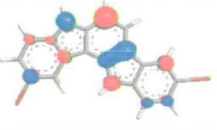

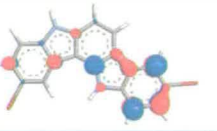

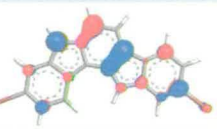
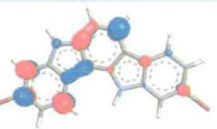

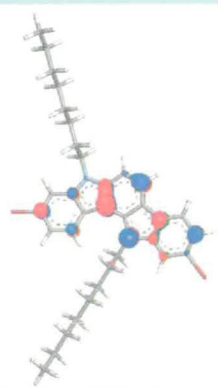
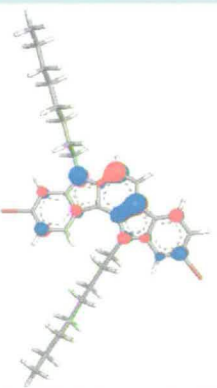

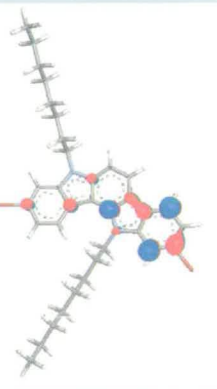
Both the absorption and emission spectra of **1c** are unusual in the context of the other diindoles. It is believed that this may be attributed to differences in the frontier orbitals. DFT calculations carried out on both **1c** and **1e** as a representative of the other 2,3-diindoles are in agreement with these conclusions. The calculations for **1e** agree with those carried out by John Henry and Dr Patricia Richardson<sup>35</sup> for **1a**, with similar frontier orbitals. However the calculated molecular orbitals for **1c** display significant differences from those calculated for the other species. This can clearly be seen from table 3.7 where both the energies of equivalent orbitals and the orientation of the orbitals vary significantly. The HOMO and HOMO-1 levels remain similar as might be seen from the absorption spectroscopy results which bear some resemblance to those of the alternative 2,3-diindoles. Differences appear in the HOMO-2, LUMO and LUMO+1 orbitals which may explain the differences seen at the high-energy end of the absorption spectra. This is discussed more thoroughly later in the Chapter in conjunction with calculations based on species **2c**.

|        | 1c   | Energy (eV) | 1e  | Energy (eV) |
|--------|--|-------------|---|-------------|
| LUMO+1 |   | -1.413      |   | -0.469      |
| LUMO   |   | -1.659      |   | -1.026      |
| HOMO   |   | -5.526      |   | -5.327      |
| HOMO-1 |   | -6.134      |   | -6.081      |
| HOMO-2 |  | -6.763      |  | -6.382      |

**Table 3.7** – Frontier orbital calculated orientations and energies for 1c and 1e

### *Indolo[3,2-a]carbazoles*

Calculations based on the indolo[3,2-a]carbazole species **2a**, **2c**, **2d**, **2e** and **3** have resulted in the molecular orbitals and predicted orbital energies seen in Table 3.8.

|             | HOMO-1  | HOMO  | LUMO   | LUMO +1   |
|-------------|---|---|--|---|
| 2a          |    |    |    |    |
| Energy (eV) | -5.284  | -5.160  | -0.623   | -0.197  |
| 2c          |    |    |    |    |
| Energy (eV) | -5.796  | -5.671  | -1.424   | -1.244  |
| 2d          |    |    |    |    |
| Energy (eV) | -5.648  | -5.543  | -1.127   | -0.671  |
| 2e          |   |   |   |   |
| Energy (eV) | -5.654  | -5.537  | -1.100   | -0.661  |
| 3           |  |  |  |  |
| Energy (eV) | -5.440  | -5.310  | -0.992   | -0.614  |

**Table 3.8** - Comparison of the calculated HOMO and LUMO-type orbitals of systems **2a**, **2c**, **2d** and **2e**

Calculations were not undertaken for **2b** due to the inability to obtain an emission spectrum and concerns over sample purity.

The resulting molecular orbitals show a number of notable similarities within the indolo[3,2-a]carbazole series. The HOMO-1 and HOMO orbitals correspond very closely across the series, with the molecular orbital evenly distributed across both indole units of the carbazole. This is indicative of the highly conjugated system expected from the indolocarbazole system.

It is noticeable that much of the occupied molecular orbital character resides on the indole nitrogen atoms. The combination of the character on both atoms is greater, in all cases, than that on atoms meta to the substituent. This is in clear agreement with the results of Section 2.3 in which the plot of oxidation potential vs. Hammett parameter suggested a significant para effect.

The LUMO and LUMO+1 orbitals of **2c** are vastly different from those of **2a**, **2d** and **2e**. The nature of the acid unit has caused the unoccupied orbitals to be largely situated on the acid groups (35%, LUMO, 30% LUMO+1). The result of this is that the orbitals are dramatically shifted with one indole unit dominating the orbital (89% LUMO, 75% LUMO+1). For the other indolo[3,2-a]carbazoles, the shift to one indole is not as drastic

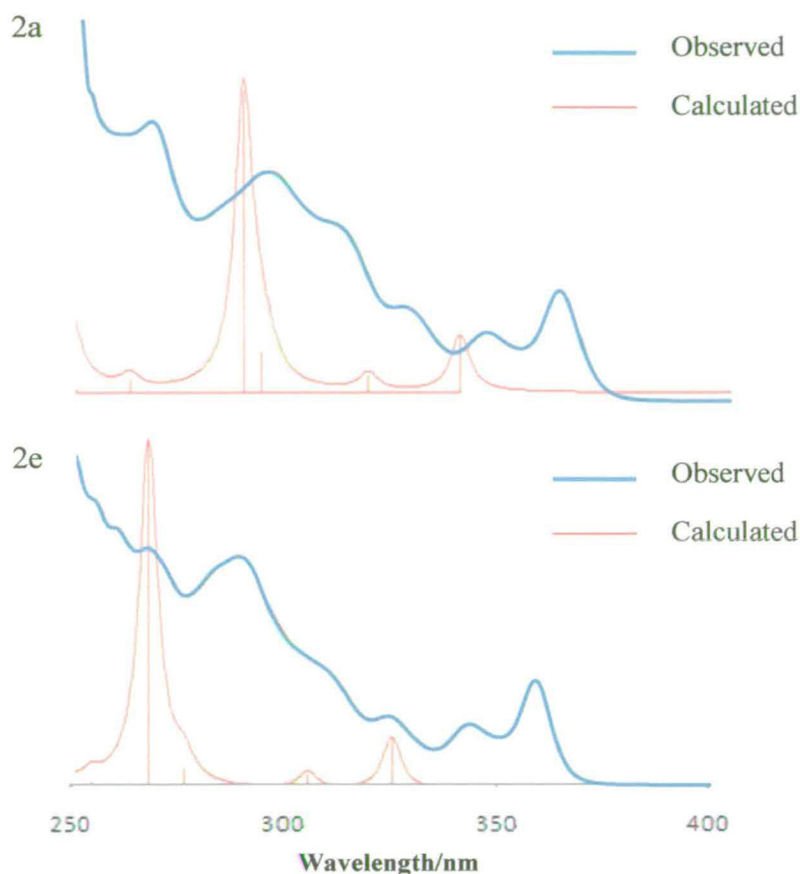
with no more than 61% of the LUMO on any one indole. The differing energies of the respective systems further emphasises the changes observed for the LUMO and LUMO+1 of **2c**. Those of **2c** are very close in energy while there is a significant gap between the LUMO and LUMO+1 of the remaining compounds. This difference in LUMO character is most likely responsible for the difference in emission spectrum of **2c** when compared to the other indolo[3,2-a]carbazoles.

The investigations into **3** also provide confirmation there is an inductive effect from the alkyl chain as 4% of the character of both the HOMO and HOMO-1 resides on the octyl groups. The presence of these chains does little to alter the general distribution of the orbitals which follows the same pattern as **2e**, however it does reduce the HOMO-LUMO gap and particularly the relative energy of the LUMO+1. This manifests itself as decreased energy of the transitions observed in the absorption spectroscopy.

### 3.7 - TD-DFT

TD-DFT calculations were carried out for species **2a** and **2e** with calculated absorption spectra for **2a** and **2e** showing significant similarities to the observed absorption spectra. The calculated spectra are displayed in Fig 3.17 while the energy, oscillator strength and composition of each transition is reported in Table 3.9 and 3.10.





**Figure 3.17** – TD-DFT calculated UV/Vis Spectra for **2a**

| Transition  | Calculated Energy (nm) | Observed Energy (nm) | f      | Composition   |
|-------------|------------------------|----------------------|--------|---|
| $S_0 - S_1$ | 318.73                 | 359                  | 0.1132 | HOMO – LUMO 63%<br>HOMO-1 – LUMO+1 27%                        |
| $S_0 - S_2$ | 300.87                 | 344                  | 0.0388 | HOMO-1 – LUMO 61%<br>HOMO – LUMO+1 27%                        |
| $S_0 - S_3$ | 274.73                 | 324                  | 0.0512 | HOMO – LUMO+1 50%<br>HOMO-1 – LUMO+1 32%<br>HOMO-1 – LUMO 18% |

**Table 3.9** – Calculated energy, oscillator strength and composition of the first three absorption transitions of **2a**

| Transition  | Calculated Energy (nm) | Observed Energy (nm) | f      | Composition         |
|-------------|------------------------|----------------------|--------|---------------------|
| $S_0 - S_1$ | 333.00                 | 363                  | 0.2225 | HOMO – LUMO 64%     |
|             |                        |                      |        | HOMO-1 – LUMO+1 23% |
|             |                        |                      |        | HOMO-1 – LUMO 11%   |
| $S_0 - S_2$ | 313.43                 | 347                  | 0.0684 | HOMO-1 – LUMO 59%   |
|             |                        |                      |        | HOMO – LUMO+1 30%   |
| $S_0 - S_3$ | 291.08                 | 329                  | 0.1642 | HOMO – LUMO+1 56%   |
|             |                        |                      |        | HOMO-1 – LUMO 25%   |
|             |                        |                      |        | HOMO-1 – LUMO+1 19% |

**Table 3.10** – Calculated energy, oscillator strength and composition of the first 3 absorption transitions of **2e**

It may be noted that in the case of both **2a** and **2e** the relative position and intensity of each transition are in agreement with the observed absorption spectra, although each transition is shifted to significantly higher energy. This is in agreement with previous calculations based on substituted indolo[3,2-b]carbazoles<sup>41</sup> in which the observed transitions were up to  $1500\text{cm}^{-1}$  lower in energy than those calculated.

The red shift in  $S_0 - S_1$ ,  $S_0 - S_2$  and  $S_0 - S_3$  transitions from **2e** to **2d** may be explained through the orbitals involved in the transitions. Each transition is primarily from either the HOMO-1 or HOMO to the LUMO or LUMO+1. As may be seen in Table 3.8 the character of each of these orbitals is based more on the 2 and 9 positions than on the 3 and 10. As such the electron withdrawing bromine group plays a more significant role in

the frontier orbitals of **2e** than **2d**. This causes an alteration to the conjugated  $\pi$ -system thus raising the transition energy.

## 3.8 - FET Measurements

### 2,3-Diindoles

In collaboration with Dr Maxim Shkunov and David Sparrowe of Merck Chemicals Ltd attempts were made to produce field-effect transistors from **1a** and **1c**.

The initial stage was the production of thin-films based on the 2,3-diindole species. This was done through spin-coating of a concentrated 2,3-diindole solution at 3000 rpm for 30 seconds before annealing. Assessment of the resulting thin-films was made through UV/Vis spectroscopy. Fig. 3.18.

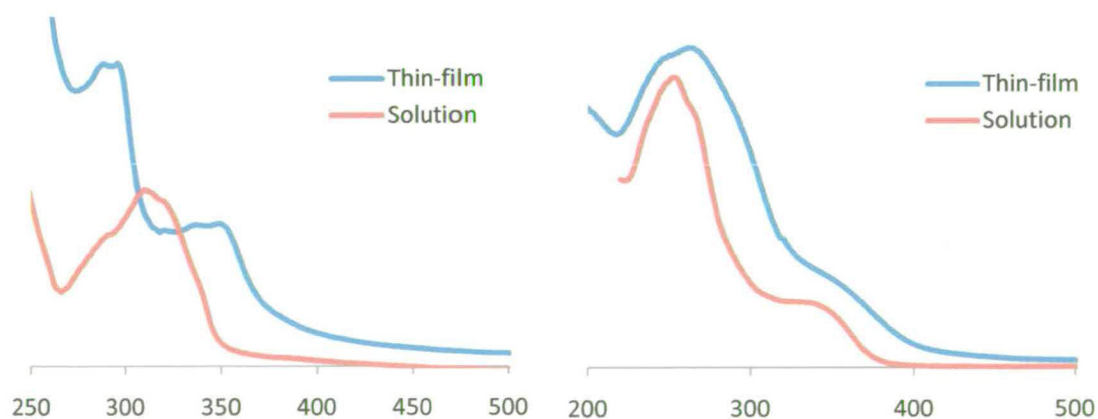
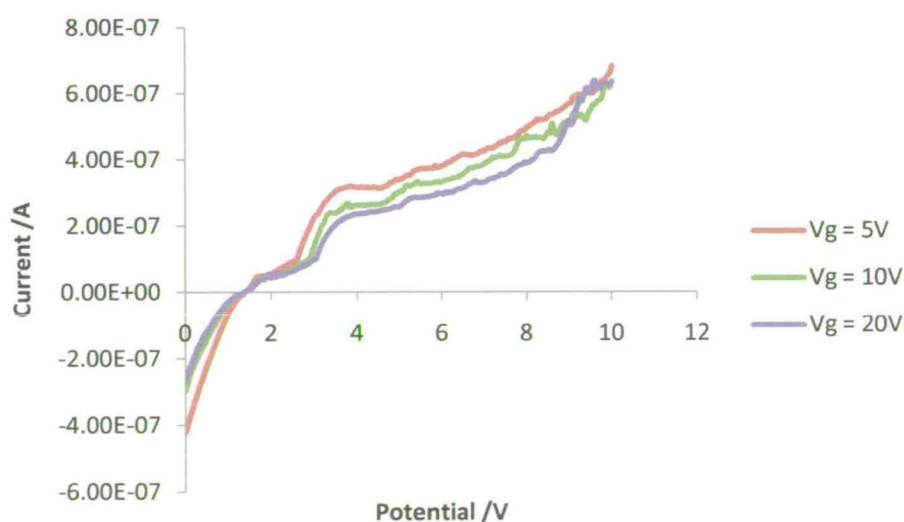


Figure 3.18 – Comparison of thin-film vs. solution UV/Vis absorption for **1a** and **1c**

The red-shift noted in both spectra is indicative of aggregation suggesting that thin-films of both species were formed successfully. When thin-film transistors were formed via the same method neither system presented semiconductor behaviour. This was attributed to the level of movement possible around the central 2,3 bond. As a result of this movement, interactions between the  $\pi$ -systems of neighbouring molecules within a film are significantly reduced, preventing charge transfer through the film.

### *Indolo[3,2-a]carbazoles*

A field-effect transistor was constructed based on compound **3**, via melting of **3** onto the pre-patterned substrate. While this results in the I-V curve in Fig 3.19 the device displays no dependence on gate voltage.



*Fig 3.19 – Current vs. Voltage graph for FET formed from 3*

The lack of any observed gate dependence may be due to a number of factors.

- Compound **3** is incapable of forming semiconducting materials.
- Compound **3** shows no semiconductor behaviour when tested through the -20V to 20V range. This has been observed for a number of other families of organic electronic materials, including numerous pentacene analogues<sup>42</sup> and the indolo[3, 2-b] carbazoles.<sup>16</sup>
- Problems with the device itself either through the nature of the substrate used or with the film formed via melt processing.

As a result of these possibilities we are as yet unable to discover the charge-mobility of **3**.

In order to ascertain the potential of indolo[3,2-a] carbazoles as functional electronic materials a more thorough attempt to assess the charge-mobility needs to be carried out. Unfortunately this is beyond the capabilities available at the University of Edinburgh at present. As such, there is now a collaboration with Professor K. Awaga at the University of Nagoya. The Awaga group will be able to study the FET behaviour of these materials more thoroughly in the coming months.

Investigation by a group with a wider range of substrates, processing capabilities and measurement equipment will help the assessment of the electronic properties of indolo[3, 2-a] carbazoles.

## 3.9 – Conclusions

This study has resulted in the successful synthesis and characterisation of a number of compounds to add to the families of both 2, 3-diindoles and indolo[3, 2-a]carbazoles. This has been achieved through the extension of an existing synthesis in the case of the 2, 3-diindoles and the adaptation of a known synthetic route to modern synthetic techniques in the case of the indolo[3, 2-a]carbazoles.

Spectroscopic data from the 2, 3-diindole species suggests that movement about the central 2, 3 bond causes the amalgamation of individual transition peaks. This results in the broad peaks observed for both the absorption and emission spectra for the 2, 3-diindoles. However this also prevents the materials from forming semiconducting films.

The nature of the HOMO levels of the indolo[3, 2-a]carbazoles appear to largely be predetermined by the heterocyclic system, with little change to geometries of the occupied frontier orbitals caused by substituent groups. The same cannot be said of the unoccupied frontier orbitals, which are greatly altered by the presence of acid groups due to the apparent introduction of new excited states centred largely on the aid groups.

Though charge mobilities have not been successfully measured for either the 2, 3-diindoles or the indolo[3, 2-a]carbazoles it is apparent from the observed electronic properties of the carbazoles that this is a very worthwhile area of research. While the observed energy gap between frontier orbitals are higher than those typically observed for the indolo[3,2-b]carbazole species, both the ease of synthesis and the significant substituent effect noted above suggest that there is much to be gained from pursuing indolo[3,2-a]carbazoles as a basis for future organic electronic materials.

## 3.10 - Experimental

### *Synthesis*

Synthesis of each 2, 3 diindole species was adapted from the previously published method.<sup>7</sup>

#### **General Procedure for 2, 3 diindole.4/3HBr Synthesis**

Indole (4 mmol) was stirred in acetonitrile (20 ml) and Br<sub>2</sub> (2 mmol) in 10 ml of acetonitrile added dropwise. The solution was left to stir for 5 minutes or until a yellow precipitate formed. The product was filtered and washed with acetone. In the case of **1d** and **1e** acetonitrile was replaced with glacial acetic acid.

**2, 3 diindole – 1a** - Yield 52%, CHN calc. For C<sub>16</sub>H<sub>12</sub>N<sub>2</sub>.4/3(HBr) C, 56.5, H, 3.6, N, 8.3%, found, C, 56.5, H, 3.6, N, 8.3%

**1b** – Yield 23% - CHN for C<sub>18</sub>H<sub>16</sub>N<sub>2</sub>.4/3(HBr) - Calc C 58.70, H 4.71, N 7.61, Found C 59., H 5.03, N 7.78 – <sup>1</sup>H-NMR (d<sub>6</sub>-DMSO) 10.96 (1H, s), 10.84 (1H, s), 7.58 (2H, m), 7.09 (3H, m), 6.79 (1H, d J<sub>H-H</sub> 0.03), 6.61 (1H, d J<sub>H-H</sub> 0.025), 6.42 (1H, s), 2.2 (6H, m) – FAB-MS: m/z 260(M<sup>+</sup>)



**1c** – Yield 48% - CHN for  $C_{18}H_{12}O_4N_2 \cdot 4/3(HBr)$  – Calc C 50.43, H 3.12, N 6.54, Found C 49.98, H 3.64, N 6.28 –  $^1H$ -NMR ( $d_6$ -DMSO) 12.05(1H, s), 11.94(1H, s), 8.87(1H, s), 8.49(1H, s), 8.22(1H, d  $J_{H-H}$  0.01), 8.08(1H, d  $J_{H-H}$  0.035), 7.92(1H, d  $J_{H-H}$  0.035), 7.79(1H, d  $J_{H-H}$  0.015), 7.66(1H, d  $J_{H-H}$  0.015), 7.13(1H, s) – FAB-MS: m/z 320(M<sup>+</sup>)

**1d** – Yield 34% - CHN for  $C_{16}H_{10}N_2Br_2$  – Calc C 48.98, H 2.55, N 7.14, Found C 47.63, H 2.34, N 6.94 –  $^1H$ -NMR ( $d_6$ -DMSO) 11.70(1H, s), 11.45(1H, s), 8.10(1H, s), 7.83(1H, m), 7.67(1H, s), 7.46(1H, d  $J_{H-H}$  0.035), 7.31(2H, m), 7.13(1H, d  $J_{H-H}$  0.035), 6.76(1H, s) – FAB-MS: m/z 392(M<sup>+</sup>)

**1e** – Yield 51% - CHN for  $C_{16}H_{10}N_2Br_2$  – Calc C 48.98, H 2.55, N 7.14, Found C 47.74, H 2.43, N 6.81 –  $^1H$ -NMR ( $d_6$ -DMSO) 11.80(1H, s), 11.68(1H, s), 8.17(2H, m), 7.90(1H, s), 7.69(2H, m), 7.52(1H, d  $J_{H-H}$  0.035), 7.32(1H, d  $J_{H-H}$  0.035), 7.01(1H, s) – FAB-MS: m/z 392(M<sup>+</sup>)

### General procedure for Indolo[3, 2-a] carbazole synthesis

2,3-diindole (0.5mmol) was suspended in acetic acid (5ml). (Dimethylamino) acetaldehyde diethyl acetal (2mmol) was added, the solution placed in a sealed tube and subjected to a microwave heating at 140° for 20 minutes at 150W power. Solution was

---

poured into a 1:1 Water : Ethyl Acetate mixture, the organic layer extracted and the solvent evaporated off. Finally the residue was purified via Column Chromatography on silica (1:1 DCM: Hexane)

**2a** – Yield 47% - CHN for C<sub>18</sub>H<sub>12</sub>N<sub>2</sub> – Calc C 84.38, H 4.69, N 10.94, Found C 82.62, H 4.76, N 10.42 – <sup>1</sup>H-NMR (d<sub>6</sub>-DMSO) 11.98(1H, s), 11.78(1H, s), 8.83(1H, d J<sub>H-H</sub> 0.035), 8.29(2H, m), 7.79(2H, m), 7.51(5H, m) – FAB-MS: m/z 256(M<sup>+</sup>)

**2b** – Yield 12% - CHN for C<sub>20</sub>H<sub>16</sub>N<sub>2</sub> – Calc C 84.51, H 5.63, N 9.86, Found C 67.48, H 6.06, N 6.68 – <sup>1</sup>H-NMR (d<sub>6</sub>-DMSO) 11.72(1H, s), 11.54(1H, s), 8.49(1H, s), 8.10(1H, d J<sub>H-H</sub> 0.035), 7.95(1H, s), 7.52(2H, m), 7.27(3H, m), 1.643(3H, t J<sub>H-H</sub> ), 1.37(3H, t J<sub>H-H</sub> 0.035) – FAB-MS: m/z 284(M<sup>+</sup>)

**2c** – Yield 42% - CHN for C<sub>20</sub>H<sub>12</sub>O<sub>4</sub>N<sub>2</sub> – Calc C 69.77, H 3.48, N 8.14, Found C 64.51, H 4.40, N 5.71 – <sup>1</sup>H-NMR (d<sub>6</sub>-DMSO) 12.53(1H, s), 12.03(1H, s), 9.43(1H, s), 8.85(1H, s), 8.42(1H, d J<sub>H-H</sub> 0.03), 8.16(2H, m), 7.79(2H, m), 7.57(1H, d J<sub>H-H</sub> 0.035) – FAB-MS: m/z 344(M<sup>+</sup>)

**2d** – Yield 64% - CHN for  $C_{18}H_{10}N_2Br_2$  – Calc C 51.92, H 2.40, N 6.73, Found C 51.59, H 2.42, N 6.14 –  $^1H$ -NMR ( $d_6$ -DMSO) 12.04(1H, s), 11.88(1H, s), 8.84(1H, s), 8.40(1H, d  $J_{H-H}$  0.035), 8.26(1H, d  $J_{H-H}$  0.035), 7.54(5H, m) – FAB-MS: m/z 416(M<sup>+</sup>)

**2e** – Yield 57% - CHN for  $C_{18}H_{10}N_2Br_2$  – Calc C 51.92, H 2.40, N 6.73, Found C 52.22, H 2.63, N 6.34 –  $^1H$ -NMR ( $d_6$ -DMSO) 11.62 (1H, s), 11.41 (1H, s), 8.47 (1H, s), 8.09 (1H, d  $J_{H-H}$  0.035), 7.93 (1H, s), 7.56 (1H, d  $J_{H-H}$  0.035), 7.48 (1H, d  $J_{H-H}$  0.035), 7.24 (3H, m) – FAB-MS: m/z 416(M<sup>+</sup>)

**Synthesis of 1, 5 dioctyl, 7, 12, dibromo 2, 3 diindole, 3** - 1.02mmol **2e**, 0.02mmol KOH, 0.05mmol  $[CH_3(CH_2)_3]_4N(HSO_4)$  and 12mmol 1-iodooctane were dissolved in 50ml acetone and heated under reflux for 24 hours. Once cool the solvent was removed and the residue dissolved in  $CH_2Cl_2$  and washed with 10% aqueous HCl. The solution was dried over  $MgSO_4$  and solvent evaporated. The remaining solid was triturated with  $CH_3CN$  to give a pale yellow solid – Yield 72% - CHN for  $C_{34}H_{42}N_2Br_2$  – Calc C 67.11, Calc H 6.91, Calc N 4.61, Found C 66.63, Found H 7.14, Found N 4.34 –  $^1H$ -NMR( $d_6$ -DMSO) 8.10 (1H, d  $J_{H-H}$  0.035), 8.07 (1H, d  $J_{H-H}$  0.035), 7.86 (1H, d  $J_{H-H}$  0.035), 7.55 (2H, m), 7.29 (3H, m), 1.20 (42H, m), 0.83 (9H, m) – FAB-MS: m/z 608(M<sup>+</sup>)

### 3.11 – References

1. O. D. Jurchescu, J. Baas, T. T. M. Palstra, *App. Phys. Lett.*, 2004, **84**, 3061
2. M. Yamagishi, J. Takeya, Y. Tominari, Y. Nakazawa, T. Kuroda, S. Ikehata, M. Uno, T. Nishikawa, T. Kawase, *Appl. Phys. Lett.*, 2007, **90**, 182117.
3. J. E. Anthony, *Chem.Rev.*, 2006, **106**, 5028
4. M. Mas-Torrent, M. Durkut, P. Hadley, X. Ribas, C. Rovira, *J. Am. Chem. Soc.*, 2004, **126**, 984
5. Y. Sun, K. Xiao, Y. Liu, J. Wang, J. Pei, G. Yu, D. Zhu, *Adv. Func. Mat.*, 2005, **15**, 818
6. N. Hu, S. Xie, Z. Popovic, B. Ong, A. Hor, *J. Am. Chem. Soc.* 1999, **121**, 5097
7. N. Robertson, S. Parsons, E.J. MacLean, R.A. Coxall, A.R. Mount. *J. Mat. Chem.*, 2000, **10**, 2043
8. M. Talarico, R. Termine, E. M. Garcia-Frutos, A. Omenat, J. L. Serrano, B. Gomez-Lor, A. Golemme, *Chem. Mater.*, 2008, **20**, 6589
9. B. Robinson, *J. Chem. Soc.*, 1963, 3097
10. G. Wille, P. Mayser, W. Thoma, T. Monsees, A. Baumgart, H.-J. Schmitz, D. Schrenk, K. Polborn, W. Steglich, *Bioorg. Med. Chem.*, 2001, **9**, 955.
11. H.-J. Kramer, M. Podobinska, A. Bartsch, A. Battmann, W. Thoma, A. Bernd, W. Kummer, B. Irlinger, W. Steglich, P. Mayser, *Chem. Bio. Chem.*, 2005, **6**, 860.
12. M. Belletete, N. Blouin, P. T. Boudreault, M. Leclerc, G. Durocher, *J. Phys. Chem. A*, 2006, **110**, 13696

13. H. Zhao, X. Tao, F. Wang, Y. Ren, X. Sun, J. Yang, Y. Yan, D. Zou, X. Zhao, M. Jiang, *Chem. Phys. Lett.*, 2007, **439**, 132
  14. J. Lu, F. Liang, N. Drolet, J. Ding, Y. Tao, R. Movileanu, *Chem. Commun.*, 2008, 5315
  15. J. Tsai, C.-C Chueh, M.-H Lai, C.-F. Wang, W.-C. Chen, B.-T. Ko, C. Ting, *Macromolecules*, 2009, **42**, 1897
  16. Y. Wu, Y. Li, S. Gardner, B. S. Ong, *J. Am. Chem. Soc.*, 2005, **127**, 614
  17. P. T. Boudreault, S. Wakim, M. L. Tang, Y. Tao, Z. Bao, M. Leclerc, *J. Mater. Chem.*, 2009, **19**, 2921
  18. Y. Li, Y. Wu, S. Gardner, B. S. Ong, *Adv. Mater.*, 2005, **17**, 849
  19. H. Moon, R. Zeis, E.-J. Borkent, C. Besnard, A.J. Lovinger, T. Siegrist, C. Kloc, Z. Bao, *J. Am. Chem. Soc.*, **126**, 15322
  20. M. Oberg, L. Bergander, H. Håkansson, U. Rannug, A. Rannug, *Toxicol. Sci.*, 2005, **85**, 935.
  21. E. Fritsche, C. Schafer, C. Calles, T. Bernsmann, T. Bernshausen, M. Wurm, U. Hubenthal, J. E. Cline, H. Hajimiragha, P. Schroeder, L. Klotz, A. Rannug, P. Furst, H. Hanenberg, J. Krutmann, *J. Proc. Natl. Acad. Sci. U.S.A.*, 2007, **104**, 8851.
  22. A. Rannug, R. Tuominen, M. Warholm, U. Rannug, *Organohalogen Compd.*, 2003, **65**, 94.
  23. S. Fabre, M. Prudhomme, *Bioinorg. Med. Chem.*, 1993, **1**, 193
  24. V. Bemanian, M. Langvik, A. Rannug, A. Goksøyr, R. Male, *Organohalogen Compd.*, 2003, **65**, 118.
  25. J. T. Kuethe, A. Wong, I. W. Davies, *Org. Lett.*, 2003, **5**, 3721
-

26. N. Wahlstrom, J. Bergman, *Tet. Lett.*, 2004, **45**, 7273
27. H. Henon, F. Anizon, R. M. Golsteyn, S. Leonce, R. Hofmann, B Pfeiffer, M. Prudhomme, *Bioorg. Med. Chem.*, 2006, **14**, 3825
28. T. Janosik, J. Bergman, *Tetrahedron*, 1999, **55**, 2371
29. E. M. Garcia-Frutos, B. Gomez-Lor, *J. Am. Chem. Soc.*, 2008, **130**, 9173
30. V. Bocchi, G. Palla, *Tetrahedron*, 1986, **42**, 5019
31. N. Wahlström, J. Slätt, B. Stensland, A. Ertan, J. Bergman, T. Janosik, *J. Org. Chem*, 2007, **72**, 5886
32. S. Aburatani J. Uenishi, *Heterocycles*, 2008, **75**, 1407
33. C. O. Kappe, *Angew. Chem. Int. Ed.*, 2004, **43**, 6250
34. L. Greci, G. Tommasi, R Petrucci, G Marrosu, A. Trazza, P. Sgarabotto, L. Righi, A. Alberti, *J. Chem. Soc., Perkin Trans. 2*, 2000, **11**, 2337
35. John Henry, *University of Edinburgh*, PhD Thesis.
36. P. Jennings, A. C. Jones, A. R. Mount, A. D. Thompson, *J. Chem. Soc., Faraday Trans.*, 1997, **93**, 3791
37. J. G. Mackintosh, A. R. Mount, D. Reed. *Mag. Res.Chem.*, 1994, **32**, 559
38. J. F. Ambrose, L. L. Carpenter and R. F. Nelson, *J. Electrochem. Soc.*, 1975, **122**, 876
39. D. Grand, A. Bemas, and E. Amouyal, *Chem. Phys.*, **44**, 73, 1979
40. P. Richardson, *University of Edinburgh*, Personal Correspondence
41. M. Belletete, P. T. Boudreault, M. Leclerc, G. Durocher, *J. Mol. Structure: THEOCHEM*, 2007, **824**, 15

42. P. Gao, D. Beckmann, H. Nok Tsao, X. Feng, V. Enkelmann, M. Baumgarten, W.

Pisula, K. Mullen, *Adv. Mater.*, 2009, **21**, 213.

## Chapter 4

# C3-Symmetric Triindoles

### 4.1 – Introduction

As noted in Chapter 1, while the presence of a large conjugated  $\pi$ -system is of fundamental importance to any potential organic electronic material, the nature of any side groups can play a significant role in the intrinsic properties of the system. These side groups may offer unusual functionality<sup>1</sup> or the potential for cheaper more readily available solution processing techniques.<sup>2</sup> While introduction of a number of side-groups may cause an increase in solubility<sup>1,3</sup> one of the most commonly used methods is the introduction of a long-chain alkyl group as observed in Chapter 3 with the increased solubility of **3** relative to **2e**. Addition of a number of long-chain alkyl groups to a large conjugated  $\pi$ - system may also have an added benefit to the engineering of subsequent devices through the formation of discotic liquid crystalline materials.



Molecules that form discotic liquid crystalline materials tend to be made of a planar, delocalised central core unit allowing strong intermolecular interactions and long side chains separating the molecules from others within the same plane, Fig 4.1. This leads to strong interactions in one dimension and weak in the others, hence the molecules tend to form columnar stacks and these stacks form liquid-crystalline mesophases.

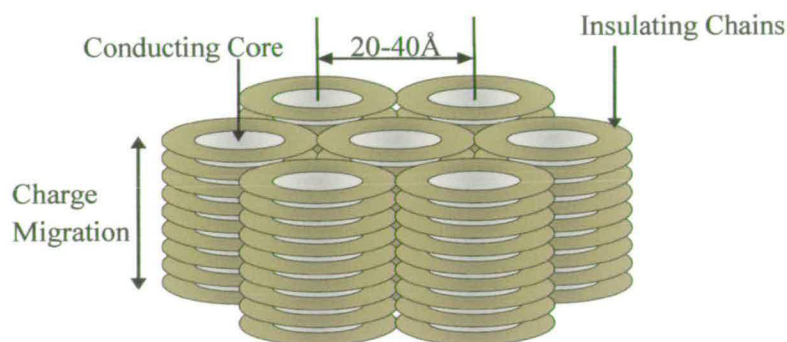


Figure 4.1 - Columnar phase in discotic liquid crystals

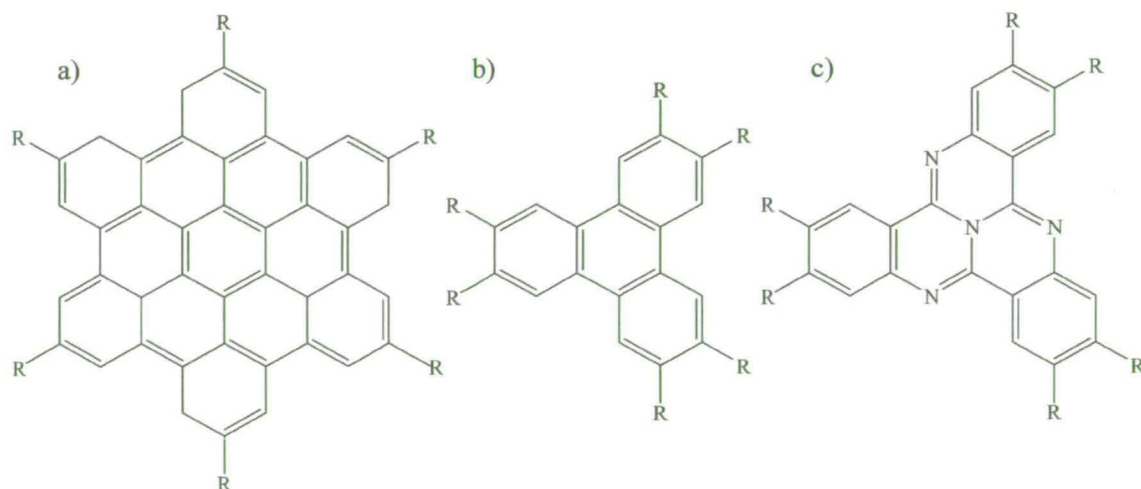


Figure 4.2 – Typical core materials for discotic liquid crystals.

As may be noted from fig 4.2 many of the systems under investigation as discotic liquid crystals bear a striking similarity to other materials already under investigation as potential organic electronic materials. One such material, the hexabenzocoronene derivative HBC-C14, Fig 4.2a (where R is C<sub>14</sub>H<sub>29</sub>), showed a charge mobility of up to 1.13cm<sup>2</sup>/Vs. <sup>4</sup>

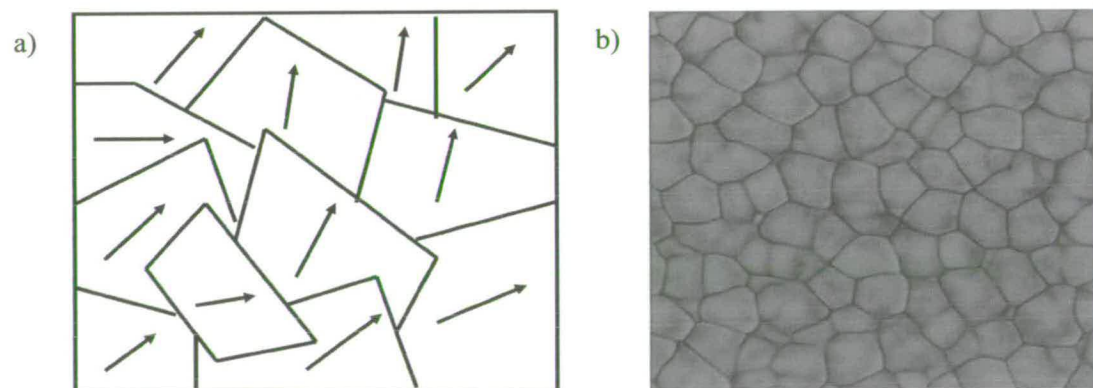
There are a number of additional advantages to the use of discotic liquid crystalline materials in the formation of organic-electronic based devices, over and above the advantages presented by other organic semiconductors.

- The columnar mesophases formed encourage one-dimensional interactions through a  $\pi$ -stack conformation, previously noted as the most effective for promoting high charge mobility.
- The strong interactions along a single dimension promote self-assembly into the columnar phases, leading to increased reproducibility between devices.
- The potential for reorientation of material within the crystalline lattice framework allows for charge transport to be encouraged within a specific direction.

The work of Christiansen et al neatly illustrates the effect liquid crystalline properties may have on an organic electronic system. <sup>5</sup> Charge mobility was increased by an order of magnitude through the realignment of a previously formed thin-film transistor of the

alternative hexabenzocoronene derivative HBC-PhC<sub>12</sub> via the application of a magnetic field. This resulted in a new monodomain film successfully avoiding the problem of grain boundaries.

Unlike single crystal based devices, molecular alignment within thin-film based devices is not always optimised, leading to multi-domain films, Fig 4.3a, and degrading the quality of the device. These domains may ultimately degrade to form polycrystalline films further decreasing device performance, Fig 4.3b.

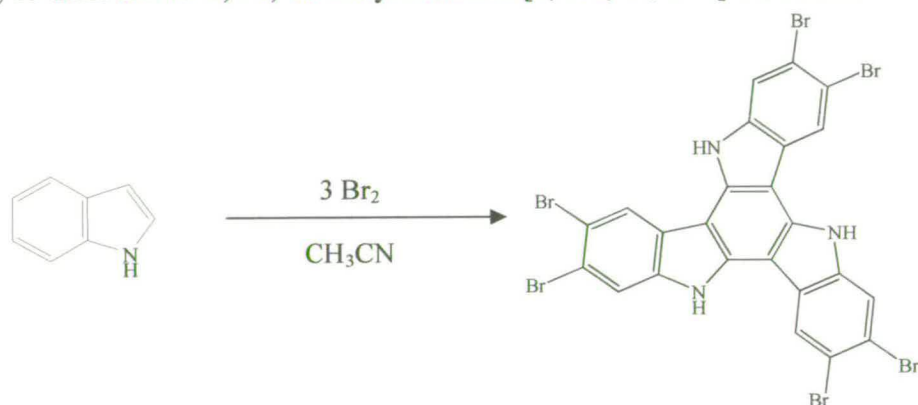


**Figure 4.3.** – a) Illustration of domains within a thin-film ( $\rightarrow$  shows direction of molecular alignment), b) AFM denoting grain boundaries within a sample <sup>6</sup>

Realignment of films via use of the liquid crystalline phase results in larger domains, reducing the possibility of significant degradation over time.

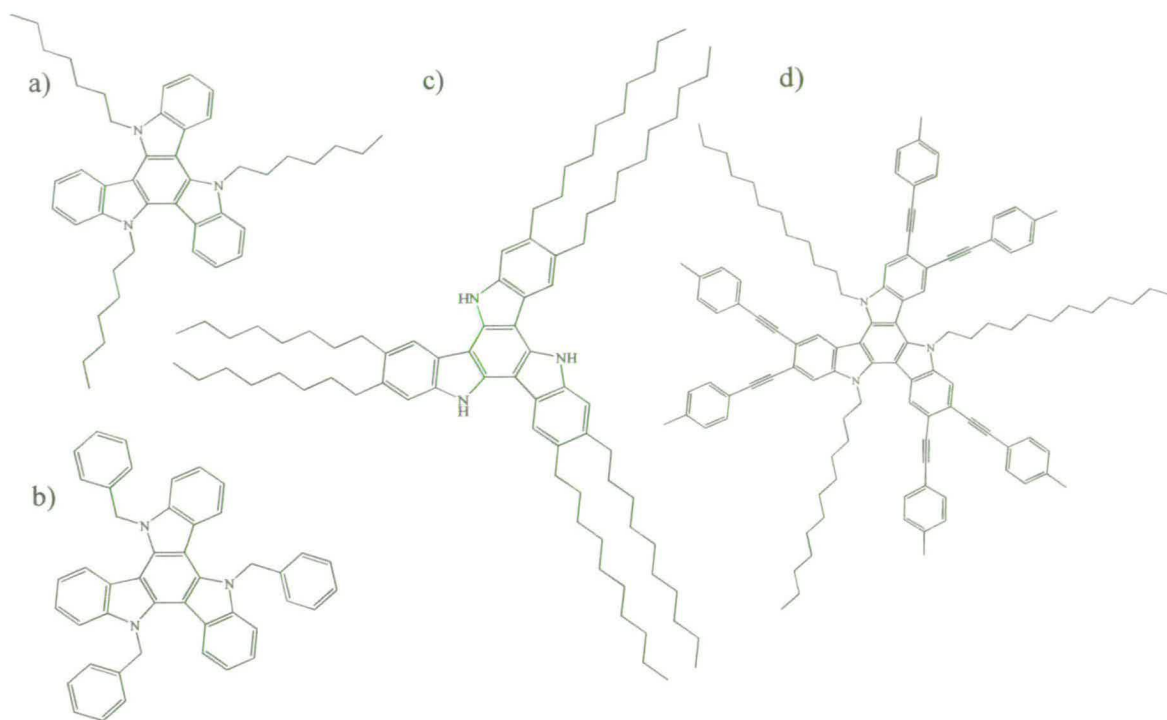
### C3 - Symmetric Triindole Species

As stated in Chapter 1 one of the most important factors in the investigation of new organic electronic materials is ease and cost of mass producing such a material. Work by Robertson et al discovered that the addition of three equivalents of Br<sub>2</sub> to indole, rather than the half equivalent required for synthesis of 2, 3 diindole results in the formation of 2, 3, 7, 8, 12, 13 hexabromo-5, 10, 15-trihydroindolo [3, 2-a, 3', 2'-c] carbazole. <sup>7</sup>



*Scheme 4.1 – Synthetic route to 2, 3, 7, 8, 12, 13 hexabromo-5, 10, 15-trihydroindolo [3, 2-a, 3', 2'-c] carbazole*

Widespread interest in the reaction has resulted in a series of C3-symmetric triindoles based on this C3-symmetric triindole starting materials, Fig 4.4. <sup>8,9,10</sup> Work by Gomez-Lor et al has resulted in the formation of a discotic liquid crystalline material based on a C3 symmetric triindole core, 2, 3, 7, 8, 12, 13 hexadecyl-5, 10, 15-trihydroindolo [3, 2-a, 3', 2'-c] carbazole, Fig 4.4c. <sup>11</sup> When a thin film FET was produced the resulting device had a charge mobility of 0.09 cm<sup>2</sup>/Vs. <sup>12</sup>

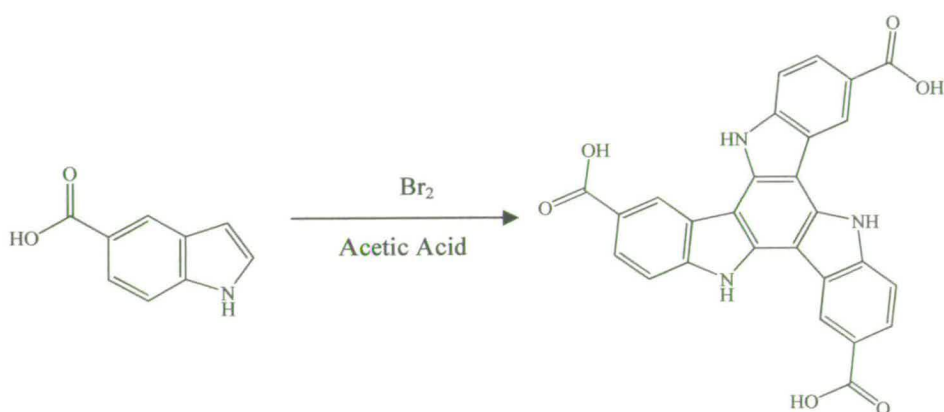


**Figure 4.4** – Selection of Molecules synthesised from 2, 3, 7, 8, 12, 13 hexabromo-5, 10, 15-trihydroindolo [3, 2-a, 3', 2'-c] carbazole starting material

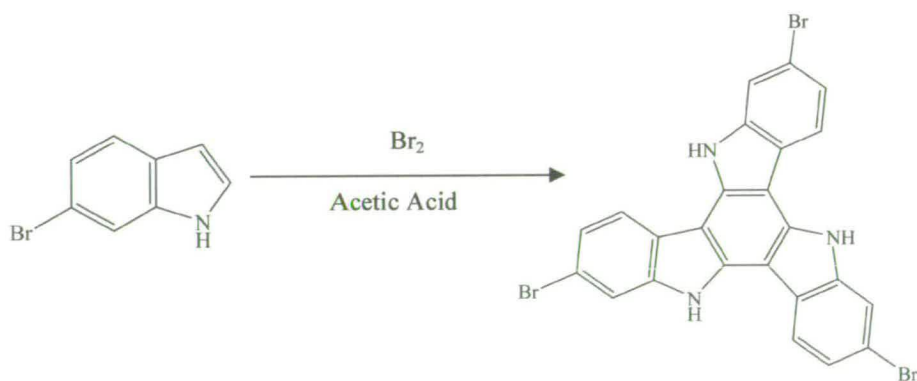
In spite of the array of possible syntheses available from the brominated triindole starting material the proximity of each bromo group to another prevents a number of potentially useful functional group conversions. This chapter reports the adaptation of the trimerisation step to produce new C<sub>3</sub>- symmetric triindole species for use as both organic electronic materials and as core materials for discotic liquid crystalline systems. These materials have been investigated through a combination of Cyclic Voltammetry, absorption and emission spectroscopy, DFT calculations and FET measurements.

## 4.2 – Synthesis

The synthesis of **4a** and **4b** has been successfully adapted from the previous synthesis of 2, 3, 7, 8, 12, 13 – Hexabromo-10, 15- dihydro-5H-indolo[3, 2-a, 3', 2'-c]carbazole <sup>7</sup> illustrated in scheme 4.1. Indole-5-carboxylic acid and 6-bromoindole were successfully oxidized using molecular bromine to form C3-symmetric cyclic substituted-triindoles, scheme 4.2 and scheme 4.3.



*Scheme 4.2 – Synthetic route to 4a*

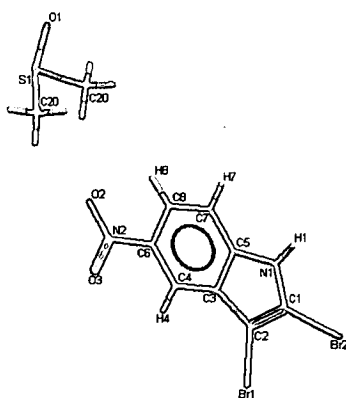


*Scheme 4.3 – Synthetic route to 4b*

As may be seen from scheme 4.1 this synthesis involves the addition of 3 equivalents of bromine to a solution of indole in acetonitrile. However, when this reaction was attempted with substituted indoles the reaction did not proceed as expected. The reaction of 5-cyano, 5-methoxy, and 5-carboxaldehyde substituted indoles resulted in a mixture of species, with no observable triindole product. It has previously been noted in Chapter 3.2 that the 5-cyano and 5-carboxaldehyde groups will preferentially react with bromine themselves, preventing the necessary formation of 3-bromo based indoles. The reaction of 5-methoxyindole gave a black solid found to be a mixture of species including the substituted 2,3-diindole that was extremely difficult to purify.

The reaction of 5-nitroindole with bromine does not give the expected product regardless of the amount of bromine added. Using 0.5 equivalents of Br<sub>2</sub> a mixture of products is formed, however using 3 equivalents of Br<sub>2</sub> a single pure product was obtained. <sup>1</sup>H-NMR analysis of this material showed only 4 peaks, 3 in the aromatic region, and suggested that the protons at the 2 and 3 positions had been removed. However a crystal structure of this material indicated that rather than triindole formation, this was due to 2,3-dibromo-substitution, Fig 4.5. From this structure it appears that in the case of 5-nitroindole reaction of the 2-position with Br is more favourable than reaction of the 3-substituted species with another monomer unit. This prevents formation of the 2,3-diindole product. The resulting 2,3-dibromo-5-nitroindole reacts with the remaining monomer to form a mixture of products. The increased addition of Br<sub>2</sub> allows the reaction to go to completion. The 2,3-dibromoindole species have long been sought

after as synthetic intermediates to a range of species.<sup>13</sup> While the one-step synthesis of a 2,3-dibrominated indole has been achieved for a number of N-alkylated species<sup>14,15</sup> it has never been successfully achieved in one-step for indoles where the Nitrogen is protonated. While polybrominated indole monomers are of particular interest in a biological context due to their apparent antibacterial and anti-fungal activity, the material properties of these systems make them unsuitable for organic electronic applications. As a result this system was not investigated further.



*Figure 4.5 – Crystal structure of the product of the reaction between 5-nitroindole and three equivalents of Br<sub>2</sub>*

The reaction of indole-5-carboxylic acid with 3 equivalents of bromine in acetonitrile gave a mixture of products, which varied in proportion based on temperature and the speed at which bromine was introduced to the reaction. At room temperature with a high rate of bromine addition the product was exclusively 2,3-dibromoindole-5-carboxylic acid however, when the rate of addition was slowed and the reaction cooled species **4a** became the dominant product. The use of acetic acid as a solvent for this reaction solved



the need for extensive purification to separate the trimer species as the excess acid catalysed the triindole formation reaction, allowing **4a** to become the kinetic product as well as the thermodynamic product.

As with the 2,3-diindoles, the use of acetic acid as a solvent allowed the investigation of 5 and 6-bromo-substituted indole species as starting materials for triindole formation. In the case of 6-bromoindole this proved extremely effective giving product **4b**. However, the reaction of 5-bromoindole gave a mixture of products that proved too difficult to separate.

In the case of 2,3,7,8,12,13-Hexabromo-10,15-dihydro-5H-indolo[3,2-a,3',2'-c]carbazole it is reported that recrystallisation of the crude product of the triindole reaction gives pure products. While this remains the case for **4a** and **4b** the quantity of product in each case makes use of this purified product for future reactions unfeasible. As a result, subsequent reactions were carried out directly from the crude product while analysis of **4a** and **4b** used the purified product. The same reaction to alkylate **2e** to form **3** was used to form **5b** from **4b**, Fig 4.6b. When the same reaction was attempted with **4a** separation of the N-alkated acid-based triindole proved impossible. However, during the reaction esterification of the three acid groups also took place giving species **5a**, Fig 4.6a, as a pure product.

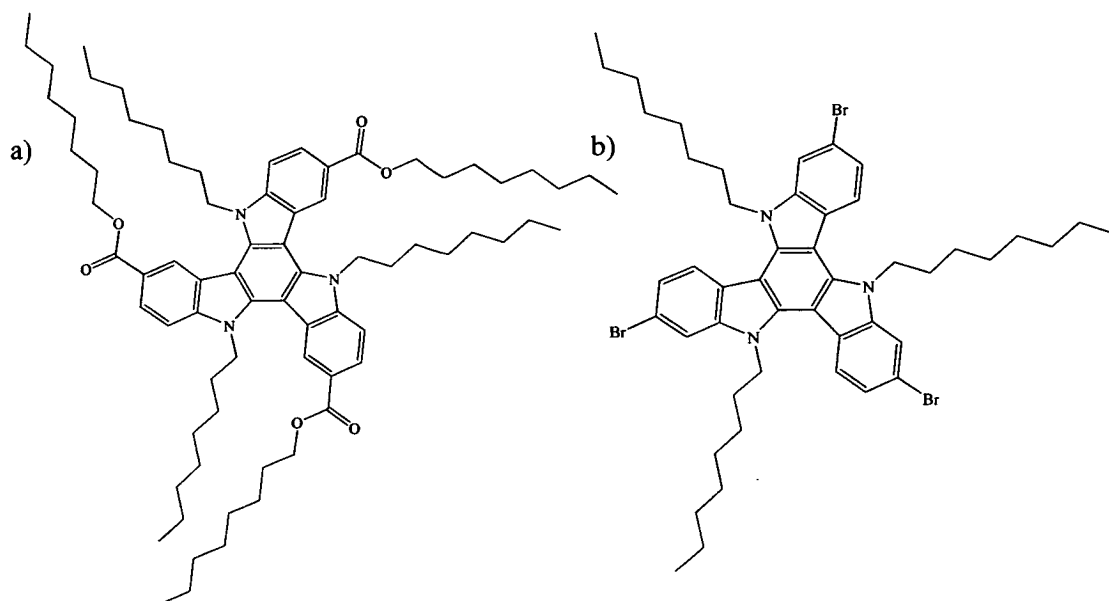
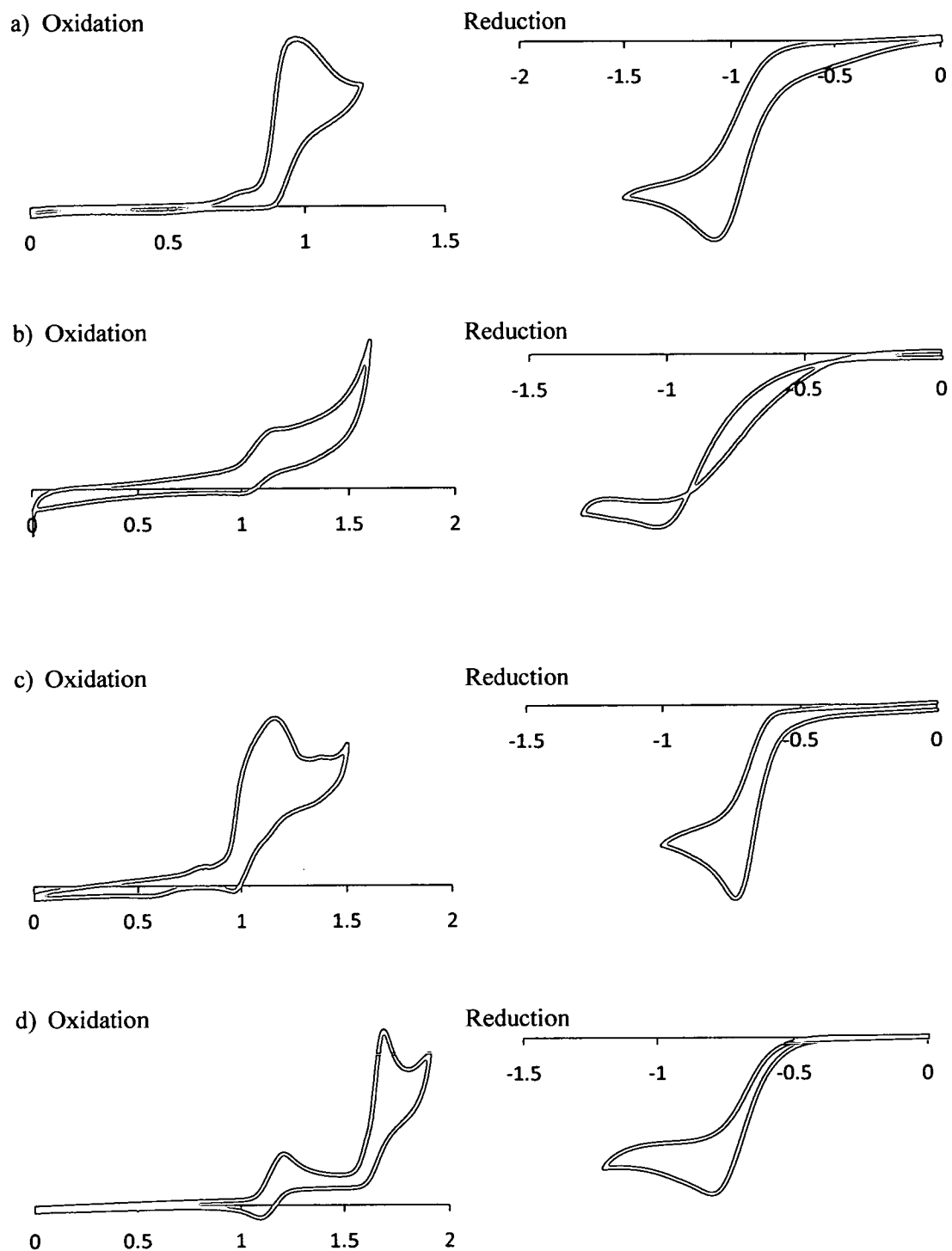


Figure 4.6 – a) Compound 5a, b) Compound 5b

## 4.3 – Electrochemistry

### *C3-Symmetric Triindoles*

Electrochemical analysis of species **4a**, **4b**, **5a** and **5b** revealed a series of oxidation and reduction potentials similar to those of the indolo[3,2-a]carbazoles. Fig. 4.6 and Table 4.1



**Figure 4.6** – Oxidation and reduction potentials of a) 4a, b) 5a, c) 4b and d) 5b

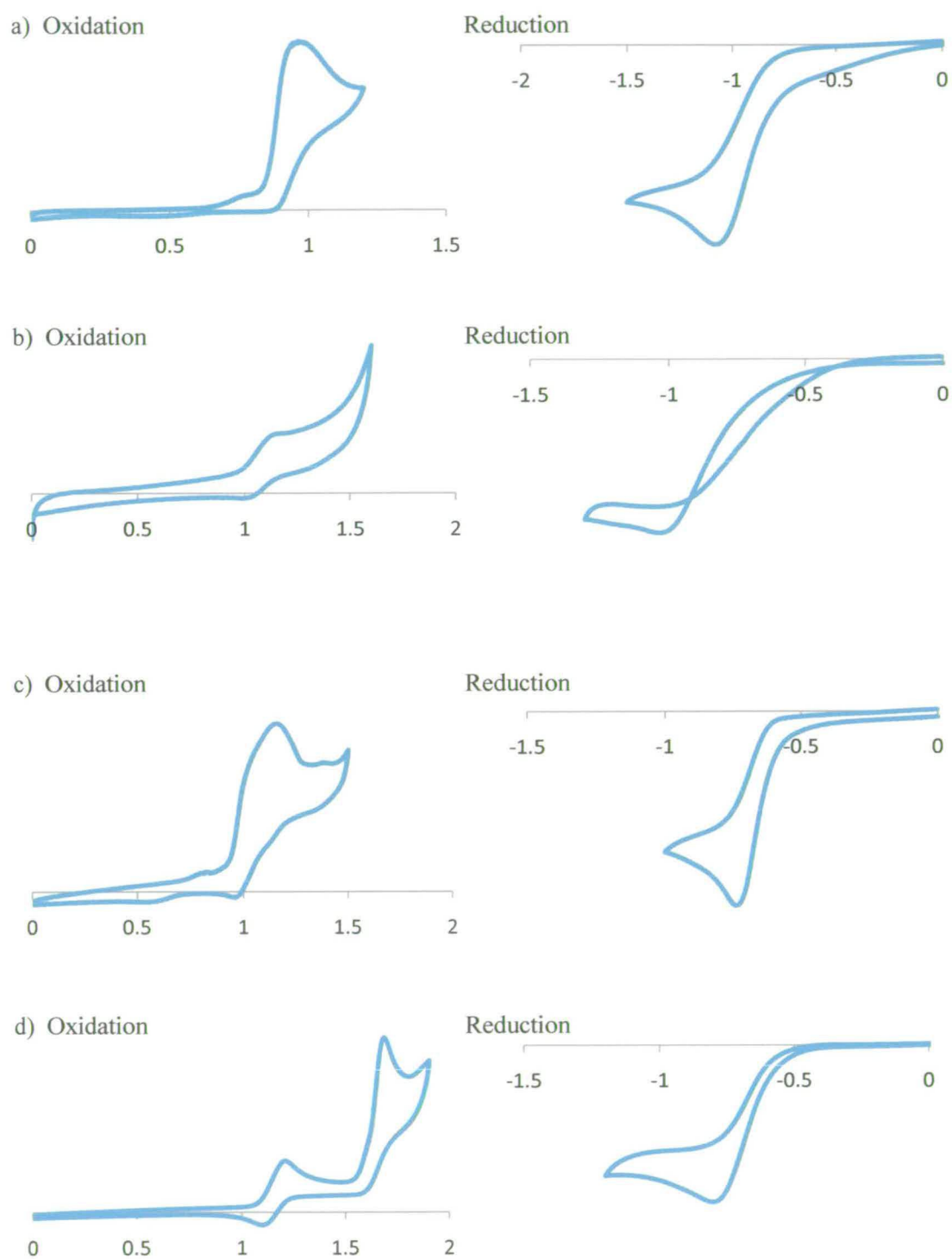


Figure 4.6 – Oxidation and reduction potentials of a) 4a, b) 5a, c) 4b and d) 5b

|    | Oxidation |       | Reduction |
|----|-----------|-------|-----------|
| 4a | 0.959     | -     | -1.084    |
| 5a | 1.054     | -     | -1.035    |
| 4b | 1.010     | -     | -0.728    |
| 5b | 1.107     | 1.631 | -0.847    |

Table 4.1 – Oxidation and reduction potentials of species **4a**, **4b**, **5a** and **5b**

Comparison of **4a** and **5a** indicates that the presence of the six octyl chains has resulted in a 0.1V increase in the oxidation potential. This suggests increased stability of the system in comparison to **4a**. This difference is repeated between species **4b** and **5b** and may be put down to extension of the inductive effect caused by the presence of the extended alkyl chains.

Analysis of **4b** and **5b** suggests a much more significant change. Now the first oxidation, which increased slightly in potential again suggesting increased stability, is fully reversible. Again this is in agreement with the work carried out by Ambrose et al,<sup>16</sup> regarding N-N cation formation in oxidized carbazole species. It is also noticeable that for **5b** this oxidation is fully reversible, while for **5a** this is not the case. Direct comparison of these systems is problematic though as different solvents were used for each system and solvent may have a profound effect on the electrochemical profile of a system.<sup>17</sup> Despite these problems it is possible to say that alkylation to form both **5a** and

**5b** resulted in a first oxidation that was more reversible than the corresponding, non-alkylated system.

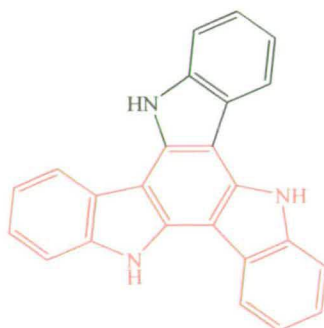
It is noticeable from the oxidation of **4b** in particular that the oxidation of the trimer species may not be a single electron oxidation process. The breadth of the oxidation peak observed for species **4a** may also indicate this s the case. Unfortunately, due to the lack of available material, differential pulse analysis could not be used to investigate the number of electrons involved.

The use of CH<sub>2</sub>Cl<sub>2</sub> as an alternative solvent for **5b** also allows a second oxidation potential to be seen due to the wider electrochemical window. It appears to be irreversible and a multi-electron-step. The nature of this oxidation will be discussed further in Section 4.6.

It is not possible to conclude that the observed reduction is substituent based as the redox potential of unsubstituted triindole remains untested however, the positions of the reduction peaks is significant.

### *Indolo[3,2-a]carbazoles vs. C3-Symmetric Triindoles*

As the C3-symmetric triindoles are based around the indolo[3,2-a]carbazole unit with the addition of an extra indole-monomer, Fig 4.7, direct comparison of the results from these species should provide a measure of the effectiveness of indole systems to form large conjugated systems.



**Figure 4.7** – Structural comparison of C3-symmetric triindole and indolo[3,2-a]carbazole (here in red)

Three of the triindole systems may also be directly compared with their equivalent indolo[3,2-a]carbazole, Table 4.2. It may be noted that the oxidation potentials reduce significantly in all three trimer systems while the reduction potentials are less negative in systems **4b** and **5b** but slightly more negative in system **4a**. Despite the slight increase in reduction potential for **4a**, the gap between oxidation and reduction potentials reduces by 0.2-0.3V in each case. This suggests that there is an increase in the conjugation in going from the carbazole to the triindole systems.

|    | Oxidation | Reduction |
|----|-----------|-----------|
| 2c | 1.270     | -1.016    |
| 4a | 0.959     | -1.084    |
| 2e | 1.182     | -0.874    |
| 4b | 1.010     | -0.728    |
| 3  | 1.170     | -0.973    |
| 5b | 1.107     | -0.847    |

*Table 4.2 – Comparison of the redox potentials indolo[3,2-a]carbazoles and the equivalent triindole species*

## 4.4 – Absorption Spectroscopy

### *C3-Symmetric Triindoles*

Previous work by Huang et al established that the unsubstituted 5, 10, 15-triheptyltriindole, Fig 4.4b, displays two characteristic absorption peaks at 316nm and 256nm,<sup>9</sup> with a number of poorly defined shoulder peaks. In the case of **4a**, **4b**, **5a** and **5b**, these shoulder peaks become much more clearly defined and a number of new transitions appear. Fig 4.7 and table 4.3

The increase in the number of transitions observed and the improved resolution of shoulder peaks between 5, 10, 15-triheptyltriindole and bromo-based trimers **4b** and **5b** may be a significant substituent effect. It may be noted that the breadth of the largest absorption peak decreases from 5000cm<sup>-1</sup> for 5, 10, 15-triheptyltriindole<sup>18</sup> to 4000cm<sup>-1</sup>



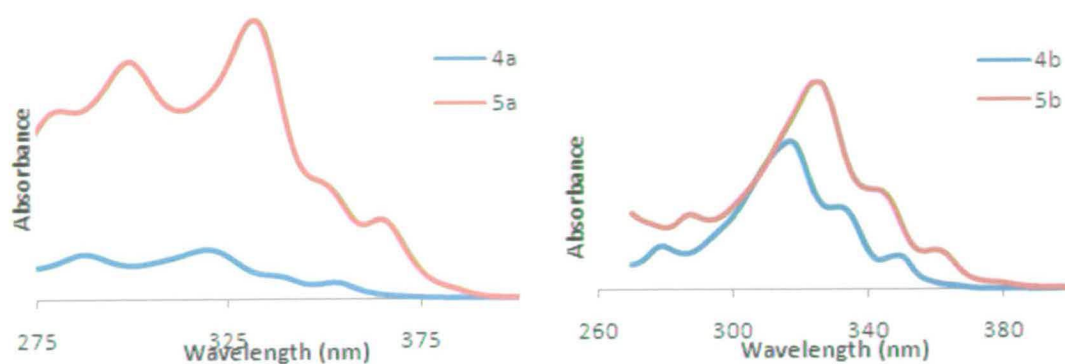


Figure 4.7 – Absorption spectra of a) Acid-based species **4a** and **5a** b) bromo-based species **4b** and **5b**

|           | Peak (nm) ( $\epsilon/M^{-1}cm^{-1} \times 10^3$ ) |             |             |            |            |
|-----------|--|-------------|-------------|------------|------------|
| <b>4a</b> | 269 (13.7)   | 288 (18.7)  | 322 (21.8)  | 339(8.9)   | 354 (7.3)  |
| <b>5a</b> | 281 (79.3)   | 299 (99.8)  | 332 (117.0) | 351(42.2)  | 365 (33.4) |
| <b>4b</b> | 279 (24.9)   | 317 (80.3)  | 331 (44.6)  | 349 (17.9) |            |
| <b>5b</b> | 287 (40.2)   | 324 (112.0) | 341 (54.2)  | 359 (21.7) |            |

Table 4.3 – Absorption peaks of **4a**, **5a**, **4b** and **5b**.

for **4b** and **5b** suggesting that there may be a significant number of transitions hidden beneath the larger transition at 316nm for 5, 10, 15-triheptyltriindole.

The number of transitions increases even further for **4a** and **5a** to five. As with the indolo[3,2-a]carbazoles this may be ascribed to differences between the frontier molecular orbitals caused by the presence of the acid and ester groups for **4a** and **5a** respectively. This is discussed more thoroughly in Section 4.6 in regard to the calculated molecular orbitals.

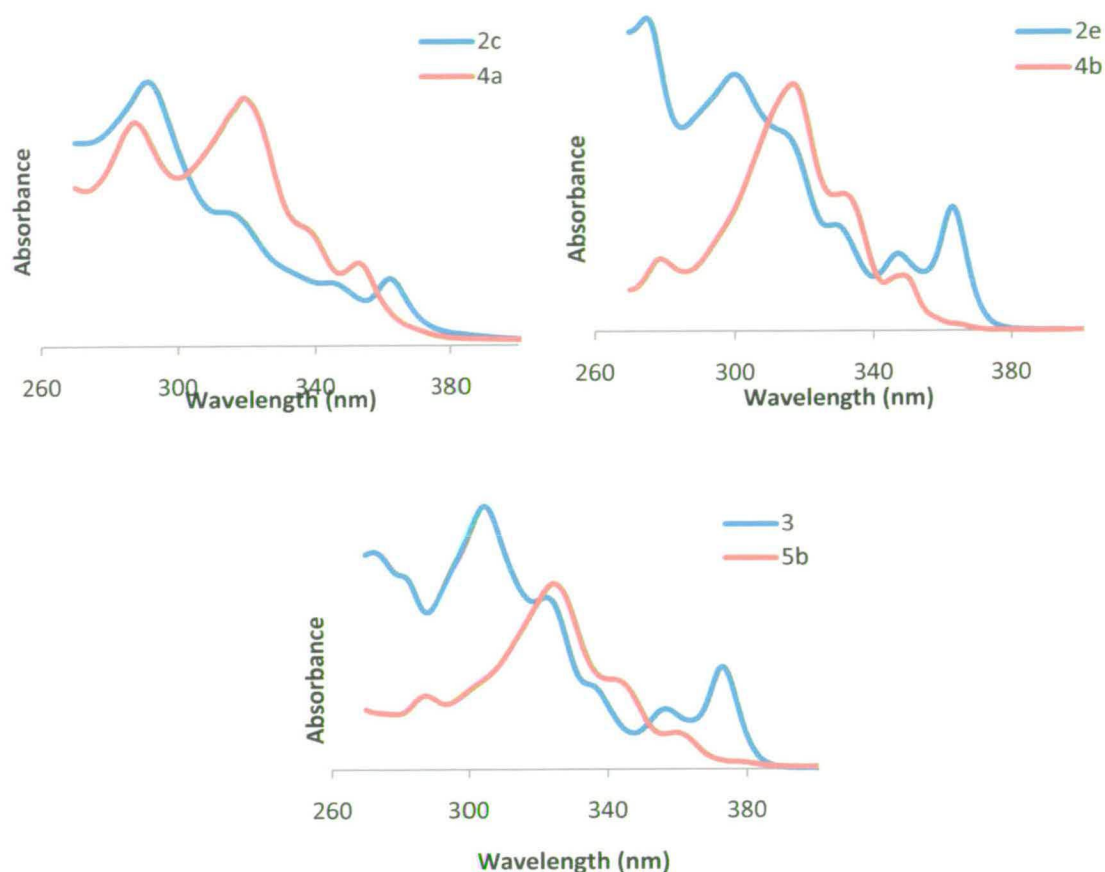
From Chapter 3 it is clear that the presence of alkyl chains on the indolic nitrogen atoms causes an inductive effect on the system ultimately leading to a  $740\text{cm}^{-1}$  red-shift in the absorption transitions. Results from the C-symmetric triindoles imply a similar inductive effect due to a red-shift of around  $1000\text{cm}^{-1}$  observed from **4a** and **4b** to **5a** and **5b**.

It should also be noted that the extinction coefficients for **4a** are significantly lower than expected based on the results for **5a**. This has been attributed to problems with solubility of the triindole species resulting in lower concentrations than accounted for and hence inaccurate determination of these values.

### *Indolo[3,2-a]carbazoles vs. C3-Symmetric Triindoles*

Direct comparison of three closely related indolo[3,2-a]carbazoles and three C3-symmetric triindoles is possible with species **2c** and **4a**, **2e** and **4b** and **3** and **5b**, demonstrating close relationships based on the presence of an extra indole monomer unit for each trimer species, Fig. 4.8 and Table 4.4.

The most noticeable difference between each triindole and the corresponding indolo[3,2-a]carbazole is that the transition energy for the lowest energy transition is lower for the indolo[3,2-a]carbazoles than the triindoles. This is contrary to what might be expected from the presence of an extra monomer unit, suggesting that the presence of the



**Figure 4.8** – Comparison of absorption spectra of a) **2c** and **4a**, b) **2e** and **4b** and c) **3** and **5b**. (Intensities not shown to scale)

|           | Peak (nm) ( $\epsilon/(M^{-1}cm^{-1} \times 10^3)$ ) |             |            |            |            |            |
|-----------|--|-------------|------------|------------|------------|------------|
| <b>2c</b> | 292 (45.1)   | 314 (23.3)  | 344 (11.0) | 362 (11.6) |            |            |
| <b>4a</b> | 269 (13.7)   | 288 (18.7)  | 322 (21.8) |            | 354 (7.3)  |            |
| <b>2e</b> | 270 (45.3)   | 300 (45.2)  | 313 (35.5) | 329 (18.6) | 347 (13.4) | 363 (21.7) |
| <b>4b</b> | 279 (24.9)   | 317 (80.3)  | 331 (44.6) | 349 (17.9) |            |            |
| <b>3</b>  | 272 (46.6)   | 305 (57.3)  | 323 (37.3) | 334 (17.4) | 356 (13.0) | 373 (21.5) |
| <b>5b</b> | 287 (40.2)   | 324 (112.0) | 341 (54.2) | 359 (21.7) |            |            |

**Table 4.4** – Comparison of absorption peaks between **2c** and **4a**, **2e** and **4b** and **3** and **5b**.

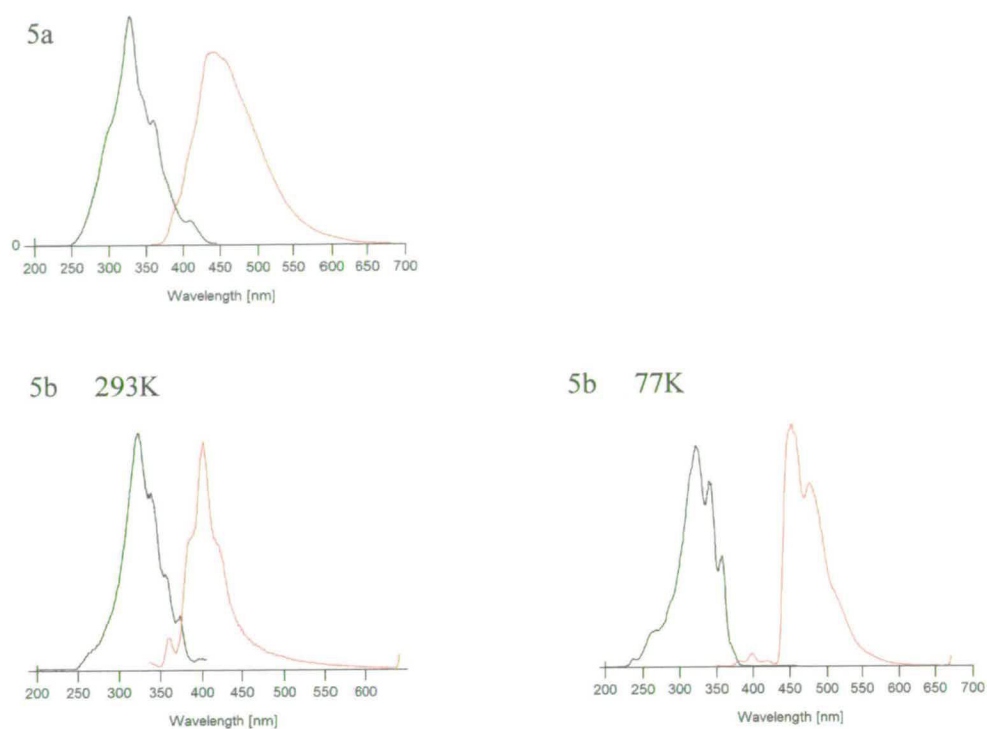
additional unit has decreased the overall conjugation of the system and increased the HOMO-LUMO gap. However, this contradicts the cyclic voltammetry results obtained for each species increased conjugation arising from the additional monomer unit. This cannot easily be explained and is further discussed in regard to DFT measurements in section 4.6.

It can also be seen that the extinction coefficients of the bromo-substituted triindoles **4b** and **5b** are significantly higher than those of the equivalent indolo[3,2-a]carbazoles **2e** and **3**. This may also be the case for **2c** and **4a** however possible solubility problems, particularly with **4a** mean quantitative analysis cannot be carried out. This is discussed further in Sections 4.6 and 4.7 in regard to the calculations undertaken based on these triindole systems.

## 4.5 – Emission Spectroscopy

### *C3 Symmetric Triindoles*

Compounds **5a** and **5b** were both found to be emissive in EtOH at 293K and studies of **5b** at 77K also discovered additional transitions, Fig 4.9, table 4.5. Species **4a** and **4b** were not studied due to lack of available product of the necessary purity.



**Figure 4.9** – Excitation and Emission Spectra of **5a** and **5b** at 293K and **5b** at 77K

|           | Emission Max  |                              |
|-----------|---------------|------------------------------|
|           | 293K          | 77K                          |
| <b>5a</b> | 435, 450, 458 | -                            |
| <b>5b</b> | 384, 401, 415 | 381, 398, 417, 453, 477, 508 |

**Table 4.5** – Emission spectra peaks for **5a** and **5b** at 293K and **5b** at 77 K Peaks

The emission spectrum of **5a** closely resembles those observed for **1c** and **2c**, being extremely broad and poorly defined. As with both **1c** and **2c**, the increased peak breadth is most likely due to the presence of alternative frontier orbitals. It may be assumed

based on the calculated orbitals of both **1c** and **2c**, that poor orbital overlap of this lower energy excited state with the ground state means that direct promotion of electrons into the lowest energy excited state is minimal, hence the similarities in absorption spectra. Interconversion of electrons in the formed excited state to this ‘new’ lower energy excited state may be followed by subsequent emission from this excited state back to the ground state. This in conjunction with emission directly from the accessible excited state back to the ground state results may well give the broad spectra. This has been discussed previously in Section 3.6 in regard to species **1c** and **2c** and will be noted further in Section 4.6.

The room temperature emission spectrum of **5b** closely resembles the expected mirror image of the excitation spectrum. This is in contrast to the hexabrominated C3 symmetric triindole, Scheme 4.1, studied by Robertson et al that was found to display no emission at room temperature. This may be attributed to the increased number of bromine atoms in the hexabrominated species, causing an increase in the heavy-atom effect, hence a greater proportion of intersystem crossing into the triplet  $T_1\pi\pi^*$  state. In the case of **5b** the rate of inter-system crossing caused by the heavy atom effect is such that the system is still fluorescent at room temperature.

The emission and excitation spectra observed for **5b** at 77K are closely related to those observed for a frozen EtOH solution of 2, 3, 7, 8, 12, 13- hexabromo-5, 10, 15-

---

trihydroindolo [3, 2-a, 3',2'-c] carbazole. The primary difference between the two species is the relative levels of phosphorescent behaviour versus fluorescent behaviour. As illustrated by the room temperature excitation spectrum a significant proportion of fluorescent behaviour is observed for species **5b**. This is not the case for hexabrominated C3 symmetric triindole.

### *Indolo [3, 2-a} carbazoles vs C3- Symmetric Triindoles*

The emission spectra of **5b** at both 293K and 77K display a number of similarities with those of **3**, Table 4.6.

|           | Emission Max  |                              |
|-----------|---------------|------------------------------|
|           | 293K          | 77K                          |
| <b>3</b>  | 376, 392      | 372, 390, 405, 446, 472, 500 |
| <b>5b</b> | 384, 401, 415 | 381, 398, 417, 453, 477, 508 |

*Table 4.6 – Comparison of the emission peaks of 3 and 5*

This suggests that excited states of **3** and **5b** are closely related. As observed through the UV/VIS spectroscopy, there are a number of differences in the excitation of both species, specifically the higher energy transition around 315nm. This difference is discussed in both Sections 4.4 and 4.6.

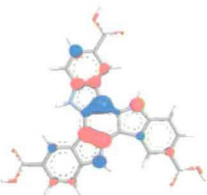
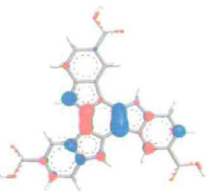
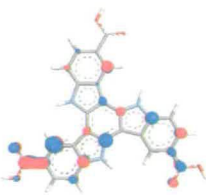
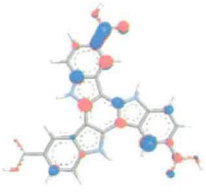
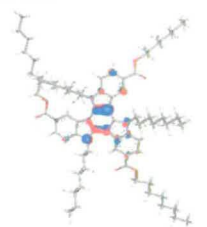
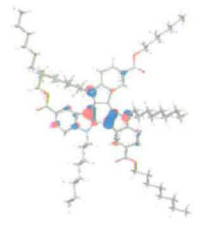
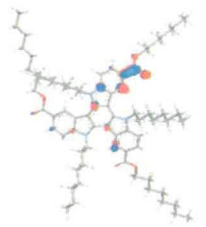
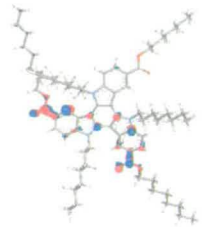
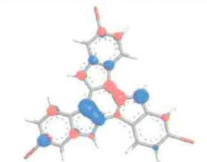
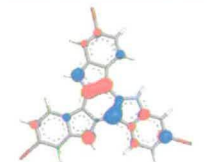
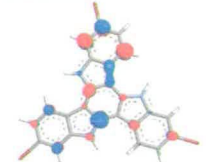
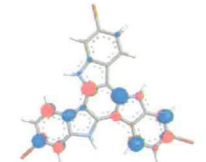
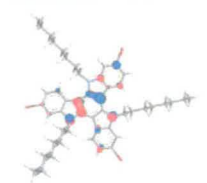
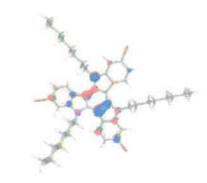
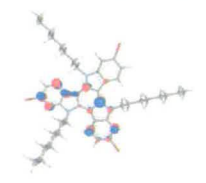
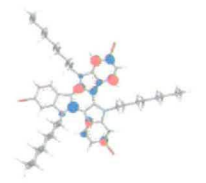
## 4.6 – DFT Calculations

### *C3-Symmetric Triindoles*

DFT calculations based on a B3LYP functional and 6-31G\* basis set have been carried out for all triindole species resulting in the calculated molecular orbitals and orbital energies noted in table 4.7

The most noticeable result of the calculations is the apparent degeneracy of the HOMO-1 and HOMO levels as well as the LUMO and LUMO+1 levels. However, given the inherent symmetry of the triindole systems it might be expected that this degeneracy would extend to the HOMO-2 and LUMO+2 as well. This is not the case with frontier orbitals closely resembling those of the indolo[3,2-a]carbazoles, along with HOMO-2 energies of -6.499eV, -5.985eV, -6.440eV and -6.099eV and LUMO+2 energies of -1.354eV -0.614eV, -1.019eV and -0.535eV for **4a**, **5a**, **4b** and **5b** respectively.



|             | HOMO-1  | HOMO  | LUMO   | LUMO+1  |
|-------------|---|---|--|---|
| 4a          |    |    |    |    |
| Energy (eV) | -5.602  | -5.601  | -1.504   | -1.504  |
| 5a          |    |    |    |    |
| Energy (eV) | -5.196  | -5.193  | -1.206   | -1.188  |
| 4b          |   |   |   |   |
| Energy (eV) | -5.466  | -5.465  | -1.046   | -1.045  |
| 5b          |  |  |  |  |
| Energy (eV) | -5.230  | -5.213  | -0.979   | -0.953  |

**Table 4.7** – Calculated geometries and energies of the frontier orbitals of 4a, 5a, 4b and 5b

The calculated HOMO-LUMO gap decreases from non-alkylated to alkylated systems from 4.10V for **4a** to 3.99eV for **5a** and from 4.42eV for **4b** to 4.23eV for **5b**. This

agrees with both the electrochemistry and the UV/Vis spectroscopy results which suggest that the addition of octyl chains to the system caused a  $1000\text{cm}^{-1}$  red-shift for the  $S_0$  to  $S_1$  transition.

As is the case for the 2,3-diindoles and indolo[3,2-a]carbazole systems, the presence of the acid and ester groups results in a significant change in the unoccupied frontier molecular orbitals, with 28% of the LUMO and LUMO+1 character residing specifically on the acid groups of **4a** and 38% of the LUMO and LUMO+1 on the ester groups of **5a**. This is in stark contrast to the 15% Br character in the LUMO and LUMO+1 of both **4b** and **5b**. This difference in functional group character of the unoccupied molecular orbitals most likely results in the differences noted between the fluorescence spectra of the acid-substituted and bromo-substituted species. However unlike the indolo[3,2-a]carbazoles there is a significant difference in the absorption spectra of the acid-substituted and bromo-substituted triindole species. These differences can be attributed to differences in orbitals further from the frontier such as those observed for the HOMO-2, fig 4.10, which has a significant proportion of functional group character for **4a** but very little for **4b**.

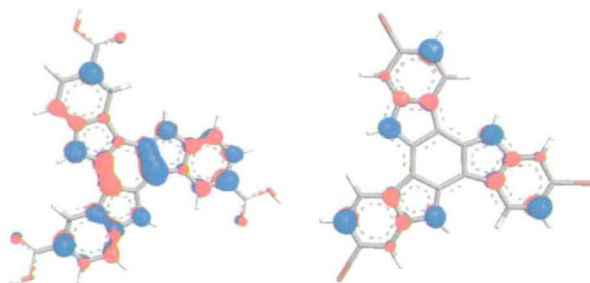
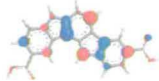
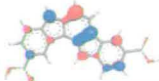
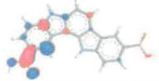
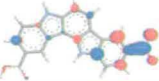




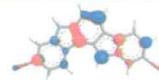
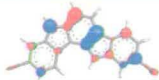
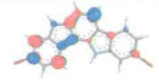
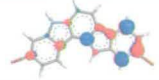










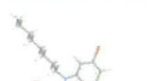



Figure 4.10 – HOMO-2 orbitals of **4a** and **4b**

### *Indolo[3,2-a]carbazoles vs. C<sub>3</sub>-Symmetric Triindoles*

The primary differences observed between the calculated molecular orbitals for the indolo[3,2-a]carbazoles and the corresponding C<sub>3</sub>-symmetric triindoles relates to the degeneracy of the HOMO-1 and HOMO and the LUMO and LUMO+1 of each triindole system. As noted in Section 3.6, seen again in Table 4.8, there is no such degeneracy between the frontier orbitals of the related indolo[3,2-a]carbazole species. This is to be expected given the lack of symmetry within the molecule. However, it is also clear from the orbital geometries displayed that there is a close relationship between the frontier orbitals of the indolo[3,2-a]carbazoles and the equivalent triindole species. This is most clearly noted via comparison of the orbital geometry on the central ring of each species. From this comparison it appears that the HOMO-1 and HOMO of **2e** and **4b** have reversed. Due to the degeneracy of the HOMO-1 and HOMO levels of **4b** this is most likely a function of the calculation itself rather than any intrinsic electronic properties of **4b** relative to **2e**.

|             | HOMO-1  | HOMO  | LUMO  | LUMO+1  |
|-------------|---|---|---|---|
| 2c          |    |    |    |    |
| Energy (eV) | -5.796  | -5.671  | -1.424  | -1.244  |
| 4a          |    |    |    |    |
| Energy (eV) | -5.602  | -5.601  | -1.504  | -1.504  |
| 2e          |    |    |    |    |
| Energy (eV) | -5.654  | -5.537  | -1.100  | -0.661  |
| 4b          |    |    |    |    |
| Energy (eV) | -5.466  | -5.465  | -1.046  | -1.045  |
| 3           |  |  |  |  |
| Energy (eV) | -5.440  | -5.310  | -0.992  | -0.614  |
| 5b          |  |  |  |  |
| Energy (eV) | -5.230  | -5.213  | -0.979  | -0.953  |

**Table 4.8** - Comparison of geometries and energies of frontier orbitals for 2c and 4a, 2e and 4b and 3 and 5b.

## 4.7 - FET Measurements

As with compound **3** in the previous chapter, a field-effect transistor based on compound **5b** was constructed via melt coating on a pre-patterned substrate. However, unlike **3** there was no characteristic I-V curve observed when a voltage was passed through the source and drain electrodes. While this may be due to **5b** being an insulator, the extremely close relationship with the known semiconductor 2, 3, 7, 8, 12, 13 hexadecyl-5, 10, 15-trihydroindolo [3, 2-a, 3', 2'-c] carbazole, Fig. 4.4a make this unlikely. The lack of necessary equipment at the University of Edinburgh has severely hampered the assessment of the charge mobility of the synthesised C3-symmetric triindoles. Fortunately, as with compound **3**, the burgeoning collaboration with the Awaga group of the University of Nagoya will allow these materials to be investigated by a group with access to the necessary equipment and techniques to thoroughly assess the electronic properties of this family of species.

## 4.8 – Conclusions

This investigation has resulted in the formation of new intermediates in the pursuit of both novel organic electronic materials and discotic liquid crystals. These provide not only new opportunities to develop a family of materials, but are also interesting functional molecules in their own right.

The electronic properties of the C<sub>3</sub>-symmetric triindoles are closely related to those of the indolo[3, 2-a]carbazoles. Like the carbazoles the presence of substituent groups appears to have little significant effect on the nature of the HOMO levels while the acid groups play a dominant role in the nature of the LUMO levels. In spite of the limited device measurements, the primary focus of this study has been achieved through the synthesis of two materials with attractive electronic properties, which offer greater scope for adaptability than other readily formed triindole materials.

## 4.9 - Experimental

### *Synthesis*

#### General Procedure for C3- Symmetric Triindole Synthesis

The substituted indole (0.5mmol) was dissolved in acetic acid (30ml) and Br<sub>2</sub> (1.1mmol) in acetic acid (20ml) was added dropwise over 5 minutes. The solution was left to stir overnight, filtered and the solid product washed with acetonitrile.

**4a** – Yield 44% - CHN for C<sub>27</sub>H<sub>15</sub>O<sub>6</sub>N<sub>3</sub> – Calc C 67.92, H 3.14, N 8.81, Found C 63.47, H 4.63, N 7.38 – <sup>1</sup>H-NMR (d<sub>6</sub>-DMSO) 12.76(3H, s), 9.42(3H, s), 8.14(3H, d J<sub>H-H</sub> 0.035), 7.87(3H, s)

**4b** – Yield 61% - CHN for C<sub>24</sub>H<sub>12</sub>N<sub>3</sub>Br<sub>3</sub> – Calc C 49.57, H 2.07, N 7.23, Found C 48.03, H 1.93, N 6.96 – <sup>1</sup>H-NMR (d<sub>6</sub>-DMSO) 12.35(3H, s), 8.81(3H, d J<sub>H-H</sub> 0.035), 8.06(3H, s), 7.75(3H, d J<sub>H-H</sub> 0.035) – FAB-MS: m/z 580(M<sup>+</sup>)

**Synthesis of 5, 10, 15 Trioctylindolo [3, 2-a, 3', 2'-c] carbazole –3, 8, 13 trioctylester, 5a - 4a**, (238mg, 0.5mmol), KOH (560mg, 0.01mol), 0.025mmol [CH<sub>3</sub>(CH<sub>2</sub>)<sub>3</sub>]<sub>4</sub>N(HSO<sub>4</sub>) (12mg, 0.025mmol) and 1-iodooctane (2.2ml, 12mmol) were dissolved in acetone (50ml) and heated under reflux for 24 hours. Once cool the solvent

was removed and the residue dissolved in  $\text{CH}_2\text{Cl}_2$  and washed with 10% aqueous HCl. The solution was dried over  $\text{MgSO}_4$  and solvent evaporated. The remaining solid was triturated with  $\text{CH}_3\text{CN}$  to give a pale yellow solid – Yield 2.09% - CHN for  $\text{C}_{75}\text{H}_{111}\text{O}_6\text{N}_3$  – Calc C 78.40, H 9.67, N 3.66, Found C 78.03, H 9.59, N 3.54 –  $^1\text{H-NMR}$  ( $d_6$ -DMSO) 9.01 (3H,s), 8.13 (3H,d  $J_{\text{H-H}}$  0.035), 7.59 (3H,d  $J_{\text{H-H}}$  0.035), 4.93 (6H, t  $J_{\text{H-H}}$  0.035), 4.37(6H, t  $J_{\text{H-H}}$  0.035), 1.91 (9H, m), 1.79 (9H, m), 1.49-1.06 (56H, m), 0.84 (9H, m), 0.71 (9H, m) – FAB-MS: m/z 1148(M<sup>+</sup>)

**Synthesis of 2, 7, 12 tribromo, 5, 10, 15 trioctyl indolo[3, 2-a, 3', 2'-c] carbazole, 5b**  
- 1.02mmol **4b** (582mg, 1.02mmol), KOH (1.12g,0.02mol),  $[\text{CH}_3(\text{CH}_2)_3]_4\text{N}(\text{HSO}_4)$  (24mg, 0.05mmol)and 1-iodooctane (2.2ml, 12mmol) were dissolved in acetone (50ml) and heated under reflux for 24 hours. Once cool the solvent was removed and the residue dissolved in  $\text{CH}_2\text{Cl}_2$  and washed with 10% aqueous HCl. The solution was dried over  $\text{MgSO}_4$  and solvent evaporated. The remaining solid was triturated with  $\text{CH}_3\text{CN}$  to give a pale yellow solid – Yield 14% - CHN for  $\text{C}_{48}\text{H}_{60}\text{N}_3\text{Br}_3$  – Calc C 63.30, H 6.59, N 4.61, Found C 62.72, H 6.49, N 4.42 –  $^1\text{H-NMR}$  ( $d_6$ -DMSO) 7.94 (3H, d  $J_{\text{H-H}}$  0.035), 7.63 (3H, s), 7.34 (3H, d  $J_{\text{H-H}}$  0.035), 1.93(6H, m), 1.04(36H, m), 0.87(9H, m) – FAB-MS: m/Z 910(M<sup>+</sup>)



## 4.10 – References

1. H. Moon, R. Zeis, E.-J. Borkent, C. Besnard, A.J. Lovinger, T. Siegrist, C. Kloc, Z. Bao, *J. Am. Chem. Soc.*, 2004, **126**, 15322
2. P. T. Boudreault, S. Wakim, M. L. Tang, Y. Tao, Z. Bao, M. Leclerc, *J. Mater. Chem.*, 2009, **19**, 2921
3. H. Usta, A. Facchetti, T. J. Marks, *J. Am. Chem. Soc.*, 2008, **130**, 8580
4. A. M. Van de Craats, J. M. Warman, A. Fechtenkotter, J. D. Brand, M. A. Harbison, K. Mullen, *Adv. Mater.*, 1999, **11**, 1469
5. I. O. Shklyarevskiy, P. Jonkheijm, N. Stutzmann, D. Wasserberg, H. J. Wondergem, P. C. M. Christianen, A. P. H. J. Schenning, D. M. de Leeuw, Z. Tomovic, J. Wu, K. Müllen, J. C. Maan. *J. Am. Chem. Soc.*, 2005, **127**, 16233
6. Y. Yang, S.C. Chang, J. Bharathan, J. Liu, *J. Mater. Sci.: Mater. Electron.*, 2000, **11**, 89
7. N. Robertson, S. Parsons, E.J. MacLean, R.A. Coxall, A.R. Mount. *J. Mat. Chem.*, 2000, **10**, 2043
8. E. M. Garcia-Frutos, B. Gomez-Lor, A. Monge, E. Gutierrez-Puelba, I. Alkorta, J. Elguero, *Chem. Eur. J.*, 2008, **14**, 8555
9. W.-Y. Lai, Q.-Y. He, D.-Y. Chen, W. Huang, *Chem. Lett.*, 2008, **37**, 986
10. B. Gomez-Lor, E. M. Garcia-Frutos, *J. Am. Chem. Soc.*, 2008, **130**, 9173
11. B. Gomez-Lor, B. Alonso, A. Omenat, J. L. Serrano, *Chem. Commun.*, 2006, **48**, 5012

12. M. Talarico, R. Termine, E. M. Garcia-Frutos, A. Omenat, J. L. Serrano, B. Gomez-Lor, A. Golemme, *Chem. Mater.*, 2008, **20**, 6589
13. Y. Liu, G. W. Gribble, *Tet. Lett.*, 2002, **43**, 7135
14. Y. Liu, G. W. Gribble, *J. Nat. Prod.*, 2002, **65**, 748
15. S. Tang, J.-H. Li, Y.-X. Xie, N.-X. Wang, *Synth.*, 2007, **10**, 1535
16. J. F. Ambrose, L. L. Carpenter, R. F. Nelson, *J. Electrochem. Soc.*, 1975, **122**, 876
17. V. Gutmann, G. Resch, W. Linert, *Coord. Chem. Rev.*, 1982, **43**, 133
18. W.-Y. Lai, Q.-Y. He, R. Zhu, Q.-Q. Chen, W. Huang, *Adv. Funct. Mater.*, 2008, **18**, 265

## Chapter 5

# Indolo[2,3-a]carbazoles

### 5.1 – Introduction

Previous chapters of this thesis have focused on materials which have been largely ignored in terms of both synthesis development and material properties. Unlike the indolo[3,2-a]carbazoles and the C3-symmetric triindoles, a wide range of synthetic literature exists in regard to indolo[2,3-a]carbazoles,<sup>1,2</sup> largely due to the use of Staurosporine, Fig 5.1, and its derivatives as anti-cancer-agents.<sup>3</sup>

Numerous syntheses of Staurosporine have been documented,<sup>4</sup> the most successful involving the synthesis of the indolo[2,3-a]pyrrolo[3,4-c]carbazol-5-one unit and subsequent reaction with a  $\gamma$ -lactam.<sup>5</sup> As a result a number of synthetic routes to indolo[2,3-a]carbazole systems have been observed.<sup>6,7</sup>

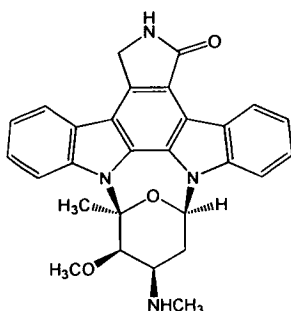
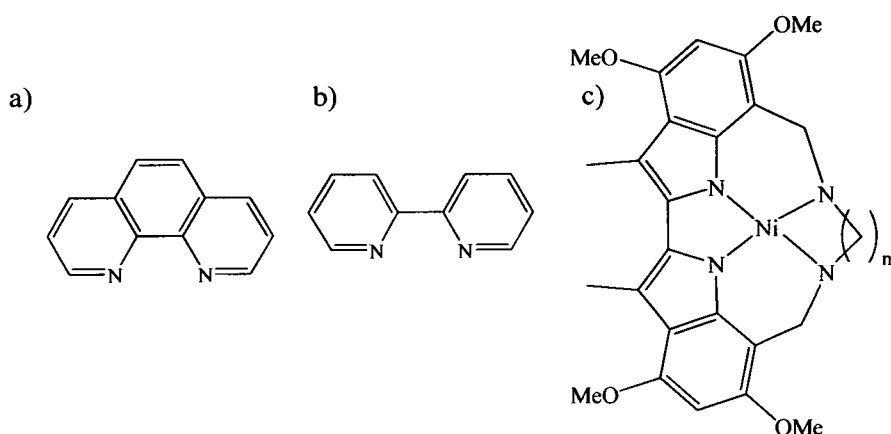


Figure 5.1 – Staurosporine.

While the biological applications of indolo[2,3-*a*]carbazoles have also been widely reported,<sup>8</sup> the material properties have largely been overlooked. Given the volume of available literature for these species and the close relationship between the indolo[2,3-*a*]carbazoles and indolo[3,2-*b*]carbazoles it is expected that the electronic properties of indolo[2,3-*a*]carbazoles may be of significant interest.

Work in this Chapter will focus on the material properties of indolo[2,3-*a*]carbazole systems. This will take two forms; the first involves the characterization of some previously synthesized indolo[2,3-*a*]carbazole-based species and analysis of these species in comparison to alternative indolocarbazoles, including those observed in Chapter 3. The second involves the synthesis and characterization of the first known coordination compound based on an indolo[2,3-*a*]carbazole species.

A number of carbazole based species have previously been used as monodentate ligands for an extremely wide-range of metals. However, despite the similarity between 1,10-



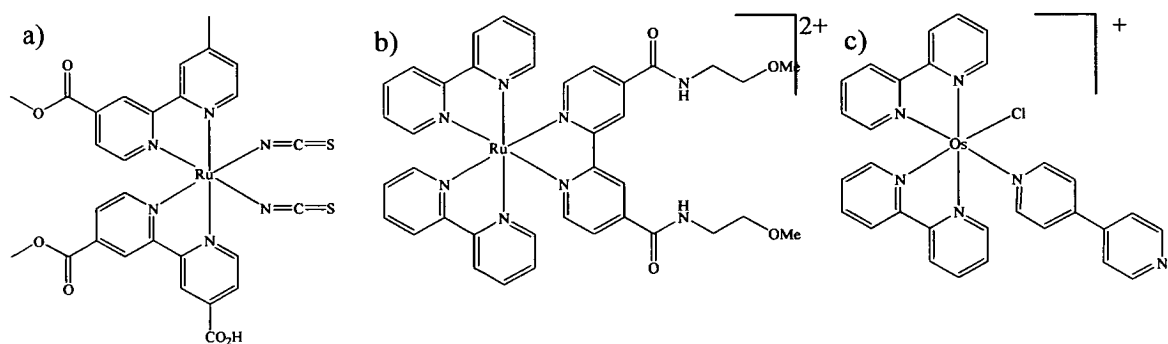
**Figure 5.2** – a) 1,10 Phenanthroline, b) 2,2-Bipyridine, c) Nickel-bisindole complex.

phenanthroline and 2,2-bipyridine, Fig 5.2, two of the most widely used bidentate ligands, and indolo[2,3-a]carbazoles, no reports of coordination compounds exist and there is only one report of a 2,2-diindole based complex, Fig 5.2c.<sup>9</sup>

The known properties of 1,10-phenanthroline and 2,2-bipyridine based complexes and expected similarities with indolo[2,3-a]carbazole complexes make compounds based on this ligand of particular interest.<sup>10,11</sup> In order to investigate the properties of the indolo[2,3-a]carbazoles as ligands, a ruthenium polypyridyl-based complex was formed. The range of known ruthenium-polypyridyl complexes available for comparison, in conjunction with the potential properties of such a system makes a ruthenium bisbipyridyl indolo[2,3-a]carbazole complex ideal for the initial investigations into indolo[2,3-a]carbazole-based species as ligands.

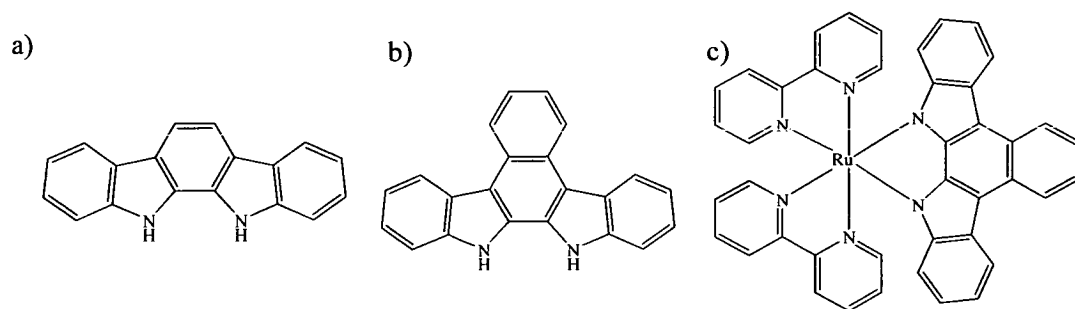
Polypyridyl-ruthenium complexes have been studied in great detail due to the impressive material properties and stability of these systems, with similar investigations now underway for polypyridyl osmium, iridium and rhodium complexes.<sup>12</sup>

Interest in polypyridyl-ruthenium complexes began in earnest when it was discovered that it was thermodynamically possible for ruthenium trisbipyridine to split water using sunlight.<sup>13,14</sup> Unfortunately the efficiency of these early systems were low due to the rate of reaction of  $\text{Ru}[\text{bipy}]_3^{2+}$  to form  $\text{Ru}[\text{bipy}]_3^{3+}$  and the high reactivity of the resulting  $\text{Ru}^{3+}$ . As a result much work has been carried out on this system to reduce the potential reactions of  $\text{Ru}^{3+}$ , including study of a range of electrolytes and heterogeneous support systems.<sup>15</sup> Ultimately this led to a greater understanding of the excited-state chemistry of ruthenium-polypyridyl complexes and to the synthesis of a vast array of materials, Fig 5.3, some of which are useful for a range of applications including; electroluminescent displays,<sup>16</sup> sensors,<sup>17</sup> dye sensitized solar cells (DSSC's)<sup>10</sup> and molecular electronic devices.<sup>18</sup> The potential applications for these materials stem from a number of interesting properties including; the stability, the absorption maximum of the MLCT transition, and the long-lived excited state. These properties may be changed through the modification or substitution of a 2,2-bipyridine ligand resulting in some of the functional molecules observed in Fig 5.3.



**Figure 5.3** – a) N719, b) Modified  $Ru[bipy]_3^{2+}$  forming an anion sensor, c) Osmium bipyridyl molecular semiconductor

As stated previously the first part of this chapter will report the properties of indolo[2,3-*a*]carbazole systems **6a** and **6b**, Fig 5.4 a and b. As with the indolo[3,2-*a*]carbazoles investigations will be carried out via cyclic voltammetry, UV/Vis spectroscopy, emission studies and DFT calculations. The second part of this chapter will describe the synthesis and properties of **7**, Fig 5.4c. This system has also been characterized by cyclic voltammetry, UV/Vis spectroscopy, emission studies and DFT calculations with the addition of spectroelectrochemistry to probe the redox states of the system.

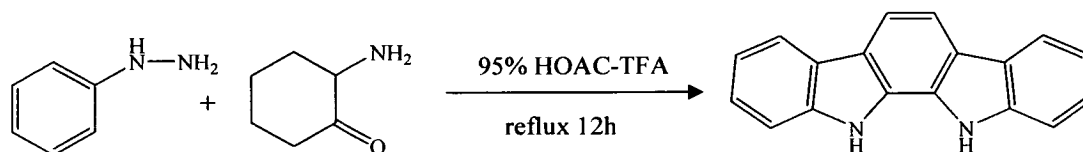


**Figure 5.4** – a) Indolo[2,3-*a*]carbazole, **6a**, b) Benzo[*c*]indolo[2,3-*a*]carbazole, **6b** and c) Ruthenium bis-bipyridyl benzo[*c*]indolo[2,3-*a*]carbazole complex, **7**

## 5.2 – Indolo[2,3-a]carbazoles

### 5.2.1 – Synthesis

While a number of possible synthetic routes to **6a** exist, that chosen, Scheme 5.1,<sup>19</sup> was used due to the expected yield and the availability of materials.



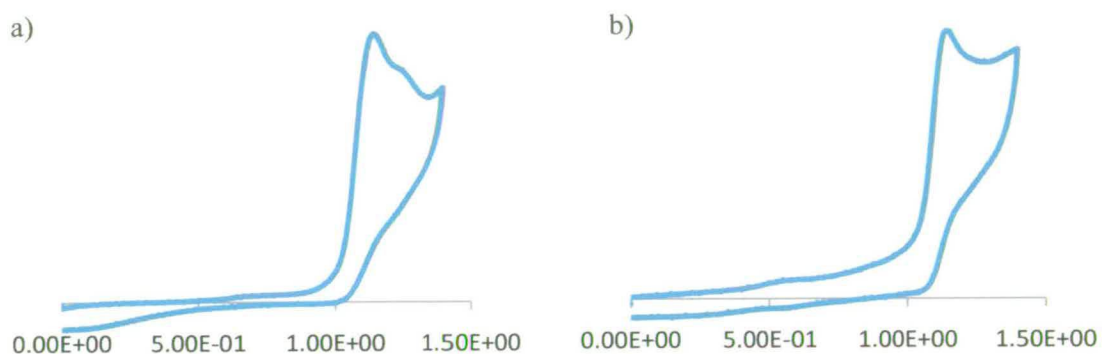
Scheme 5.1 – Synthesis of **6a**

The synthesis of **6b** was carried out using the only reported synthetic route.<sup>19,20</sup>

### 5.2.2 – Electrochemistry

Upon electrochemical analysis of species **6a** and **6b**, Fig. 5.5 and Table 5.1, both display an oxidation around 1.1V and no reduction peaks. The potential of **6b** is 0.04V higher than that of **6a**. This may be indicative of increased stability towards oxidation for **6b** against **6a** which might be expected from the addition of the benzene ring to **6b**. However due to the proximity of the oxidation potentials it is difficult to draw conclusions in this regard with any certainty.



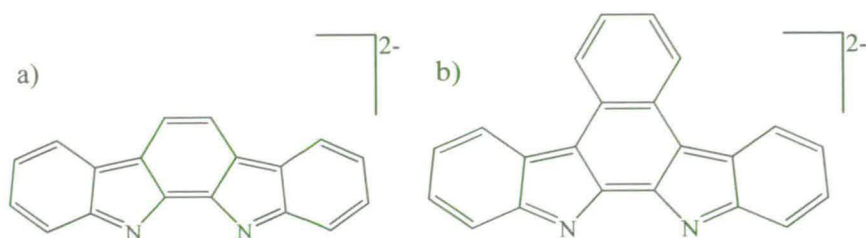


**Figure 5.5** – Electrochemical oxidation potential of a) **6a** and b) **6b** against Ag/AgCl reference in 0.1MTBABF<sub>4</sub>/DMF

|           | Oxidation |       |
|-----------|-----------|-------|
|           | <b>6a</b> | 1.117 |
| <b>6b</b> | 1.154     | -     |

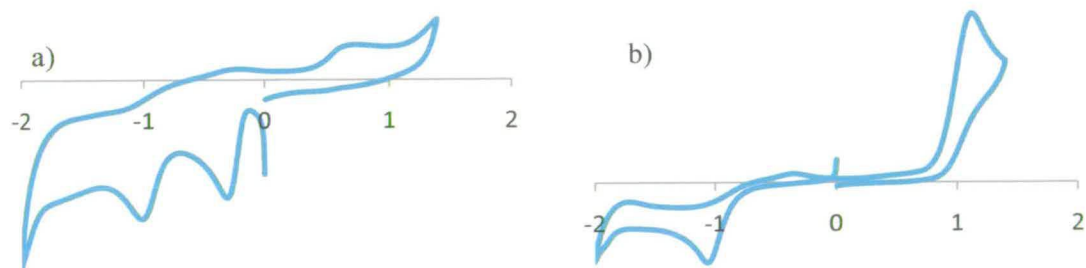
**Table 5.1** – Electrochemical potentials of **6a** and **6b**

The major difference between the species is the appearance of a second oxidation peak for **6a**. The oxidation of **6a** and **6b** is expected to result in the species seen in Fig. 5.6a and b respectively. Oxidation of **6a** and **6b** to these species would be the result of a 2-electron oxidation. Due to the added stability of the  $\pi$ -structure of **6b** it would be expected that the 2 oxidations required would be closer together so it is believed that the oxidation process of **6b** is a 2-electron process whereas that of **6a** suggests two single-electron processes despite the proximity of the two processes.



**Figure 5.6** – Expected oxidized forms of a) **6a** and b) **6b**

After bulk oxidation of **6a**, with two electrons transferred per molecule, cyclic voltammetry of the newly oxidised species showed two reduction peaks and a single, small return oxidation peak. Fig 5.7a.

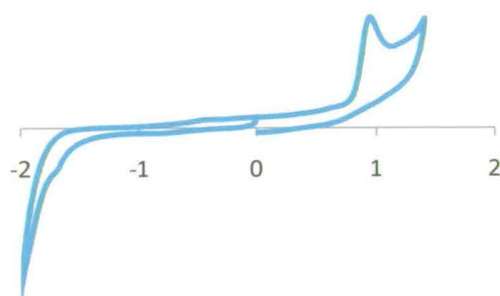


**Figure 5.7** – Coulometry results a) Cyclic voltammetry after bulk oxidation, b) cyclic voltammetry of oxidised species with 2 equivalents triethylamine

The position of the first reduction peak at  $-0.35\text{V}$  is indicative of reduction of  $\text{H}^+$  as seen in Chapter 3.3. This is expected as oxidation of **6a** will liberate two equivalents of  $\text{H}^+$  which, upon reduction will be lost as  $\text{H}_2$  gas. The liberation of  $\text{H}_2$  makes reduction of the

oxidized species to reform **6a** impossible hence subsequent oxidations do not follow the same process, resulting in the change observed in oxidation potential.

Quantitative addition of triethylamine removes  $H^+$  from the solution so reduction to  $H_2$  is no longer observed and reduction to **6a** is possible as reformation of the pyrrole rings strips the protons from triethylamine. As a result the oxidation potential returns to 1.12V, Fig 5.7b. This process is reversible and bulk reduction of **6a** results in the electrochemical profile observed in Fig 5.8, with no reduction peak observed.



*Figure 5.8 – Cyclic voltammetry after bulk reduction of oxidised species*

***Indolo[2,3-*a*]carbazoles vs. Indolo[3,2-*a*]carbazoles vs. Indolo[3,2-*b*]carbazoles***

A comparison between the cyclic voltammogram of **2a** and **6a** along with that of 5,11-dioctylindolo[3,2-*b*]carbazole, Fig. 5.9, **OINCb**,<sup>21</sup> shows some significant differences, Table 5.2. (Electrochemical analysis of unsubstituted indolo[3,2-*b*]carbazole has never been undertaken.)

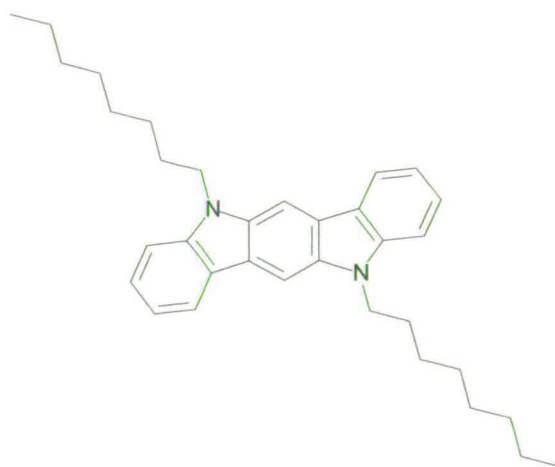


Figure 5.9 – 5,11-Dioctylindolo[3,2-*b*]carbazole, **OINCb**.

|              | Oxidation |
|--------------|-----------|
| <b>2a</b>    | 1.089     |
| <b>6a</b>    | 1.117     |
| <b>OINCb</b> | 0.856*    |

\* Adapted from results from SCE reference to equivalent for value for sat KCl Ag/AgCl reference

Table 5.2 – Electrochemical potentials of Indolocarbazoles.

Though the octyl chains on **OINCb** may make some difference to the oxidation potential it is more likely that the same pattern as that of **2e** and **3** will be followed and the oxidation will become reversible but remain in the same position. The 0.25V shift in potential between **OINCb** and those of **2a** and **6a** may be due to the indolic nitrogen atoms being para to each other rather than ortho or meta. The importance of the nitrogens to the properties of indolo[3,2-*a*]carbazoles has been noted previously. The two nitrogen atoms being para to each other would be expected to have a significant effect on the nature of the HOMO and LUMO levels and hence on the HOMO-LUMO gap and the oxidation and reduction processes.

Unfortunately neither indolo[2,3-*b*]carbazole or indolo[2,3-*c*]carbazole have been analyzed electrochemically. These systems might be expected to have oxidation potentials related to **2a** and **6a** for indolo[2,3-*b*]carbazole and **OINCb** for indolo[2,3-*c*]carbazole but this hypothesis cannot be fully tested via electrochemical analysis.

### 5.2.3 – UV/Vis Spectroscopy

The most noticeable difference between the absorption spectra of **6a** and **6b**, Fig 5.10 and Table 5.3 is the strength of the lowest energy transitions, with a 5-fold increase in  $\epsilon$  for the  $S_0$  to  $S_1$  transition from **6a** to **6b** and a 2-fold increase for  $S_0$  to  $S_2$ . This increase

in  $\epsilon$ , along with the red-shift in absorption maxima may be attributed to the increase in the size of the  $\pi$ -structure.

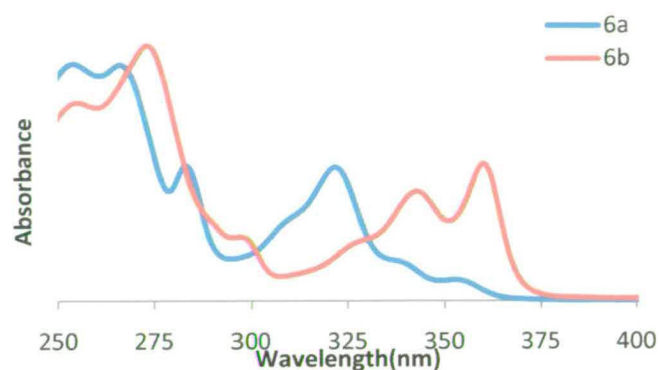


Figure 5.10 – UV/Visible Absorption Spectra for 6a and 6b

|    | Peak (nm) ( $\epsilon/ M^{-1}cm^{-1} \times 10^3$ ) |            |            |            |            |            |
|----|---|------------|------------|------------|------------|------------|
| 6a | 254 (46.2)  | 266 (46.1) | 283 (21.0) | 322 (22.9) | 336 (7.6)  | 353 (3.8)  |
| 6b | 255 (26.2)  | 273 (30.2) | 297 (9.0)  | 330 (8.6)  | 343 (19.2) | 360 (23.8) |

Table 5.3 – UV/Visible Absorption Peaks for 6a and 6b

### Indolocarbazole Comparison

A comparison between the spectra of 2a, 6a, OINCb,<sup>21</sup> 1-methylindolo[2,3-*b*]carbazole,<sup>22</sup> Fig 5.11a and 5,8-dimethylindolo[2,3-*c*]carbazole,<sup>23</sup> Fig 5.11b, show some significant differences, Table 5.4.

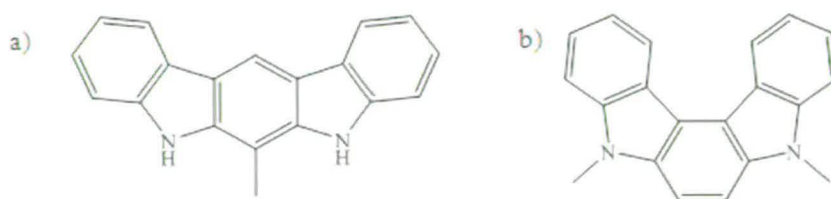


Figure 5.11 – a) 1-methylindolo[2,3-*b*]carbazole b) 5,8-dimethylindolo[2,3-*c*]carbazole

|  | Peak (nm) * |            |            |
|--|-------------|------------|------------|
| 2a   | 324 (18.5)  | 344 (16.6) | 359 (33.2) |
| 6a   | 322 (25.9)  | 336 (7.6)  | 353 (3.8)  |
| 1-methylindolo[2,3- <i>b</i> ]carbazole      | 320 (11.3)  | 343 (10.1) | 358 (15.4) |
| 5,8-dimethylindolo[2,3- <i>c</i> ]carbazole  | 379 (5.4)   | 393 (4.7)  | 401 (8.5)  |
| 5,11-dimethylindolo[3,2- <i>b</i> ]carbazole | 372 (3.2)   | 396 (4.4)  | 419 (7.2)  |

Table 5.4 – Absorption peaks of Indolocarbazole systems

The absorption spectra of other, non-alkylated indolo[2,3-*b*]carbazole, indolo[2,3-*c*]carbazole and indolo[3,2-*b*]carbazoles have never been measured. However, given that the difference in the energy of transitions of species **2e** and alkylated analogue **3** is around  $740\text{cm}^{-1}$ , the differences between the alkylated indolocarbazole species and their non-alkylated analogues cannot account for the differences observed between the various indolocarbazole species. The differences between spectra appear to agree with the hypothesis put forward after the Section 5.2.2, the decreasing energy of the HOMO-LUMO gap between the synthesised species and **OINCb** may be attributed to the effect of para indolic nitrogen atoms. In the case of both **OINCb** and 5,8-dimethylindolo[2,3-

c]carbazole the  $S_0$  to  $S_1$ ,  $S_0$  to  $S_2$  and  $S_0$  to  $S_3$  transitions are all at significantly lower energy than the equivalent transitions in **2a**, **6a** and 1-methylindolo[2,3-*b*]carbazole.

Comparison of the extinction coefficients of the various carbazole species show a pattern emerging which suggests that **6a** is particularly unusual. For all indolocarbazole species with the exception of **6a**, the  $S_0$  to  $S_1$  transition is significantly stronger than the  $S_0$  to  $S_2$  and  $S_0$  to  $S_3$  transitions. This is also true of **6b**, indicating that this holds true of all indolocarbazole species and a fundamental characteristic of **6a** causes this difference. This is discussed in Chapter 5.2.5 in regard to TD-DFT calculations of the expected absorption spectra.

#### 5.2.4 – Emission Studies

The emission and excitation spectra of **6a** and **6b** have been recorded at 293K in EtOH, Fig 5.12, Table 5.5

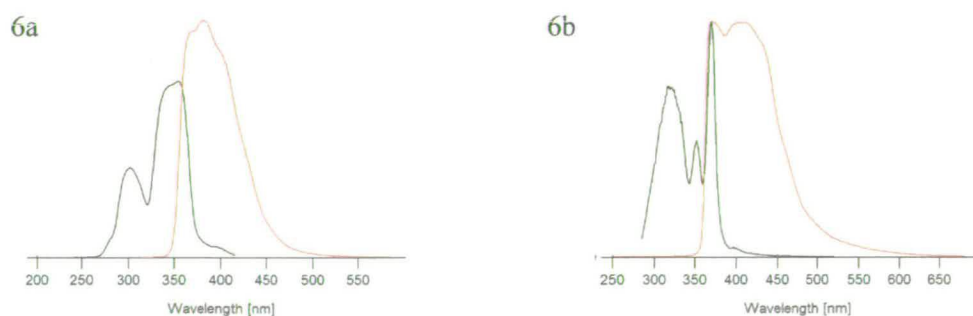


Figure 5.12 – Emission Spectra of **6a** and **6b** at 293K



|    | Emission Max  |
|----|---------------|
|    | 293K          |
| 6a | 367, 380, 398 |
| 6b | 370, 394, 404 |

Table 5.5 – Emission peaks for 6a and 6b at 293K

The excitation spectra of both **6a** and **6b** show three transitions with a red-shift in those from **6b** accounted for by the increase in  $\pi$ -structure. The close relationship between the systems implies that the excited states of **6a** and **6b** are closely related.

### Indolocarbazole Comparison

Comparison of the emission spectra of **2a** and **6a**, Table 5.6, indicates that unlike the absorption spectra, the emission spectra of **2a** and **6a** are closely related. From this it may be inferred that while the structure of the indolocarbazole unit has a significant effect on the ground state, the excited state is less dependent on the molecular arrangement of the indolocarbazole than on the nature of indolocarbazoles as a species. Unfortunately emission studies have not been carried out on any of the indolo[2,3-b]carbazoles, indolo[2,3-c]carbazoles or indolo[3,2-b]carbazoles so this cannot be confirmed.

|    | Emission Max  |
|----|---------------|
|    | 293K          |
| 2a | 363, 374      |
| 6a | 367, 380, 398 |

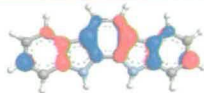
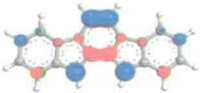


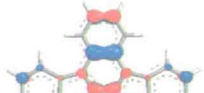
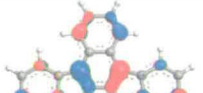
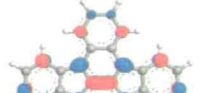
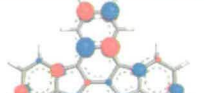
Table 5.6 – Emission peaks for 6a and 6b at 293K

### 5.2.5 – DFT Calculations

#### *Indolo[2,3-*a*]carbazoles*

Calculations based on the indolo[2,3-*a*]carbazole species **6a** and **6b** have resulted in the molecular orbitals and predicted orbital energies observed in Table 5.7.

It is immediately apparent that the energy of the occupied frontier orbitals of **6a** and **6b** have reversed, with the HOMO-1 of **6a** closely related to the HOMO of **6b** and vice versa. The same cannot be said of the unoccupied frontier orbitals, with the LUMO and LUMO+1 of **6a** seemingly related to the equivalent orbital of the **6b**. This may well give rise to the observed differences between the electronic spectra of **6a** and those of alternative indolocarbazole systems, including **6b**.

|             | HOMO-1  | HOMO  | LUMO   | LUMO +1   |
|-------------|---|---|--|---|
| <b>6a</b>   |  |  |  |  |
| Energy (eV) | -5.362  | -5.136  | -0.782   | 0.122   |
| <b>6b</b>   |  |  |  |  |
| Energy (eV) | -5.324  | -5.108  | -1.095   | -0.014  |

**Table 5.7** - Calculated geometries and energies of the frontier orbitals of **6a** and **6b**

This may be explained via the extent of the role played by the extra phenyl ring in both of the observed frontier occupied molecular orbitals. This redistribution of the electron density reduces the electron density located around the nitrogen atoms in what is the HOMO for **6a** and the HOMO-1 for **6b**. As a result, the size of the anti-bonding interaction between the nitrogen atoms and the 2,2-bond is reduced. Thus the energy of this particular molecular orbital is reduced for **6b** to such an extent that it is no longer the highest energy occupied orbital.

### 5.2.6 - TD-DFT

TD-DFT calculations were carried out for both **6a** and **6b**, Fig. 5.13. The energies, oscillator strength and composition are reported in Table 5.8 and 5.9.

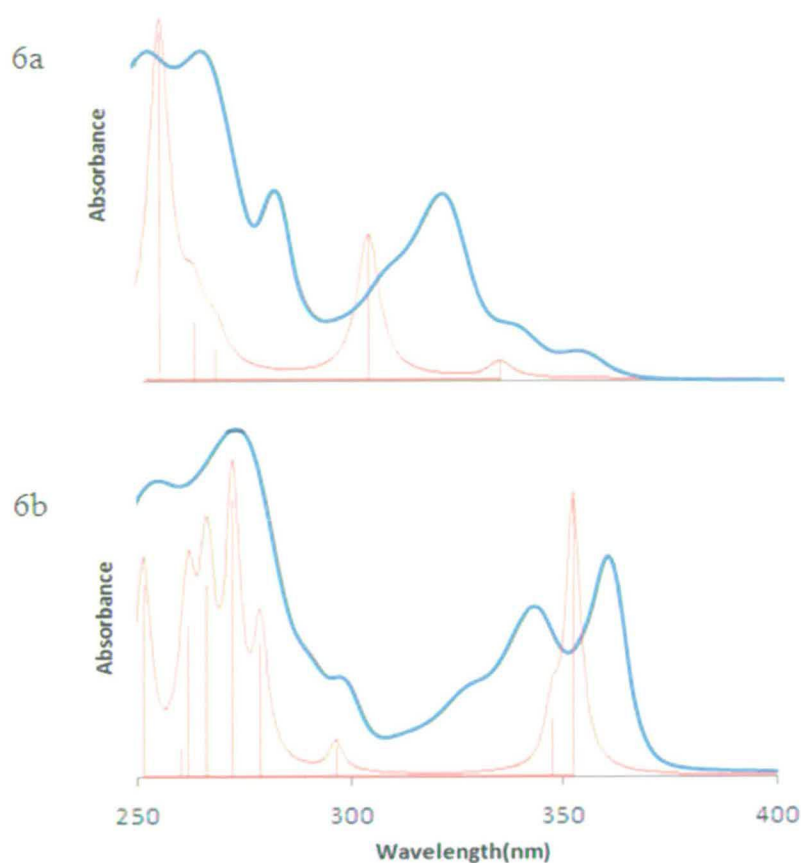


Figure 5.13 – Comparison between observed and calculated absorption spectra for 6a and 6b

| Transition  | Calculated Energy (nm) | Observed Energy (nm) | f      | Composition   |
|-------------|------------------------|----------------------|--------|---|
| $S_0 - S_1$ | 331.09                 | 353                  | 0.0642 | HOMO – LUMO 67%   |
| $S_0 - S_2$ | 301.68                 | 336                  | 0.5555 | HOMO-1 – LUMO 63%<br>HOMO – LUMO+1 23%                      |
| $S_0 - S_3$ | 267.82                 | 322                  | 0.1194 | HOMO-2 – LUMO 42%<br>HOMO – LUMO+1 39%<br>HOMO – LUMO+2 27% |

Table 5.8 – Calculated energy, oscillator strength and composition of first 3 absorption transitions of 6a

| Transition  | Calculated Energy (nm) | Observed Energy (nm) | f      | Composition                            |
|-------------|------------------------|----------------------|--------|--|
| $S_0 - S_1$ | 350.38                 | 360                  | 0.4955 | HOMO – LUMO 65%<br>HOMO-1 – LUMO+1 15% |
| $S_0 - S_2$ | 345.48                 | 343                  | 0.1044 | HOMO-1 – LUMO 65%<br>HOMO – LUMO+1 23% |
| $S_0 - S_3$ | 295.97                 | 330                  | 0.0536 | HOMO-2 – LUMO 65%<br>HOMO – LUMO+2 18% |

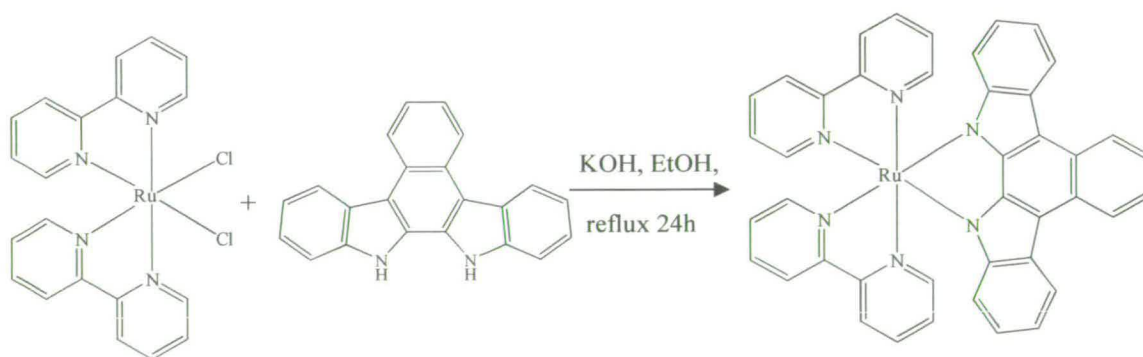
*Table 5.9 – Calculated energy, oscillator strength and composition of first 3 absorption transitions of 6e*

The calculated spectra of both **6a** and **6b** bear some resemblance to the observed spectra however, the calculated spectra of **6b** is significantly closer to that observed. For **6a**, while the calculated transitions are slightly higher in energy than expected from the results of **2a** and 2,8 diphenyl-6,12-diethylindolo[3,2-b]carbazole,<sup>24</sup> the relative intensities of each transition are far removed from the extinction coefficients. The composition of the transitions does not vary between **6a** and **6b**. This is in agreement with the suggestion put forward in Chapter 5.2.4 that the differences in the observed spectra may be due to the apparent switching of the HOMO-1 and HOMO levels between **6a** and **6b**.

## 5.3 -Ruthenium bisbipyridyl-benzo[*c*]indolo[2,3-*a*]carbazole

### 5.3.1 – Synthesis

The synthesis of **7** was carried out heating Ru[bipy]<sub>2</sub>Cl<sub>2</sub> and **6b** to reflux in the presence of a strong base, Scheme 5.2. Compound **7** was successfully identified by both <sup>1</sup>H-NMR and FAB-MS, however CHN analysis is inconclusive. As the ratio of C:H:N is in agreement with that expected if another material with no further C, H or N is present within the sample, this has been attributed to an inorganic impurity. Due to the ‘extra’ mass observed through CHN analysis the most likely inorganic impurity appears to be a fractional proportion of Cl. This is discussed more thoroughly in Section 5.3.



*Scheme 5.2 – Synthetic route taken to 7*

### 5.3.2 - Electrochemistry

The electrochemical analysis of **7**, Fig. 5.14, Table 5.10, is particularly unusual displaying two reversible oxidations at 0.16V and 0.58V. In comparison to a number of alternative ruthenium bis-bipyridyl species, Fig 5.15, the potential of these oxidations is unique. It may be observed that neither  $[\text{Ru}^{\text{II}}(\text{bipy})_3]^{2+}$ , Fig 5.14a, or  $[\text{Ru}^{\text{II}}(\text{bipy})_2(\text{BiBzImH}_2)]^{2+}$  Fig 5.15b, are neutral species. This makes it significantly more difficult to remove further electrons, thus giving a higher oxidation potential however,  $[\text{Ru}^{\text{II}}(\text{bipy})_2(\text{bqdi})]$ , Fig 5.15c, is neutral with a first oxidation potential even higher, though the oxidized form of  $\text{Ru}^{\text{II}}(\text{bipy})_2(\text{BiBzIm})$  displays an oxidation peak at 0.43V. However, no second oxidation peak is observed indicating that the transition from Ru(III) to Ru(IV) is not trivial, emphasizing the unusual nature of **7**. Similarly related species previously studied include  $[\text{Ru}(\text{bipy})_2(\text{Hpzpzth})]^{2+}$  and  $[\text{Ru}(\text{bipy})_2(\text{pzpzth})]^+$ , Fig. 5.16.<sup>28</sup> These also suggest that **7** has a range of unusual properties. The first oxidation changes from 1.09V for  $[\text{Ru}^{\text{II}}(\text{bipy})_2(\text{Hpzpzth})]^{2+}$  to 0.87V for  $[\text{Ru}^{\text{II}}(\text{bipy})_2(\text{pzpzth})]^+$ . This does not account for the three oxidation peaks observed for **7** and thus it appears that **6b** has some very interesting characteristics as a ligand. The ease of oxidation of **6b** to produce the oxidized form observed in Fig 5.6b suggests that **6b** may act as a non-innocent ligand, with different electronic conformations to stabilize the various oxidation states of the metal centre.

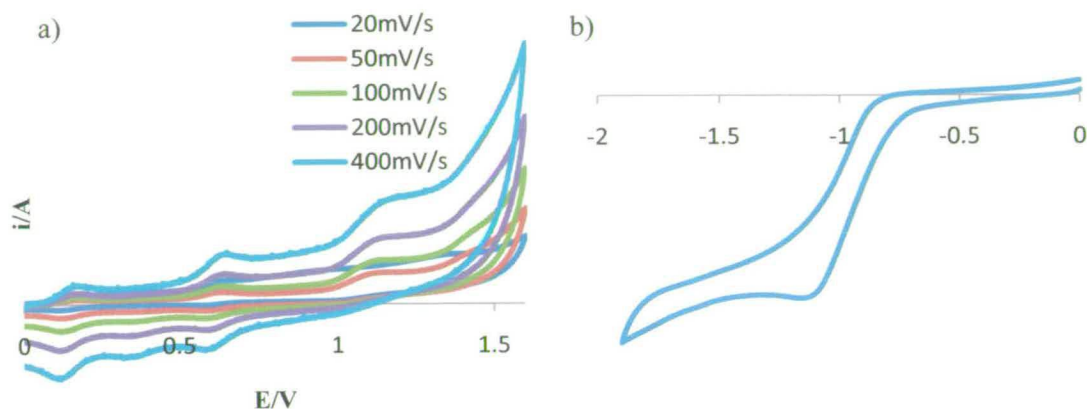


Figure 5.14 – a) Oxidation and b) reduction of **7** against Ag/AgCl reference in 0.1MTBAPF<sub>4</sub>/DMF

|   | Oxidation         |      |                   | Reduction          |
|---|-------------------|------|-------------------|--------------------|
| <b>6b</b>   | 1.15 <sup>†</sup> | -    | -                 | -1.00 <sup>†</sup> |
| <b>7</b>  | 0.16              | 0.58 | 1.15 <sup>†</sup> | -1.18 <sup>†</sup> |
| <b>Ru(bipy)<sub>3</sub><sup>2+*</sup></b>                       | 1.35              | -    | -                 | -1.37              |
| <b>Ru(bipy)<sub>2</sub>(BiBzImH<sub>2</sub>)<sup>2+**</sup></b> | 0.93              | 1.48 | -                 | -1.60              |
| <b>Ru(bipy)<sub>2</sub>(BiBzIm)<sup>**</sup></b>                | 0.43              | -    | -                 | -1.58              |
| <b>Ru(bipy)<sub>2</sub>(bqdi)<sup>***</sup></b>                 | 1.42              | -    | -                 | -0.45              |

Table 5.10- Observed redox peaks for **6b**, **7** and a number of alternative ruthenium polypyridyl systems. All processes are chemically and electrochemically reversible unless marked <sup>†</sup>. \*Taken from 25 \*\* Taken from 26, \*\*\* Taken from 27

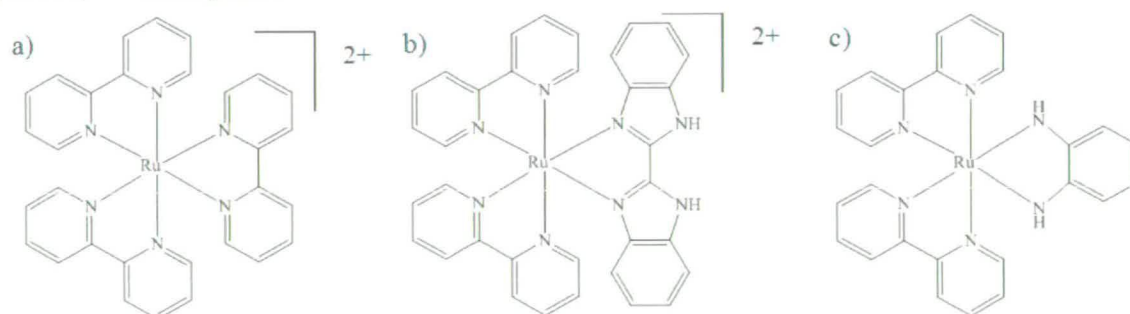


Figure 5.15 – Analogous ruthenium complexes a) Ruthenium tris-2,2'-bipyridine, Ru(bipy)<sub>3</sub>, b) Ruthenium bis-2,2'-bipyridyl 2,2'-bibenzimidazole, Ru(bipy)<sub>2</sub>(BiBzImH<sub>2</sub>) c) Ruthenium bis-2,2'-bipyridyl benzoquinone diimine, Ru(bipy)<sub>2</sub>(bqdi)



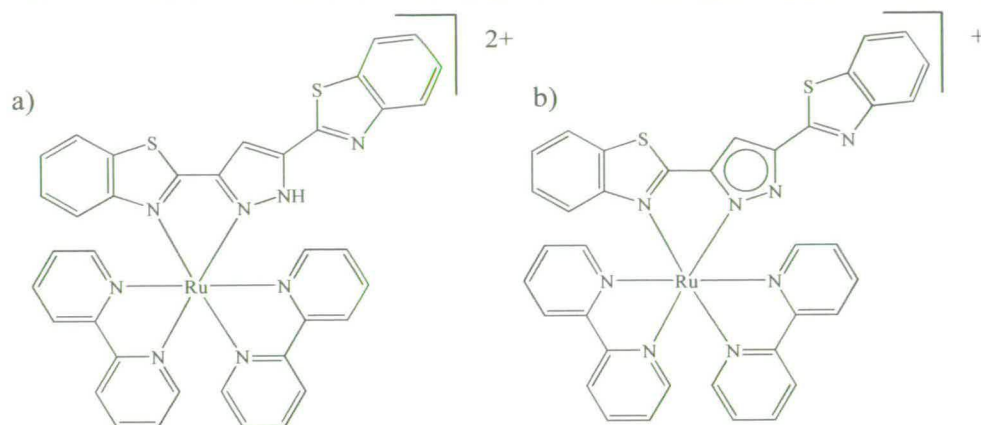


Figure 5.16 – a)  $Ru(bipy)_2(Hpmpzth)$ , b)  $Ru(bipy)_2(pzpzth)$

As the ‘extra’ mass noted via CHN analysis may belong to  $Cl^-$ , it might be assumed that species **7** exists in two forms at atmospheric conditions; one in which the ligand **6b** is in the reduced form and one in which it is in the oxidised form but with  $Cl^-$  counter-ions. However, the relative peak heights of the various oxidation processes dispute this. This leads to the conclusion that the ‘extra’ mass is at present an unexplained, but benign, impurity.

While no other ruthenium bis-bipyridyl systems have been synthesised with nitrogen-based non-innocent ligands ruthenium bis-bipyridyl dithialoto complexes, Fig 5.17, have been observed.<sup>29</sup> The dithialoto ligands may take on two forms, Fig 5.17a and c, and this has the effect of lowering the first two oxidation potentials of the complex. Cyclic voltammetry of these species show three reversible oxidations, Table 5.11. These compare much more closely to **7** than the nitrogen based systems previously noted

suggesting that these systems are indeed non-innocent systems though this will be investigated more thoroughly throughout this Chapter.

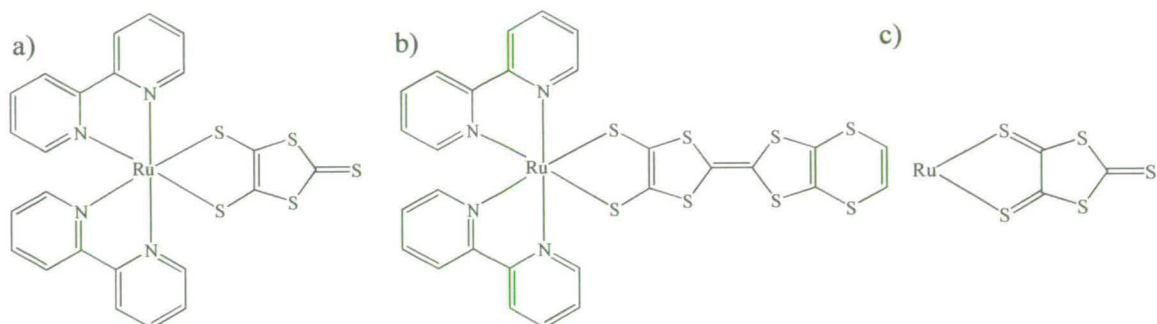


Figure 5.17 – a), b) Ruthenium dithialoto based systems, c) second possible conformation of the dithialoto ligand

|   | Oxidation |      |      |
|---|-----------|------|------|
|   |           |      |      |
| Ru(bipy) <sub>2</sub> (C <sub>3</sub> S <sub>5</sub> ), Fig 5.17a               | 0.00      | 0.67 | 0.80 |
| Ru(bipy) <sub>2</sub> (C <sub>8</sub> H <sub>4</sub> S <sub>8</sub> ) Fig 5.17b | -0.30     | 0.31 | 0.79 |

Table 5.11 – Oxidation potentials of ruthenium bisbipyridyl dithialoto complexes

### 5.3.3 – UV/Vis Spectroscopy

The most notable aspect of the absorption spectrum of **7** is the number of transitions observed in the ultraviolet and visible regions, Fig 5.18, Table 5.12. This may well be attributed to the increased  $\pi$ -structure of **6b** in comparison to the other ligands noted. The increase in the size of the  $\pi$ -structure has the potential to increase the number of  $\pi$ - $\pi^*$  transitions. It is also noticeable that S<sub>0</sub> to S<sub>1</sub> transition for **7** and Ru(bipy)<sub>2</sub>(BiBzIm) are at significantly lower energy than Ru(bipy)<sub>3</sub><sup>2+</sup> and

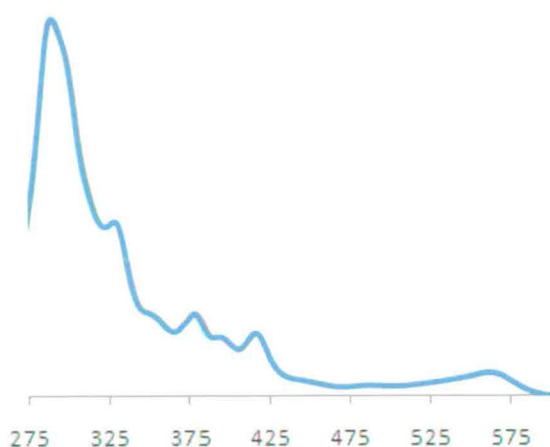


Figure 5.18 – Absorption spectrum of 7

|                                | Peak (nm) ( $\epsilon/ M^{-1}cm^{-1} \times 10^3$ ) |           |           |           |          |          |
|--------------------------------|---|-----------|-----------|-----------|----------|----------|
| 7                              | 289(46.0)   | 328(23.1) | 378(11.5) | 393(8.3)  | 416(8.9) | 561(6.1) |
| $Ru(bipy)_3^{2+*}$             | 284(71.0)   | 436(11.4) | 448(12.5) |           |          |          |
| $Ru(bipy)_2(BiBzImH_2)^{2+**}$ | 290(63.1)   | 328(37.5) | 347(45.8) | 469(11.3) |          |          |
| $Ru(bipy)_2(BiBzIm)^{**}$      | 295(54.7)   | 333(30.4) | 543(8.4)  |           |          |          |

Table 5.12 – Observed absorption peaks for 7 and a number of alternative ruthenium polypyridyl systems

$Ru(bipy)_2 (BiBzImH_2)^{2+}$ . In previous studies this red-shift has been rationalized as anionic, weakly  $\pi$ -accepting ligands raising the energy of ruthenium(II) d-orbitals<sup>30</sup> and this is the case with analogous halide and oxalate systems, as well as with the similar dipyrin ligands, Fig 5.19.<sup>31</sup> From previous studies this transition may be assigned as the result of a <sup>1</sup>MLCT absorption as is the case with other known ruthenium bis-bipyridyl complexes.

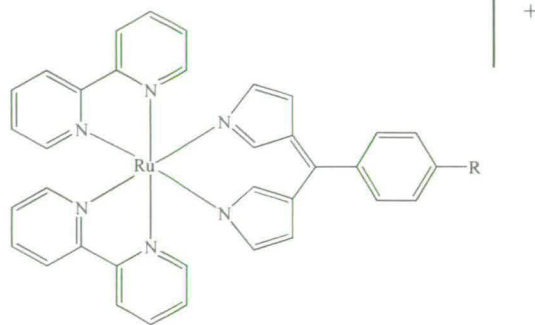


Figure 5.19 – Ruthenium bisbipyridyl dipyrin systems

### 5.3.4 – Emission Spectroscopy

Emission studies of **7** showed no emission at 298K or 77K. Work carried out by Keri McCall at the University of Edinburgh <sup>32</sup> has noted that ruthenium polypyridyl complexes display increasingly weak emission as spatial separation between the HOMO and LUMO increases. This is discussed in Section 5.3.6.

### 5.3.5 – Spectroelectrochemistry

The oxidised forms of **7** were studied through spectroelectrochemistry to allow more effective assessment of frontier molecular orbitals. Studies were carried out in 0.1M TBABF<sub>4</sub>/DMF, Fig 5.20.

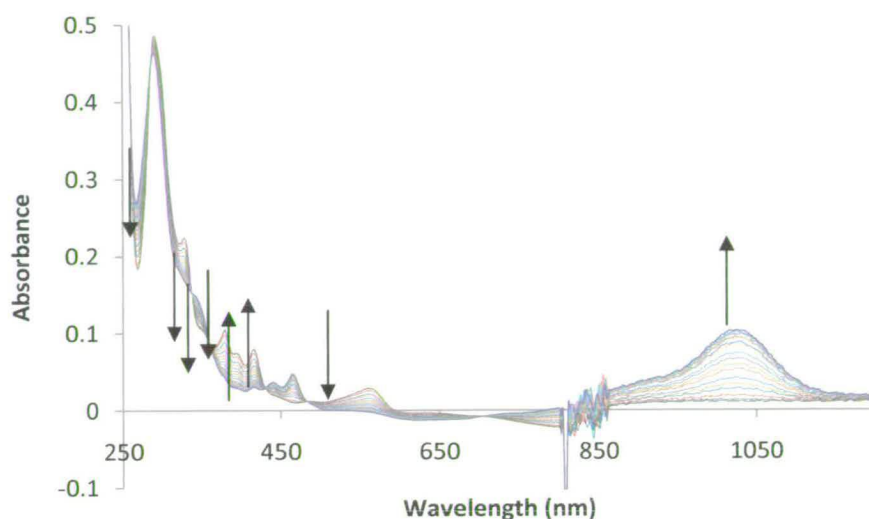


Figure 5.20 – Dioxidation study of 7 in 0.1M TBABF<sub>4</sub>/DMF with an applied potential of 0.7V vs Ag/AgCl.

When the system was oxidised at 0.3V to assess the first oxidation no change was observed and only when the potential was increased to 0.7V, past the point of the second oxidation, was any change in spectrum noted. Past 0.7V the spectrum shows five isosbestic points, the band at 561nm collapses and there is a partial collapse of the three transitions between 378nm and 416nm, while two new transitions appear in the visible region at 465nm and 441nm and another band appears in the near-IR region at 1025nm. These changes were completely reversible upon regeneration of the parent compound at 0.5V.

The changes observed are suggestive of ruthenium oxidation with the decrease in the MLCT transitions and the new peak at 1025nm typical of a LMCT transition ligand to Ru(III).<sup>30,32</sup> Changes in the spectrum at higher energy, such as the appearance of peaks at 441nm and 465nm and the collapse of the peaks at 378nm and 393nm might also arise from interactions with a new Ru(III) centre. However the quantity of transitions in the high energy region makes it difficult to use these transitions in the identification of the new species.

As only the dioxidised species causes a change in the absorption spectra, the mono-oxidised species appears particularly unusual. As the changes in the spectra are indicative of a Ru(III) centre not Ru(IV) the first oxidation appears to be entirely situated on the benzo[c]indolo[2,3-a]carbazole ligand. This situation will be investigated further through DFT calculations.

### ***5.3.6 – DFT Calculations***

Calculations undertaken into the geometry and orbitals of **7** have resulted in the predicted geometry and molecular orbitals observed in Table 5.13 and the energies and orbital occupancies noted in Table 5.14.

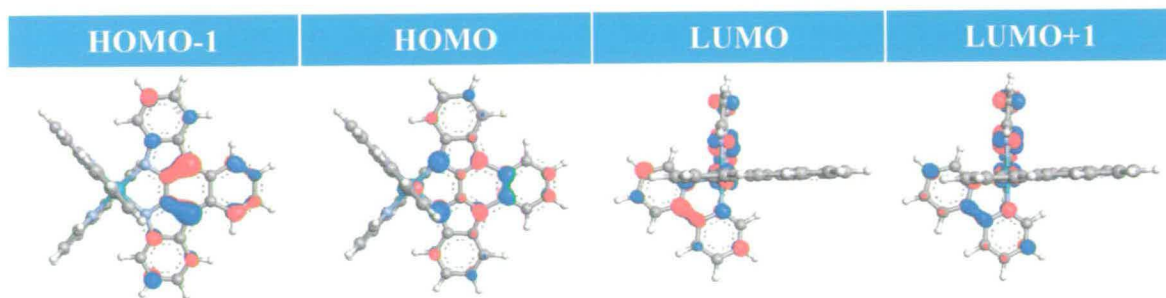


Table 5.13 – Calculated geometries of the frontier orbitals of **7**

|        | Energy (eV) | Percentage Occupancies |       |        |
|--------|-------------|------------------------|-------|--------|
|        |             | Ru                     | BiPy  | Indole |
| LUMO+2 | -1.585      | 2.58                   | 96.36 | 1.07   |
| LUMO+1 | -2.320      | 12.41                  | 86.29 | 1.25   |
| LUMO   | -2.376      | 6.99                   | 90.96 | 1.29   |
| HOMO   | -3.640      | 8.52                   | 8.10  | 83.35  |
| HOMO-1 | -3.882      | 0.18                   | 0.24  | 99.49  |
| HOMO-2 | -4.280      | 17.99                  | 4.50  | 77.51  |

Table 5.14 – Calculated orbital energies and occupancies of **7**

The most obvious difference between the orbital geometries of **7** relative to those of the free species **6b** is the lack of unoccupied frontier orbital character on the indole species. This is in agreement with previous calculations on ruthenium bis-bipyridyl complexes which have found the LUMO to be predominantly on the bipyridyl complexes while the HOMO is largely located on the ruthenium and the non-bipyridyl ligands.<sup>33</sup> This is in agreement with the absorption spectroscopy results observed for **7** due to the similarities between a number of the transitions observed for **7** and those of other ruthenium bipyridyl complexes. One further difference of note is the apparent reversal of the

HOMO-1 and HOMO levels of **7** relative to **6b**. This may be attributed to the orbital node between the indole-based nitrogen atoms and the central ruthenium ion causing an increase in the relative energy of this orbital in comparison to that of **6b**.

The lack of any observable emission may well be due to the limited orbital overlap observed between frontier orbitals. In the case of both the occupied and unoccupied frontier orbitals the only point of overlap, i.e. the central ruthenium(II) ion displays very little orbital character. As such transitions between the excited state and ground state are effectively so slow that no luminescence can be seen as non-radiative processes will dominate.

The energies of the HOMO and HOMO-1 levels lie close together while also displaying an extremely low level of ruthenium character. The spectroelectrochemical results suggest that the first oxidation causes no change to the ruthenium centre, i.e. the ruthenium centre remains ruthenium(II). In spite of the computational results obtained this is not easily explained. The first oxidation may be entirely based on the indolocarbazole, while the second oxidation is based much more on the ruthenium centre and as such, result in the change observed in the absorption spectra. The nature of the calculated HOMO-1 orbital suggests there is not only a minor level of ruthenium character involved in the orbital but there is also very little indole-based nitrogen character involved. Hence the interactions between the ruthenium centre and the

---



surrounding ligands remain largely unchanged by the first oxidation. However without complex TD-DFT studies beyond the scope of this investigation this cannot be fully ascertained.

## 5.4 – Conclusion

The electronic properties of two species have been assessed for the first time with the results showing striking similarities to both the indolo[3, 2-*a*]carbazoles and other previously assessed indolocarbazole species. Unusual features in the spectra of **6a** appear to be as a result of the proximity between the two nitrogen atoms in comparison to other indolocarbazole systems.

The electronic properties observed through the study of indolo[2, 3-*a*]carbazoles, the indolo[3, 2-*a*]carbazoles from Chapter 3 and the reported properties of indolo[2, 3-*b*]carbazoles and indolo[2, 3-*c*]carbazoles suggest that while much emphasis has been placed in the device potential of indolo[3, 2-*b*]carbazoles the remaining indolocarbazole species may well have their own roles to play as functional electronic materials.

A novel ruthenium bipyridyl complex has been synthesised and characterised, which contains the first example of the use of an indolo[2, 3-a]carbazole as a ligand. This species displays some highly unusual properties. The ruthenium(II)bisbipyridyl benzo[c]indolocarbazole displays two reversible oxidation at 0.16V and 0.59V however, the spectroelectrochemical analysis of the system at 0.7V points towards a Ru(III) centre.

The ‘non-innocent’ nature of this ligand may play a significant role in the unusual first oxidation of **7**. Though this cannot be stated with certainty due to the lack of expected changes to the  $\pi - \pi^*$  transitions which may occur if the oxidation were ligand based. It is clear that subsequent studies of the nature of indolo[2, 3-a]carbazoles as ligands will present a significant challenge and opportunity given the unusual characteristics exhibited by this species.

## 5.5 - Experimental

### *Synthesis*

Synthesis of Indolo[2, 3-a] carbazole <sup>18</sup> and benzo[e] indolo [2, 3-a] carbazole <sup>19,20</sup> followed literature procedures. Ru(bipyridyl)<sub>2</sub>Cl<sub>2</sub> synthesised by Keri McCall following published methods <sup>34</sup> from RuCl<sub>3</sub>.2H<sub>2</sub>O kindly loaned by Johnson Matthey.

**Indolo[2,3-a]carbazole, 6a** – Yield 11% - CHN for C<sub>18</sub>H<sub>12</sub>N<sub>2</sub> – Calc C 84.38, H 4.69, N 10.94, Found C 82.27, H 4.11, N 9.02

**Benzo[c]indolo[2,3-a]carbazole, 6b** – Yield 26% - CHN for C<sub>22</sub>H<sub>14</sub>N<sub>2</sub> – Calc C 86.27, H 4.58, N 9.15, Found C 85.79, H 4.37, N 9.01

**Synthesis of Ruthenium bis-bipyridyl benzo[c]indolo[2,3-a]carbazole, 7** - Ru(bipyridyl)<sub>2</sub>Cl<sub>2</sub> (72mg, 0.144mmol) **6b** (43mg, 0.144mmol) and KOH (16mg, 0.288mmol) were dissolved in ethanol (30ml) and refluxed for 18 hours. After cooling the solution was filtered and washed with methanol – Yield 33% - CHN for RuC<sub>42</sub>H<sub>28</sub>N<sub>6</sub> – Calc C 70.29, H 3.91, N 11.72, Found C 65.48, H 3.03, N 9.93 – <sup>1</sup>H-NMR (d6-DMSO) 8.49 (2H, d J<sub>H-H</sub> 0.03), 8.30 (2H, d J<sub>H-H</sub> 0.03), 8.07 (2H, m), 7.81 (6H, m), 7.59 (2H, d J<sub>H-H</sub> 0.035), 7.44 (2H, t J<sub>H-H</sub> 0.035), 7.18 (2H, t J<sub>H-H</sub> 0.035), 6.99 (4H, m), 6.44

(2H, t  $J_{\text{H-H}}$  0.035), 6.28 (2H, t  $J_{\text{H-H}}$  0.035), 5.21 (2H, d  $J_{\text{H-H}}$  0.035) – FAB-MS:  $m/z$  717(M<sup>+</sup>)

## 5.6 – References

1. J. Bergman, T. Janosik, N. Wahlstrom, *Adv. Heterocycl. Chem.*, 2001, **80**, 1.
2. G. Bartoli, M. Bosco, R. Dalpozzo, P. E. Todesco, *J. Org. Chem.*, 1986, **51**, 3694
3. S. Fabre, M. Prudhomme, *Bioinorg. & Med. Chem.*, 1993, **1**, 193
4. B. Hugon, F. Anizon, C. Bailly, R. M. Golsteyn, A. Pierre, S. Leonce, J. Hickman, B. Pfeiffer, M. Prudhomme, *Bioinorg. & Med. Chem.*, 2007, **15**, 5965
5. J. Bergman, B. Pelcman, *Tet. Lett.*, 1987, **28**, 4441
6. J. T. Kuethe, I. W. Davies, *Tet. Lett.*, 2004, **45**, 4009
7. C. A. Merlic, D. M. McInnes, *Tet. Lett.*, 1997, **38**, 7661
8. J. A. Bush, B. H. Long, J. J. Catino, W. T. Bradner, K. J. Tomita, *Antibiot.*, 1987, **40**, 668
9. D. S. Black, N. Kumar, L. C. H. Wong, *J. Chem. Soc. Chem. Commun.*, 1985, 1174
10. B. O'Regan, M. Gratzel, *Nature*, 1991, **353**, 737
11. G. Liebsch, I. Klimant, O. S. Wolfbeis, *Adv. Mater.*, 1999, **11**, 1296
12. T. Albrecht, A. Guckian, J. Ulstrup, J. G. Vos, *Trans. Nanotech. IEEE*, 2005, **4**, 430
13. G. Sprintschnik, H. W. Sprintschnik, P. P. Kirsch, D. G. Whitten, *J. Am. Chem. Soc.*, 1976, **98**, 2337

14. G. Sprintschnik, H. W. Sprintschnik, P. P. Kirsch, D. G. Whitten, *J. Am. Chem. Soc.*, 1977, **99**, 4949
15. K. Kalyanasundaram, M. Gratzel, *Angew. Chem., Int. Ed. Engl.*, 1979, **18**, 781
16. S. Weller, K. Brunner, J. W. Hofstraat, L. De Cola, *Nature*, 2003, **421**, 54
17. J. K. Barton, A. T. Danishefsky, J. M. Goldberg, *J. Am. Chem. Soc.*, 1986, **108**, 2081
18. Y.-Z. Hu, Y.-Q. Chen, *Synlett.*, 2005, **1**, 42
19. M. Saulnier, D. B. Frennesson, M. S. Deshpande, D. M. Vyas, *Tet. Lett.*, 1995, **36**, 7841
20. G. Abbiati, A. Arcadi, E. Beccali, G. Bianchi, F. Marinelli, E. Rossi, *Tetrahedron*, 2006, **62**, 3033
21. P. T. Boudreault, S. Wakim, N. Blouin, M. Simard, C. Tessier, Y. Tao, M. Leclerc, *J. Am. Chem. Soc.*, 2007, **129**, 9125
22. M. L. Swindells, M. L. Tomlinson, *J. Chem. Soc.*, 1956, 1135
23. H. Weller, K.-H. Grellemann, *J. Am. Chem. Soc.*, 1983, **105**, 6268
24. M. Belletete, P. T. Boudreault, M. Leclerc, Gilles Durocher, *J. Mol. Structure: THEOCHEM*, 2007, **824**, 15
25. P. A. Mabrouk, M. S. Wrighton, *Inorg. Chem.*, 1986, **25**, 526
26. A. M. Bond, M. Haga, *Inorg. Chem.*, 1986, **25**, 44507
27. H. Masui, A. B. P. Lever, E. S. Dodsworth, *Inorg. Chem.*, 1993, **32**, 258
28. Baitalik, U. Florke, K. Nag, *J. Chem. Soc., Dalton Trans.*, 1999, 719
29. K. Natsuaki, M. Nakano, G. Matsubayashi, R. Arakawa, *Inorg. Chim. Acta*, 2000, **299**, 112

30. G. Wolfbauer, A. M. Bond, D. R. MacFarlane, *Inorg. Chem.*, 1999, **38**, 3836
31. S. J. Smalley, M. R. Waterland, S. G. Telfer, *Inorg. Chem.*, 2009, **48**, 13
32. Keri McCall, *University of Edinburgh*, PhD Thesis, 2008.
33. G. Wolfbauer, A. M. Bond, D. R. MacFarlane, *J. Chem. Soc., Dalton Trans.*, 1999, 4363
34. B. P. Sullivan, D. J. Salmon, T. J. Meyer, *Inorg. Chem.*, 1978, **17**, 3334

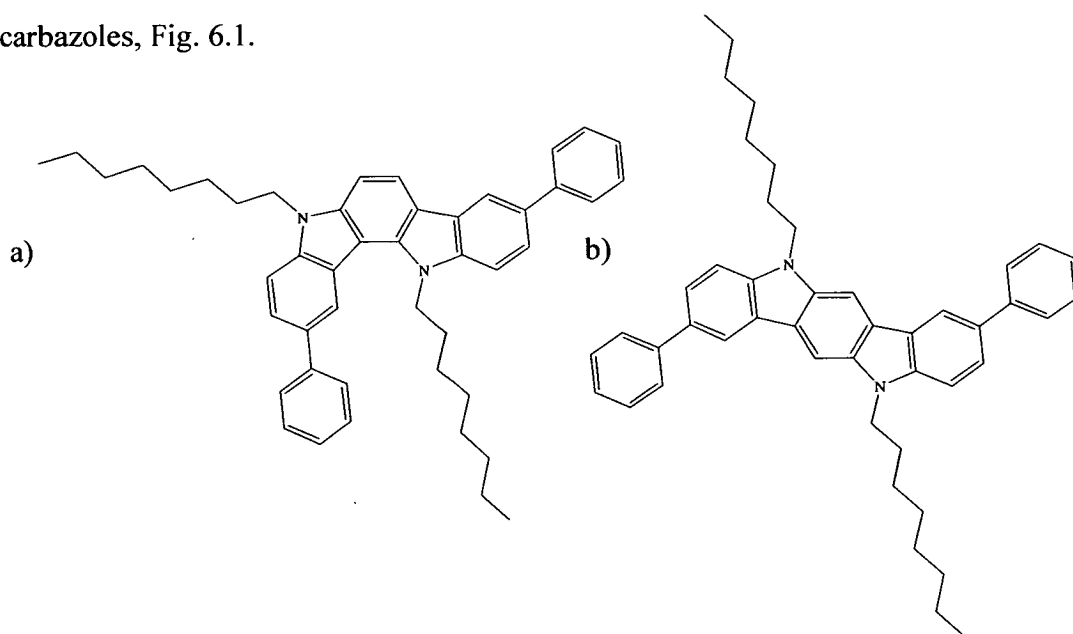
## **Chapter 6**

# **Future Work**

Throughout the course of this thesis much has been made of the potential of the indole-based species investigated with a view towards electronic applications, both as a purely organic material, and in the case of the indolo[2,3-a]carbazoles, as useful ligand in the creation of new inorganic compounds.

The original premise of this thesis was to both synthesise and characterise a new family of organic electronic materials, ultimately leading to the formation of devices from said materials and a thorough understanding of the potential of said material. Over the course of this research the aim of this thesis has been revised and ultimately appears to be the first step in a number of exciting projects to be undertaken by the Robertson group and collaborators.

The new synthetic route to indolo[3,2-a]carbazoles, and the potential for further functionalisation of the new species offer a cheap and synthetically simple route to complex conjugated organic species. This has been recognised by the further work currently underway within the Robertson group in collaboration with Professor K. Awaga of the University of Nagoya, into the charge mobility of these ‘building block’ indolo[3,2-a]carbazoles. Ultimately this will lead to the investigation of comparable indolo[3,2-a]carbazoles to the analogous and already investigated indolo[3,2-b]carbazoles, Fig. 6.1.



**Figure 6.1** – a) 2,9-Diphenyl-5,12-dioctylindolo[3,2-a]carbazole, b) 3,9-Diphenyl-5,11-dioctylindolo[3,2-b]carbazole

A similar goal has been set for separate research into the C3-symmetric indole trimer derivatives. The potential for **4a**, **4b** and **5b** as building blocks towards alternative organic electronic materials is too great to ignore and is also being further investigated in conjunction with Professor K. Awaga.



Finally the innovative use of indolo[2,3-a]carbazole species as ligands is being studied by Nina Chadwick of the University of Edinburgh. The apparent non-innocent nature of these ligands, as well as the potential applications for the complexes formed has lead to EPSRC funding to further develop understanding of these species.